Final Technical Report
Contract: NAS1-02056-6008
Solicitation/PR/Tracking No.: RFK-1224
GTRI Project A6972

Pulsed Lidar Performance / Technical Maturity Assessment

By:

Gary G. Gimmestad, Leanne L. West, and Jack W. Wood
Georgia Tech Research Institute

and

Rod Frehlich
National Center for Atmospheric Research

Prepared for:

National Aeronautics and Space Administration
Langley Research Center
NASA Technical Monitor: David K. Rutishauser
9A Langley Boulevard
MS 156A, Bldg. 1168, Rm. 113
Hampton, VA 23681-2199

Submitted by:

GEORGIA INSTITUTE OF TECHNOLOGY
A Unit of the University System of Georgia
Georgia Tech Research Institute
Atlanta, GA 30332-0800

February 2004

Contents

Figures

Tables

Executive Summary

The performance and technical maturity of the Coherent Technologies, Inc. (CTI) WindTracer lidar have been assessed for wake vortex detection and tracking at airports. The performance assessments described here were conducted with Monte Carlo simulations, and general plans were developed for field tests to validate the simulations.

To quantify the performance of CTI's algorithm, simulated lidar data were generated for various vortex and lidar parameters, and the results of CTI's algorithm (which was implemented on a mainframe computer at the National Center for Atmospheric Research) were compared with the known input parameters or "truth". This approach permits a rigorous statistical analysis of the detection of the vortex and the accuracy of the resulting estimates of vortex location and strength as a function of the lidar Signal to Noise Ratio (SNR), the key lidar signal quality parameter.

For each set of input parameters, 1,000 realizations were generated in order to insure good statistical accuracy. The lidar signals were generated with sophisticated algorithms that accounted for the fact that a wake vortex is much smaller than the lidar pulse, and realistic atmospheric conditions such as the background turbulence were included. An ambient wind speed of 3 m/s away from the lidar was assumed.

Simulations were performed for two different aircraft selected by NASA - the Boeing 737 for a smaller aircraft and the Boeing 747 for a large aircraft. Two cases were considered: an ideal analytic vortex model with no turbulence, and the same vortex model with an added turbulent velocity field satisfying a von Karman spatial spectrum and having an energy dissipation rate of 0.001 m^2/s^3.

The CTI algorithm is an approximation of the maximum likelihood (ML) estimator, which has optimal performance for many estimation problems. The research team therefore modified an existing ML estimation algorithm developed at the University of Colorado to produce optimal estimates of wake vortex parameters, as a reference for the performance of the CTI algorithm. To ensure robust results, both the simulations of lidar signals and the calculation of the ML estimates were produced with minimal approximations, which resulted in an intensive computational load. The vortex and lidar parameters were selected by NASA and CTI to match the conditions at the 2001 San Francisco airport (SFO) tests.

CTI's algorithm operates in two distinct modes: a detection mode and a tracking mode. Therefore, two situations were simulated: 1) a detection scenario where many realizations of the first 4 scans of lidar data were generated and processed, and 2) a tracking scenario where 22 scans of the vortex were generated and analyzed. Three main statistical metrics were produced: the probability of detection of the vortex, and the bias and the standard deviation of the resulting estimates of the vortex parameters. In addition, the probability density function (histogram) of the estimates was also produced to quantify the performance of CTI's algorithm. The simulations results are illustrated in 66 figures.

In general, the performance of the CTI algorithm was very good. For SNR = 10, the errors in the CTI vertical and horizontal track measurements were often very small compared to the vortex dimensions, in the 0.2 m range. The largest biases observed were 4 m, with a random error of about 1 m. The results for vortex circulation showed that the lidar algorithm was very accurate when the vortex was first detected, but that it overestimated circulation more and more as the vortex decayed. Circulation biases as large as 60 m^2/s were observed for vortices 100 seconds old. The addition of turbulence increased the standard deviations of the estimates but had little effect on bias. An investigation of algorithm performance as a function of SNR showed that the probability of vortex detection is very high for SNR values over 0.5, and for SNR = 1 or greater, the tracking errors are very small. Bias error in the circulation estimates is a function of SNR, however, growing larger as SNR decreases.

The second aspect of the project was to develop test plans for validating the simulation results. At the time this report was written, tests of the CTI WindTracer lidar were being conducted at the St. Louis International Airport (STL) by the Volpe National Transportation Systems Center. No detailed documentation of these tests was available, so the research team visited the site and developed a written description of them. The description includes several diagrams and photographs to illustrate the position and scan patterns of the lidar, as well as the positions of associated instruments such as wind lines. Auxiliary information and the data collection and processing procedures were also documented.

One lidar had been installed, and a second, identical lidar was being procured for STL. The second lidar was to be installed further up the glide slope from the first, and the existence of two lidars at one airport provided a unique opportunity for cost-effective add-ons to the STL tests. Plans for validation field tests were therefore developed in two categories: 1) tests that could be conducted as add-ons to the current STL series of tests; and 2) tests that would require a separate series of tests in a restricted airspace. In both cases, the objective of the tests was to validate the results of the numerical simulations.

Two short-term tests using the two lidars were recommended for STL. In the first test, the lidars were to be installed adjacent to each other, scanning in adjacent vertical planes, so as to measure the same vortices simultaneously with both lidars. A statistical analysis of the vortex track and circulation data files would then provide a measure of the random measurement errors of the two lidars. In the second test, the lidars were to face each other across the glide slope, again scanning adjacent vertical planes. An analysis of the resulting track files would then determine any track bias along the range direction.

Tests of two CTI lidars together cannot be used to validate the circulation biases in low SNR shown by the simulations. Circulation bias will require a separate type of instrument. Scanning the lidar in a vertical plane adjacent to a vertical array of acoustic anemometers was recommended, while wake vortices were transported across the array by the ambient wind. Point sensors cannot characterize the vortex wind field with the temporal and spatial resolution of the lidar, but acoustic anemometers do provide fast, accurate, three-axis wind measurements. The tower supporting the sensor array would have to be fairly tall, so this test was to be conducted in controlled airspace, not at a commercial airport.

1 Introduction

This report describes the results of investigations performed by the Georgia Tech Research Institute (GTRI) and the National Center for Atmospheric Research (NCAR) under a task entitled "Pulsed Lidar Performance/Technical Maturity Assessment" funded by the Crew Systems Branch of the Airborne Systems Competency at the NASA Langley Research Center under Contract NASI-02056-6008. The investigations included two tasks, 1.1(a) and 1.1(b).

Task 1.1(a), performed by NCAR in Boulder, Colorado was an analysis of the lidar system to determine its performance and capabilities based on results from simulated lidar data with analytic wake vortex models provided by NASA, which were then compared to the vendor's claims for the operational specifications of the lidar. Task 1.1(a) is described in Section 3, including the vortex model, lidar parameters and simulations, and results for both detection and tracking of wake vortices generated by Boeing 737s and 747s.

Task 1.1(b) was performed by GTRI in Atlanta, Georgia and is described in Section 4. Task 1.1(b) includes a description of the St. Louis Airport (STL) field test being conducted by the Volpe National Transportation Systems Center, and it also addresses the development of a test plan to validate simulation studies conducted as part of Task 1.1(a). Section 4.2 provides a description of the Volpe STL field tests, and Section 4.3 describes 3 possible ways to validate the WindTracer lidar simulations performed in Task 1.1(a).

The Tasks discussed in this report are in support of the NASA Virtual Airspace Modeling and Simulation (VAMS) program and are designed to evaluate a pulsed lidar that will be required for active wake vortex avoidance solutions. The Coherent Technologies, Inc. (CTI) WindTracer LIDAR is an eye-safe, 2-micron, coherent, pulsed Doppler lidar with wake tracking capability [1]-[3]. The actual performance of the WindTracer system was to be quantified. In addition, the sensor performance has been assessed and modeled, and the models have been included in simulation efforts.

The WindTracer LIDAR was purchased by the Federal Aviation Administration (FAA) for use in near-term field data collection efforts as part of a joint NASA/FAA wake vortex research program. In the joint research program, a minimum common wake and weather data collection platform will be defined. NASA Langley will use the field data to support wake model development and operational concept investigation in support of the VAMS project, where the ultimate goal is to improve airport capacity and safety.

2 Background

The detection and tracking of wake vortices from commercial aircraft is important for efficient use of major airports and general aviation safety. To prevent hazardous wake turbulence encounters, airports operate with the Instrument Flight Rules (IFR) longitudinal spacing requirement. The spacing requirement is based on factors such as the geometry of the airspace/runways and the size of the aircraft involved. The main concern at airports is the drifting of a vortex into the path of an aircraft during landing. In addition, the ability to track the location and vortex strength at higher altitudes would help quantify and predict the risk of hazardous encounters.

The detection and tracking of a wake vortex has been investigated using various techniques and instruments [3]-[7]. Because the spatial extent of the vortex is typically 10-50 m, high-resolution velocity measurements are required to accurately resolve the vortex [3][6][7]. Therefore, a suitable instrument for wake vortex detection and tracking is a high-resolution Doppler lidar.

Through the Aircraft Wake VOrtex Spacing System (AVOSS) project, NASA set the goal of demonstrating a technology that could provide aircraft with real-time wake avoidance information, thereby allowing a greater capacity of aircraft landings by reducing the longitudinal spacing requirement. As part of the AVOSS project, pulsed lidar prototypes have been field-tested for wake vortex tracking capability.

The technique for identification of a wake vortex using profiles of radial velocity measurements at various elevation angles has been verified by Brockman et al. [6] and Kopp et al. [7] using data from a CTI lidar. A clear signature of the vortex can be produced in the coherent Doppler lidar signal spectrum when the range gate of the processing interval completely encompasses the vortex with an optimal scanning geometry [4]. Producing the clear signature requires the accumulation of signal spectra from multiple lidar shots that sample the range and altitude of the complete vortex at a beam angle that is perpendicular to the vortex axis while scanning the lidar beam from zero elevation to a maximum elevation determined by the range to the runway and the maximum altitude of the vortex, as shown in Figure 1.

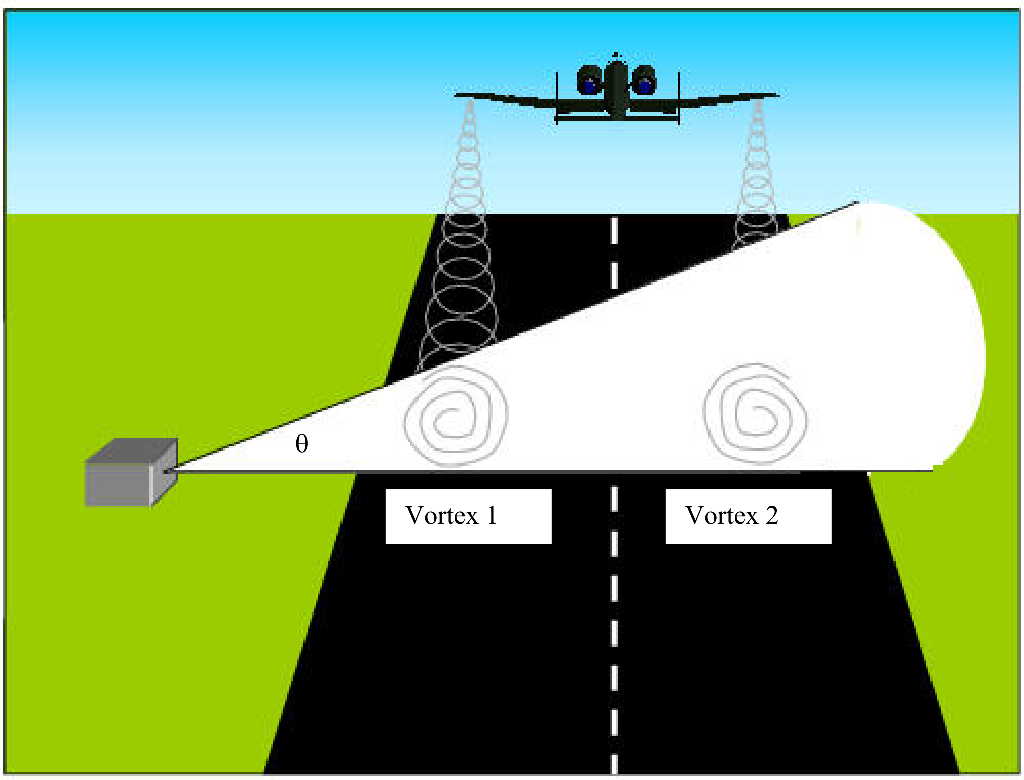

Figure 1. Geometry of wake vortex detection and tracking with coherent Doppler lidar

3 Task 1.1(a)

3.1 Introduction to Task 1.1(a)

Experimental verification of wake vortex detection and tracking with a pulsed Doppler lidar is difficult because an accurate independent measurement of the vortex parameters is not readily available. Since the goal of this effort was to quantify the performance of CTI's algorithm, simulated lidar data was generated for various vortex and lidar parameters, and the results of

CTI's algorithm were compared with the known input parameters or "truth". This approach permits a rigorous statistical analysis of the detection of the vortex and the accuracy of the resulting estimates of vortex location and strength as a function of the lidar Signal to Noise Ratio (SNR), the key lidar signal quality parameter.

The statistical accuracy of the results is determined by the number of realizations generated for each set of input parameters. The ability to generate many realizations of the lidar data for controlled conditions is a major advantage of numerical simulations over similar comparisons in a field campaign. However, accurate simulations of lidar signals for a wake vortex, which is much smaller than the lidar pulse, require careful simulation algorithms [8]-[12]. In addition, it is important to include realistic atmospheric conditions such as the background turbulence, which is always present.

The research team has chosen two benchmark cases for the two different aircraft selected by NASA (the Boeing 737 for a smaller aircraft and the Boeing 747 for a large aircraft). The first case is an ideal analytic vortex model with no turbulence, and the second is the same vortex model with an added turbulent velocity field satisfying a von Karman spatial spectrum [9],[11]-[13].

In a preliminary review of lidar based vortex detection and tracking algorithms, the research team found no quantitative predictions of performance for a given set of vortex, lidar, and atmospheric parameters. It is consequentially difficult to compare CTI's algorithm with other techniques. The CTI algorithm [4] is an approximation of the maximum likelihood (ML) estimator, which has optimal performance for many estimation problems. The research team has therefore modified an existing ML estimation algorithm developed at the University of Colorado to produce optimal estimates of wake vortex parameters as a reference for the performance of the CTI algorithm.

To ensure robust results, both the simulations of lidar signals and the calculation of the ML estimates were produced with minimal approximations, which resulted in an intensive computational load. The vortex and lidar parameters were selected by NASA and CTI to match the conditions at the San Francisco airport (SFO) tests. To simplify the analysis, it was decided that the aerosol backscatter over the vortex region is constant.

CTI's algorithm operates in two distinct modes: a detection mode and a tracking mode. Therefore, two situations were simulated: 1) a detection scenario where many realizations of the first 4 scans of lidar data were generated and processed, and 2) a tracking scenario where 22 scans of the vortex were generated and analyzed. Three main statistical metrics were produced: the probability of detection of the vortex, and the bias and the standard deviation of the resulting estimates of the vortex parameters. In addition, the probability density function (histogram) of the estimates was also produced to quantify the performance of CTI's algorithm.

3.2 Wake Vortex Model

The simulation of lidar data requires a realistic analytical model for the vortex time evolution. The vortex pair time evolution was provided by NASA based on the Burnham-Hallock model, which represents the tangential velocity $v_\theta(r, t)$ of the vortex as [14]

$$v_\theta(r, t) = \frac{\Gamma(t)}{2\pi r}\frac{r^2}{r^2 + r_C^2} \tag{1}$$

where r is the distance from the vortex core, Γ is the circulation strength, and r_C is the vortex core radius, which also indicates the location of the maximum tangential velocity. A vortex pair is established with the two counter-rotating vortices satisfying Eq. (1) with the same altitude H(t) with a downward velocity

$$w(t) = \frac{\Gamma(t)}{2 \pi b_0} \quad (2)$$

where b_0 is the initial vortex pair horizontal separation. The decay of the vortex strength is given by

$$\frac{\Gamma(t)}{\Gamma_0} = 1 - \frac{t}{T_0} \quad (3)$$

where Γ_0 is the strength at the creation time t=0 and T_0 is the decay time of the vortex.

3.3 Wake Vortex and Atmospheric Parameters

The vortex parameters depend on the aircraft type and to a lesser extent, on the atmospheric conditions. To reduce the numerical effort, only two aircraft were considered: the Boeing 737 and the Boeing 747. NASA provided the vortex parameters, given in Table 1. For both aircraft, the center of the vortex pair is located a distance y=1120 m from the lidar at an altitude of 150.0 m at the time of vortex creation.

Table 1. Vortex Parameters

Aircraft	Γ_0 (m^2/s)	b_0 (m)	r_c (m)	T_0 (s)
737	220	22.3	0.669	108
747	500	50.5	1.5	145

Another important input is the background wind field which was given by NASA as a constant horizontal ambient velocity $v_{ambient}$ = 3 m/s away from the lidar to produce realistic vortex motion. To include more realistic velocity fields, such as the effect of turbulence, the research team produced a set of results for an added homogeneous isotropic von Karman radial velocity field [10]-[13] with an energy dissipation rate of $\varepsilon = 0.001\ m^2/s^3$ and an outer scale L_0=50 m consistent with Doppler lidar turbulence measurements in the boundary layer [15]. The random turbulent wind field is generated with algorithms that produce the correct spatial statistics of the velocity field at the simulation grid points [9]-[13]. One disadvantage of the added turbulent field is the possible errors introduced in the definition of the true vortex parameters. To simplify the interpretation of the performance of the ML and CTI estimates, the research team assumed that the true vortex parameters are not altered by the turbulent field. This assumption can be investigated with further analysis of the simulated wind fields and Doppler lidar data. An example of the time evolution of the vortex parameters and the CTI estimates from simulated data with high SNR is shown in Figure 2 for the decay of a vortex from a Boeing 737. The statistical performance of estimates such as these was determined for vortex detection (the first measurement) and for tracking (the remaining measurements after detection).

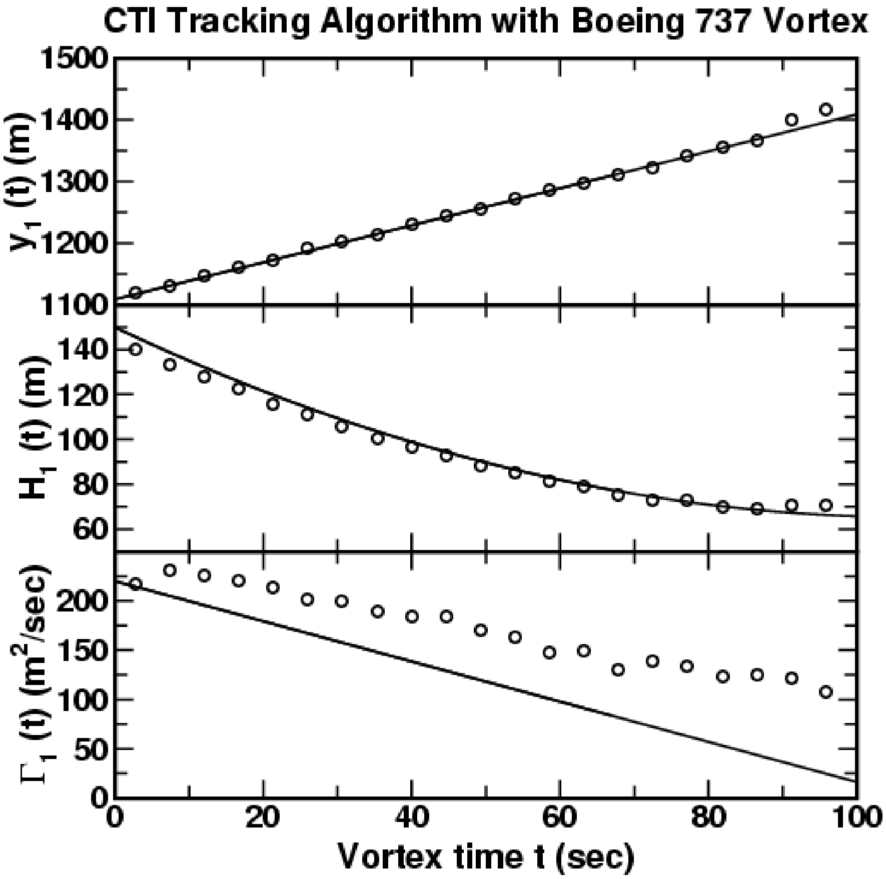

Figure 2. Temporal evolution of the Boeing 737 vortex parameters (solid line) and CTI estimates from simulated data (circle) of distance y_1, altitude H_1, and strength Γ_1 for vortex 1 and SNR=10

3.4 Lidar Parameters

The lidar parameters were provided by NASA to match the CTI WindTracer system [16] used during a September 2001 installation at SFO. These parameters are given in Table 2, and the lidar data sampling geometry is illustrated in Figure 3, for 737 vortices. The lidar is 3 m above the surface and an ambient velocity $v_{ambient}$= 3.0 m/s away from the lidar is also assumed. The lidar heterodyne Signal to Noise Ratio (SNR) in a 50 MHz bandwidth is the key free parameter that was varied to sample typical operating conditions. The CTI algorithm was modified to output an estimate of the SNR in the tracking files. The statistical analysis of these estimates was also included in the performance evaluation.

Table 2. CTI WindTracer Lidar Parameters

laser wavelength, λ	2.0225 μm
Full Width at Half Maximum (FWHM) Gaussian pulse width, Δt	0.32 μs
FWHM pulse width in range, Δr	48 m
pulse repetition frequency (PRF)	500 Hz
sampling rate for real data, F_{samp}	100 MHz
data samples per range gate, M	64
number of spectral points per range-gate, N_{bin}	32
range-gate processing length, Δp	96 m
range-gates range offset	11 data samples (16.5 m)
accumulated spectra per range gate, N	20
spectra per Line-Of-Sight (LOS) N_{spec}	48
number of LOS's N_{LOS}	70
lidar beam elevation angle scan rate θ_{scan}	3.3° /s
first elevation angle θ_1	0.25°
time between the start of each elevation scan t_{scan}	4.65 sec

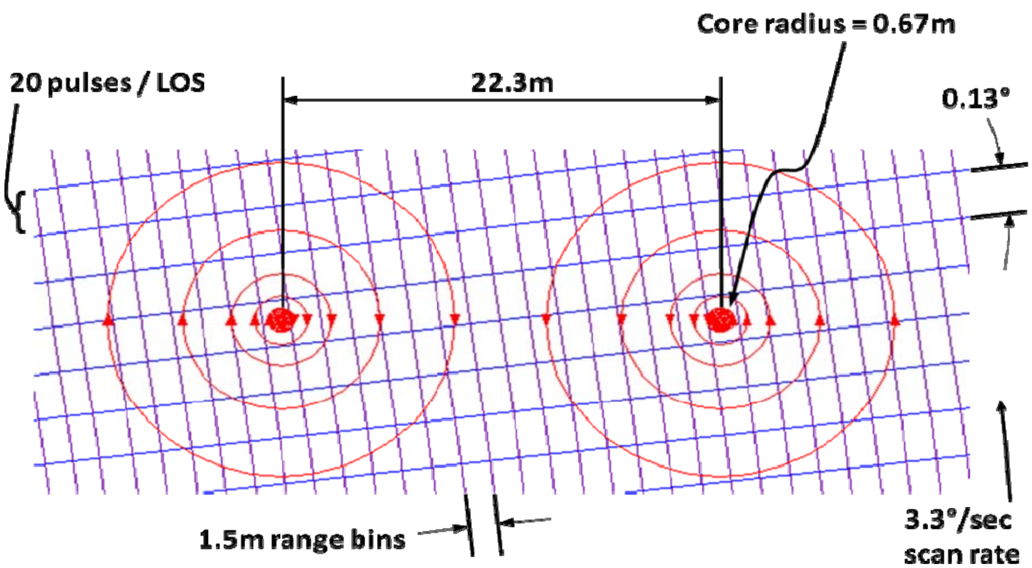

Figure 3. SFO Lidar data sampling for 737 vortices

3.5 Lidar Simulations

Minimal assumptions and approximations were made in order to produce accurate results from the simulated lidar data. The raw lidar data is generated with a standard Monte-Carlo simulation algorithm assuming constant backscatter over the analysis domain [9]. The backscattered laser field from slabs of the atmosphere transverse to the lidar beam axis is represented by a Gaussian random process assuming the central limit theorem is valid, i.e., there are a large number of illuminated aerosols for each slab. The signal level is defined by the coherent Doppler lidar signal to noise ratio (SNR), which is assumed constant over the region around the vortex, which is essentially equivalent to assuming a constant aerosol backscatter coefficient. For the simulations, the radial velocity v (z,θ) is calculated as a function of range z along the lidar beam axis and elevation angle θ at a range spacing Δz for each LOS based on the wake vortex model and the ambient velocity $v_{ambient}$. An example of the radial velocity profile from the Boeing 737 case for 3 different LOS's (above, centered and below the vortex) and the range-gates centered around the vortex at time t=0 is shown in Figure 4. The radial velocity profiles are clearly different for the 3 LOS's. Note that the pulse extent Δr= 48 m is half the range-gate length Δ p= 96 m, and the vortex size is less than the lidar pulse.

To produce rigorous results with minimal assumptions, the lidar signal from each lidar shot was simulated and processed using CTI's spectral estimation algorithm. For the vortex detection analysis, 1000 realizations of the resulting spectra were simulated for 4 complete elevation angle scans of the lidar with a time of 4.65 sec between each scan. Each of the 1000 realizations represents a statistically independent collection of randomly located aerosol particles for the analytic vortex model. In addition, for the case with background turbulence, each realization consisted of a statistically independent turbulent wind field for each elevation angle scan, i.e., we make the assumption that the small scale turbulence has a correlation time less than the 4.65 second interval between scans. This is a good approximation for typical surface layer conditions with a 3 m/s ambient velocity. However, there are few reliable measurements of background turbulence in typical airport conditions, which will be different from previous boundary-layer measurements because of the heated runways and local terrain.

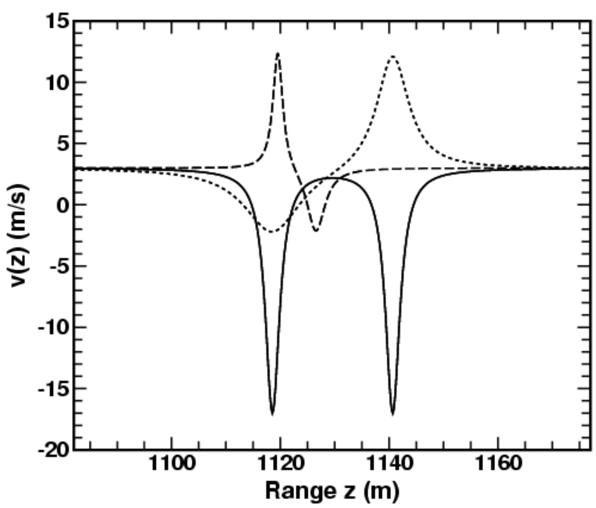

Figure 4. Radial velocity profiles for 3 LOS range-gates surrounding the Boeing 737 vortex: (solid line) range-gate centered on vortex; (dotted line) range-gate 5 m below vortex; (dashed line) and 5 m above the vortex

An example of the accumulated spectra from simulated lidar data with N=20 shots for a single elevation scan is shown in Figure 5 as a function of the elevation angle or equivalently the LOS index for a range-gate centered on the vortex and an SNR=10. The spectra are normalized by the average spectrum with no signal present (average noise spectrum). Zero velocity is located at bin 16 with positive radial velocity (away from the lidar) for bins less than 16 and negative radial velocity (towards the lidar) for the bins above 16. This is the sign convention used in the CTI WindTracer lidar. The large spectral power at bin 13 indicates the contribution from laser scattering from aerosols with the background ambient velocity. The radial velocity profiles of Figure 4 are reflected in the spectra at the upper section of the image around LOS index 52, where the variations in the radial velocity produce distinctive features in the accumulated Doppler lidar spectra. The enhanced signal power to the right of the background signal at LOS 52 reflects the large negative velocity for the lidar beam centered on the vortex, i.e., the solid line of Figure 4. The smaller two features to the left of the background spectra at LOS number 50 and 55 indicate the smaller positive vortex radial velocity from the lidar beam below and above the vortex, i.e., the dotted and dashed curves of Figure 4.

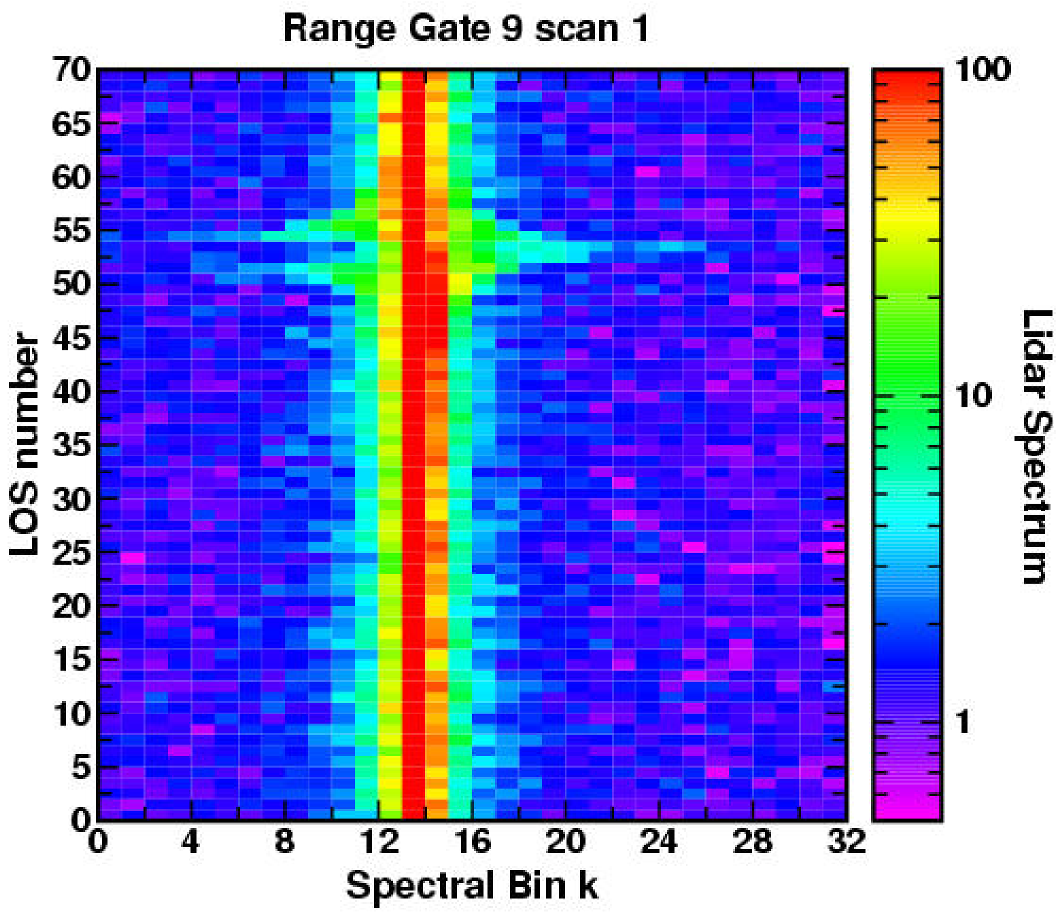

Figure 5. Accumulated or average spectra vs. LOS number (elevation angle) for a range-gate centered on the vortex

3.6 Lidar Simulation Convergence Test

The accuracy and numerical effort of the simulations depend on the grid size Δz. The most obvious signature of the vortex is contained in the small spectral features away from the ambient mean velocity. As $\Delta z \to 0$, the statistics of the spectral estimates must approach the correct limiting value. The criterion for selecting an acceptable Δz is based on the difference between the average and standard deviation of the lidar signal spectral estimates S(k,Δz) and the correct value in the limit of Δz→0. This test should be performed for the spectral bins k that are most sensitive to the vortex feature. A convergence test using 10,000 simulated spectra was performed for spectral bin k=23 and LOS number 53 of Figure 5, which is clearly produced by the vortex. The results are shown in Figure 6. As the grid size Δz→0, the two test statistics approach a constant to within the statistical accuracy of the estimates. For this case, a grid size Δz=0.1875 m will accurately represent the Doppler lidar signal. Similar results are produced for the Boeing 747 vortex and therefore the grid size Δz=0.1875 m was used for all the simulations.

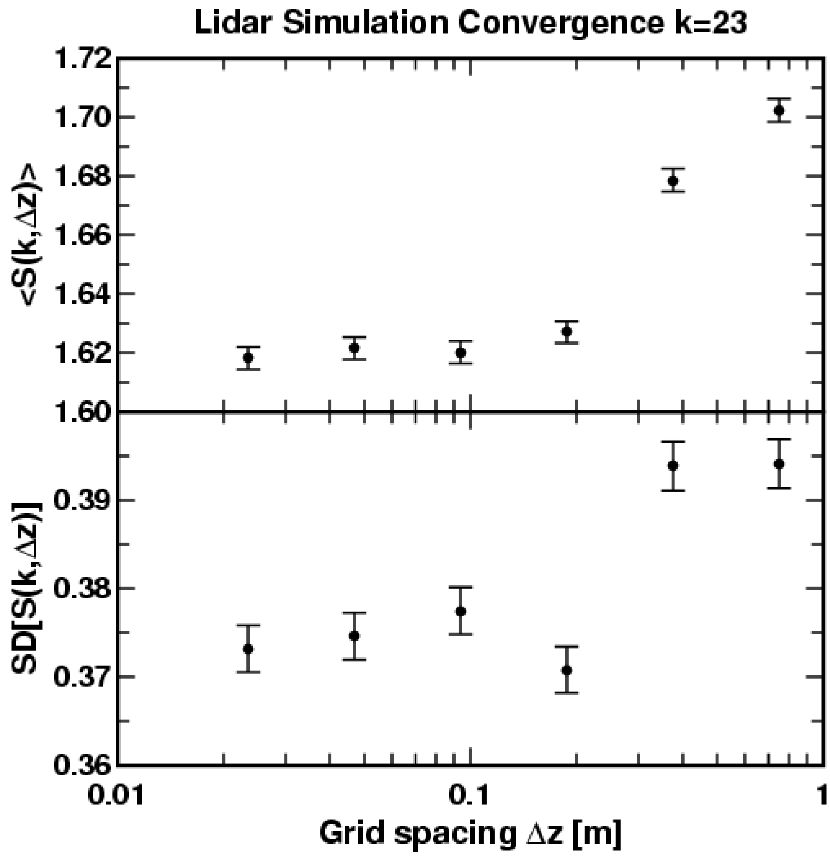

Figure 6. Convergence test for the optimal simulation range grid size Δz, based on the average spectrum <S(k, Δz)> and the standard deviation SD[S(k, Δz)] vs the grid size Δz, with 1-σ error bars indicated

3.7 Maximum Likelihood Estimation Algorithm

A complete analysis of the performance of the CTI vortex detection and tracking algorithm requires a comparison with other algorithms or the theoretical best performance given by the Cramer Rao Bound (CRB) [17]. Unfortunately, the calculation of the CRB for the vortex problem is not feasible. In addition, there are no quantitative performance metrics published for any comparable algorithm. Because the performance of the exact ML estimator approaches the CRB in the limit of large samples, an approximate ML estimator was used as a reference for ideal performance, which was also a logical choice since the CTI algorithm is an approximate ML estimator.

The reference algorithm chosen for the performance of CTI's algorithm is an approximation of the exact maximum likelihood estimator assuming the spectral estimates S(k) are statistically independent χ^2 random variables with mean $S_m(k,\Theta) = <S(k,\Theta)>$ and 2N degrees of freedom where <> denotes ensemble average over the random location of the aerosol particles and Θ denotes the unknown vortex parameters. The maximum likelihood estimator, $\hat{Q}$, of the parameters, Θ, are those values that maximize the log likelihood function which can be written as [18]

$$L(\Theta) = C - N \sum_{k=1}^{M_T} [S(k)/S_m(k, \Theta) + \ln S_m(k, \Theta)], \tag{4}$$

where C is a constant, k denotes spectral index, and M_T is the total number of spectral estimates from the range-gates in the region around the vortex. The ML estimator requires knowledge of the functional form of the average spectral bins S_m (k,Θ) and therefore the unknown parameters Θ depend on the assumptions used for the vortex model, i.e., the functional form and the unknown parameters. The most efficient ML estimator uses the minimum number of unknown parameters.

We investigated two ML estimators. The first ML algorithm (ML 3 par) was chosen to optimize vortex detection for the early stages of the vortex evolution. Therefore, both vortex pairs are assumed to have the same altitude H, vortex radius r_C, and circulation strength Γ. We also assumed the vortex pair separation, b_0, and core radius, r_C, are given by the aircraft type. For most cases of interest, the lidar SNR and background ambient velocity could be accurately estimated from the spectral data (see Figure 5) and were assumed to be known. Therefore, the unknown parameters for the ML estimator were the vortex altitude H, the distance y to the center of the vortex pair, and the vortex circulation strength Γ.

The second ML estimator (ML 6 par) was similar to the CTI algorithm, i.e., it estimated the vortex location and strength for each of the vortex pairs assuming the SNR is known. Since no approximations are made, this ML estimator is numerically intensive but provided a lower bound for performance. The ML estimates were produced by calculating the log likelihood function L(Θ) for a fixed grid of the unknown variables Θ around the true value using a pre-computed table of the values S_m (k,Θ) [12]. The ML estimates were those values that maximized L(Θ) based on a parabolic interpolation around the grid value with the maximum of L(Θ). The CTI algorithm does not produce an estimate for a given vortex if the signal is not sufficiently high to pass a threshold test on the likelihood function L(Θ). The fraction PD of estimates produced was therefore defined as the detection probability and was a useful metric of performance in the low SNR regime.

3.8 Results for Detection of Boeing 737 Vortex

The statistical properties of an estimate x are completely defined by the probability density function (PDF). Other important statistics are the bias, defined by

$$\mathrm{BIAS}_x = < x > - \mu \tag{5}$$

where <> denotes ensemble average and μ is the correct ensemble average of the random variable x, and the random error described by the variance

$$\mathrm{VAR}[x] = < [x - < x >]^2 > \tag{6}$$

or the standard deviation $SD[x]=VAR[x]^{1/2}$. The correct values of the estimates of the vortex parameters are difficult to define exactly because the vortex is changing during the measurement.

Therefore, for the CTI estimates and the full ML estimator the correct vortex parameters are defined as the value of the analytic model when the lidar beam passes through the center of the given vortex. For the ML estimates that assume the vortex pairs have the same parameters with a known separation, truth is defined as the values of the analytic model when the lidar beam passes through the center of the vortex pair.

The PDF of the CTI estimates of the closest vortex, vortex 1, the farthest vortex, vortex 2, and three different ML estimates of the vortex parameters for the first lidar scan of the Boeing 737 case are shown in Figure 7 to Figure 11, respectively, for a high SNR case and no background turbulence (ε=0). The biases of the ML estimates are small and the random errors are very low. The bias of the CTI estimates is small except for the vortex strength Γ, which is larger than for the ML estimators. This is probably due to the approximations used to increase the numerical efficiency of the CTI algorithm. The random error for vortex location is very small, especially compared with the dimensions of the vortex, and the CTI estimator has slightly larger error than the ML estimators.

To investigate the source of the bias, the lidar data was simulated with the same lidar and processing parameters but for a time independent vortex, i.e., a frozen vortex embedded in the ambient flow. This is the best case scenario because the ML estimator assumes a vortex model that is frozen in space and time. The corresponding results are shown in Figure 12 to Figure 16. The 3 parameter ML estimator, Figure 14, has the smallest bias and the 0.05 m bias in the height is produced by the 2 m spacing in the height variable of the log likelihood table. The larger bias in the 6 parameter ML estimator, Figure 15 to Figure 16, is also produced by the finite grid size of the log-likelihood table and by the interaction of the different variables, however, the biases are still acceptably small. There are many issues for optimizing a ML estimator such as the chosen grid of unknown parameters Θ of the log-likelihood table, the calculation of the mean spectra for the various vortex models, and the interpolation used to determine the maximum of the log likelihood function. The biases in the CTI estimates are larger than the ML estimators for the vortex locations but still acceptable; however, the bias in the vortex strength is noticeably larger. This is to be expected since the vortex strength is the most difficult parameter to estimate and would be the most sensitive to approximations that are required to speed up the ML algorithm. Note that the standard deviation of the CTI strength estimates are smaller than the ML estimates. This result is most likely related to the smaller average value of the CTI estimates.

The effects of the additive turbulence for the high SNR case are shown in Figure 17 to Figure 21. The standard deviation of all the estimates has increased. However, there is little effect on the bias of the estimates. Most of the PDF's are approximately Gaussian.

The performance of the CTI algorithm is conveniently summarized by plotting the detection probability, PD, the bias, and the standard deviation of the estimates of the vortex parameters and the estimates of SNR as a function of the true SNR. The bias and standard deviation of the ML estimators provides a reference for the best possible performance. The ML with only 3 parameters estimated (ML 3 par) is ideally suited for the first detection of the vortex. The ML estimator with 6 parameters estimated (ML 6 par) is required for tracking the vortex and like the CTI algorithm, produces independent estimates of the parameters of each vortex. However, this estimator assumes the aircraft type has been determined from the first detected scan and the vortex radius, r_C, is known.

The results for the Boeing 737 vortex simulations are shown in Figure 22 to Figure 29. The CTI estimator of the vortex parameters has a small bias except for the estimates of vortex strength Γ in lower SNR. There is a consistent bias in the CTI estimates of the SNR, i.e., -20% bias at low SNR to –40% bias at high SNR. As expected, for the ML estimates, the estimation of more independent parameters increase the standard deviation or estimation error of the estimates and the added turbulence produces an additional increase in the estimation error. However, there is only a small impact on the bias of the estimates reflecting the robust nature of the ML estimator. The ML 3 parameter estimator has excellent performance even for an SNR=0.2. However, the ML 6 parameter estimator has random outliers for SNR<1.0.

Table 3 summarizes the simulations that were performed in order to evaluate the performance of the detection algorithms for the Boeing 737. The results are shown in Figure 7 through Figure 29.

Table 3. Performance Simulations of Detection Algorithms - 737

ε	Estimator	Vortex	Figure No.
PDFs – SNR, H, Y, Γ. SNR = 10			
0	CTI	1	7
0	CTI	2	8
0	ML 3	Both	9
0	ML 6	1	10
0	ML 6	2	11
With frozen vortices			
0	CTI	1	12
0	CTI	2	13
0	ML 3	Both	14
0	ML 6	1	15
0	ML 6	2	16
With turbulence			
0.001	CTI	1	17
0.001	CTI	2	18
0.001	ML 3	Both	19
0.001	ML 6	1	20
0.001	ML 6	2	21
Bias vs. SNR – SNR, H, Y, Γ			
0	All	1	22
0	All	2	23
0.001	All	1	24
0.001	All	2	25
PD, SD(H), SD(Y), SD(Γ)			
0	All	1	26
0	All	2	27
0.001	All	1	28
0.001	All	2	29

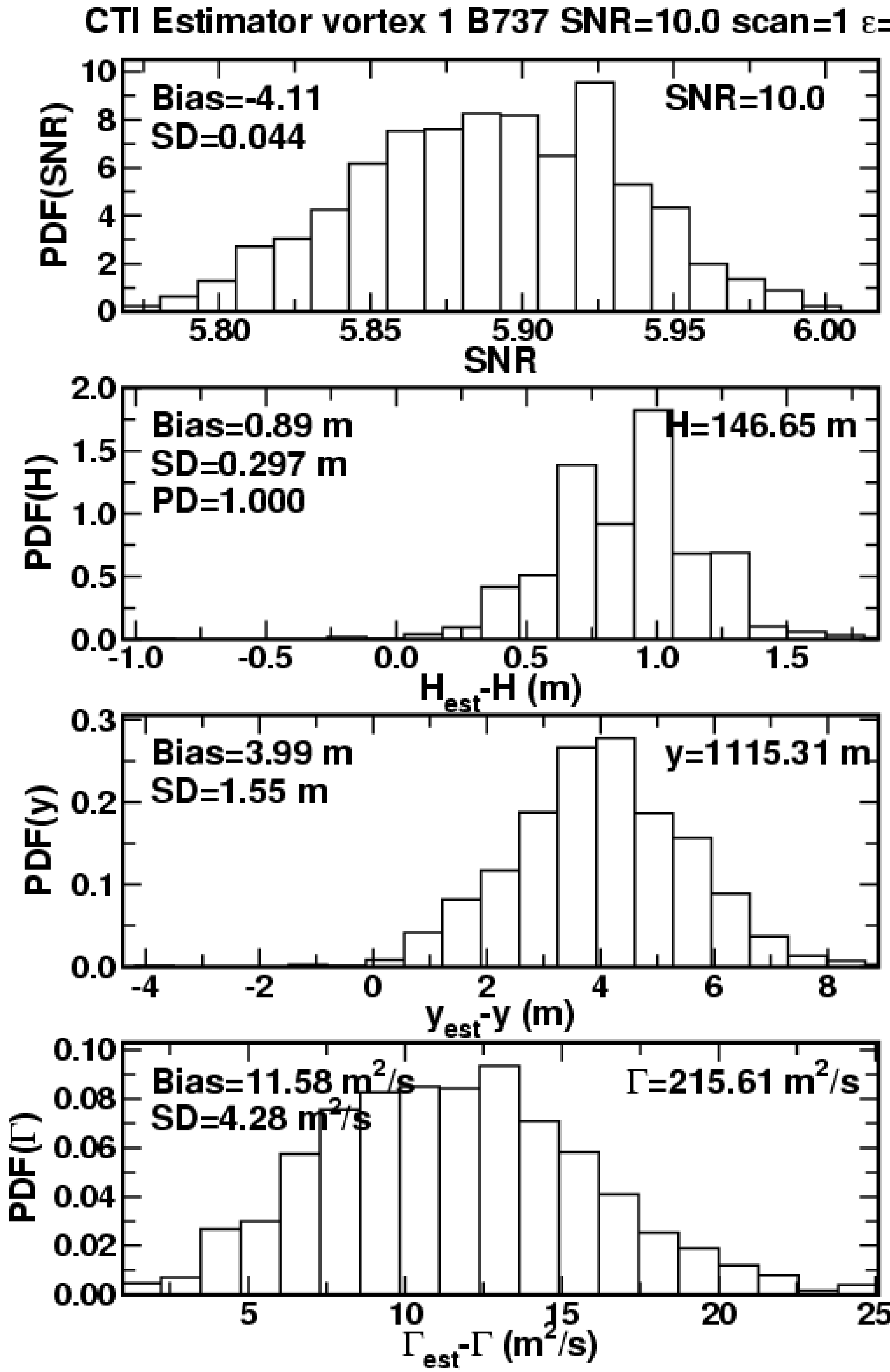

Figure 7. PDF of CTI estimates of the parameters of vortex 1. The bias and standard deviation (SD) are shown on the left and the correct values are shown on the right. The detection probability PD is also shown.

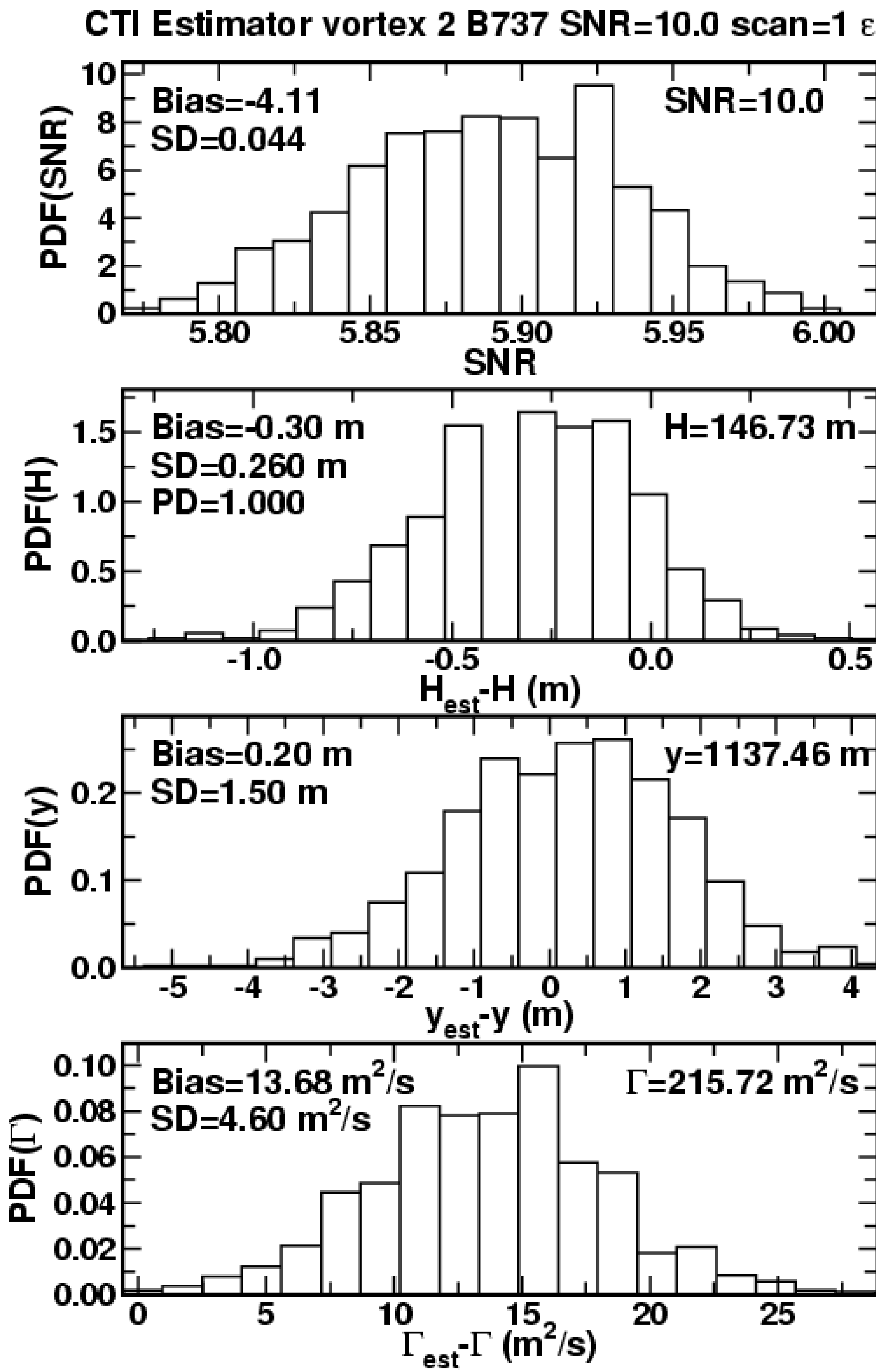

Figure 8. PDF of CTI estimates of the parameters of vortex 2. The bias and standard deviation (SD) are shown on the left and the correct values are shown on the right. The detection probability PD is also shown.

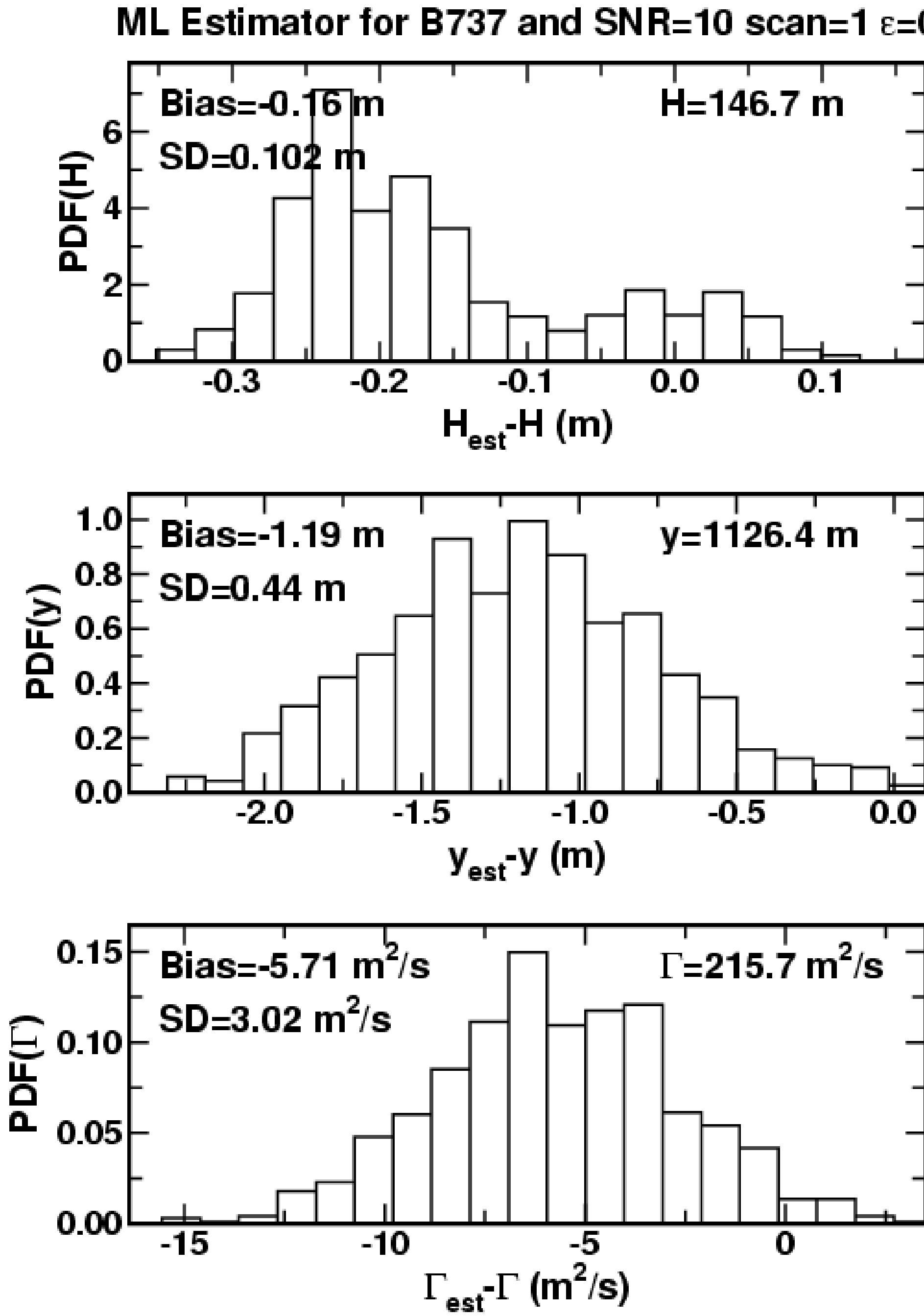

Figure 9. PDF of ML estimates of the vortex parameters assuming each vortex has the same parameters and the spacing between the vortices is known. The bias and standard deviation (SD) are shown on the left and the correct values are shown on the right.

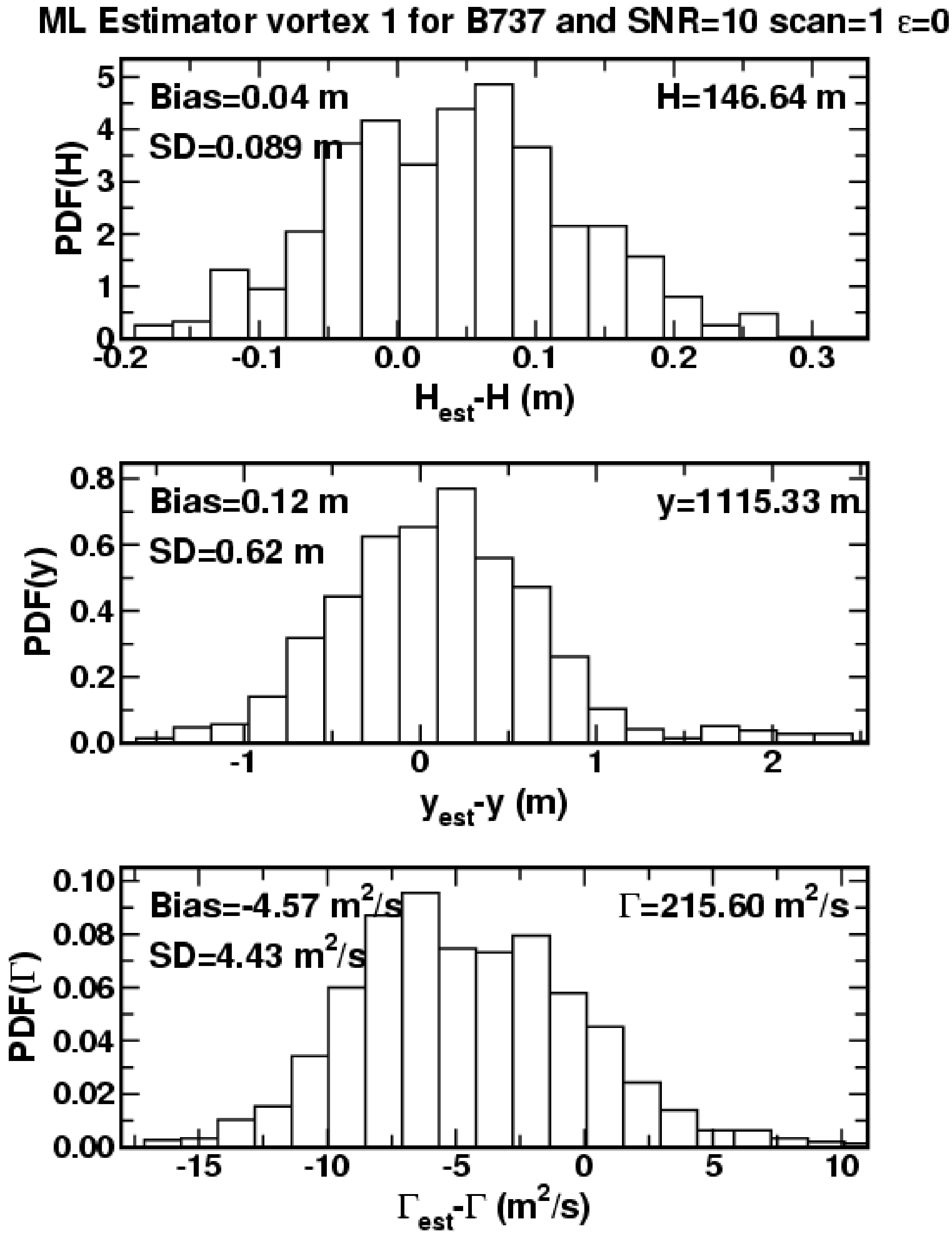

Figure 10. PDF of ML estimates of the parameters of vortex 1. The bias and standard deviation (SD) are shown on the left and the correct values are shown on the right.

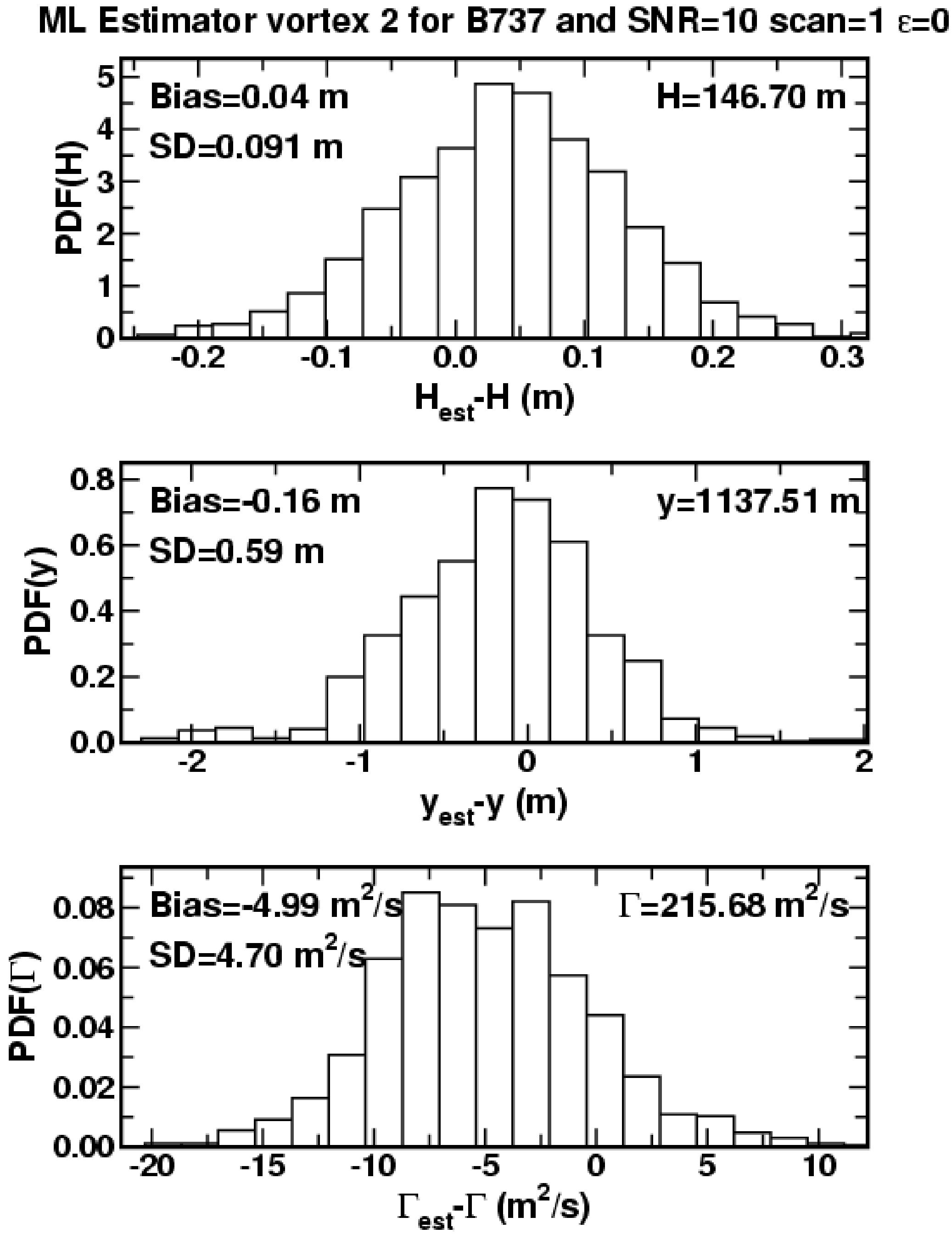

Figure 11. PDF of ML estimates of the parameters of vortex 2. The bias and standard deviation (SD) are shown on the left and the correct values are shown on the right.

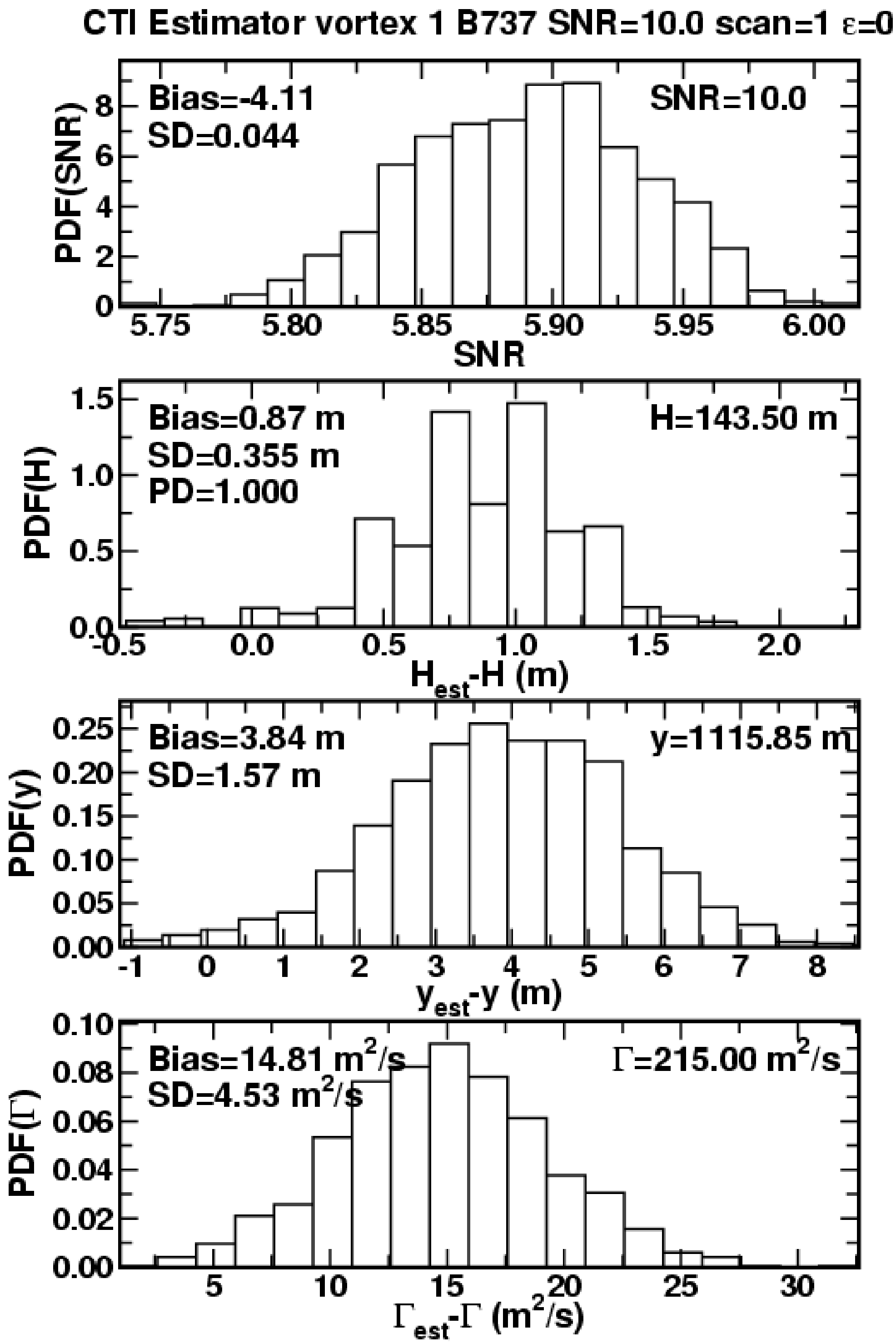

Figure 12. PDF of CTI estimates of the parameters of a frozen vortex 1. The bias and standard deviation (SD) are shown on the left and the correct values are shown on the right. The detection probability PD is also shown.

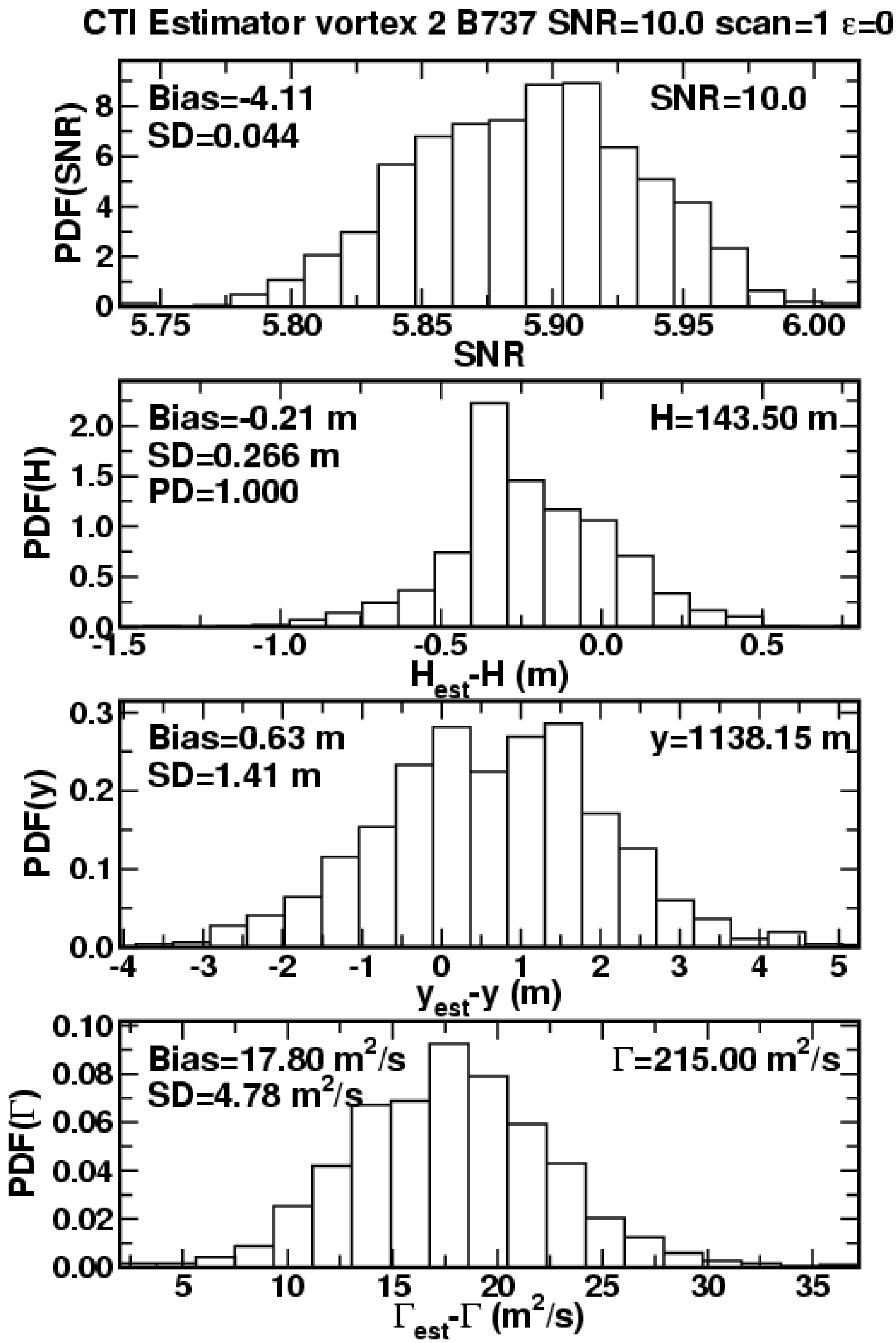

Figure 13. PDF of CTI estimates of the parameters of a frozen vortex 2. The bias and standard deviation (SD) are shown on the left and the correct values are shown on the right. The detection probability PD is also shown.

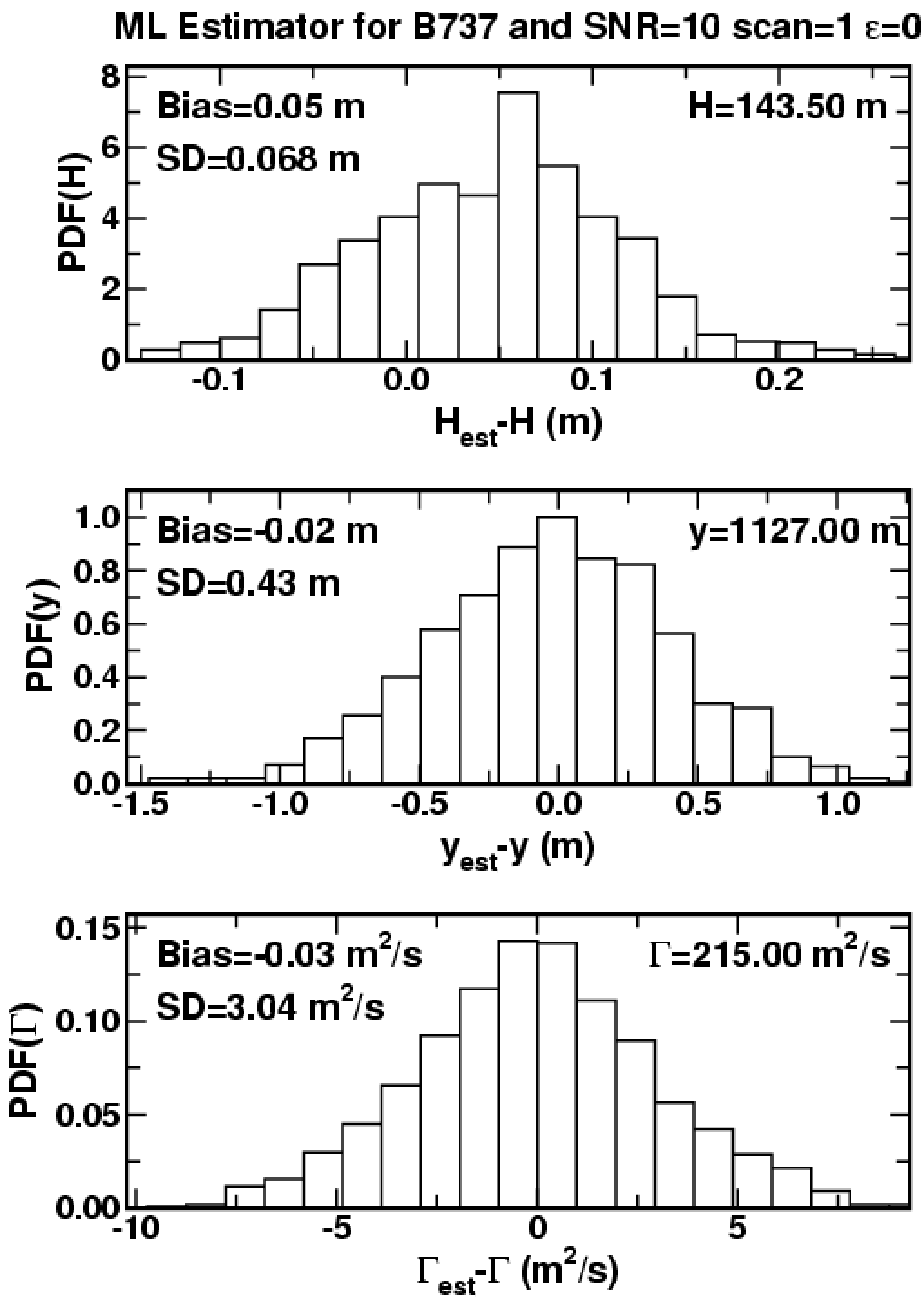

Figure 14. PDF of ML estimates of a frozen vortex parameters assuming each vortex has the same parameters and the spacing between the vortices is known. The bias and standard deviation (SD) are shown on the left and the correct values are shown on the right.

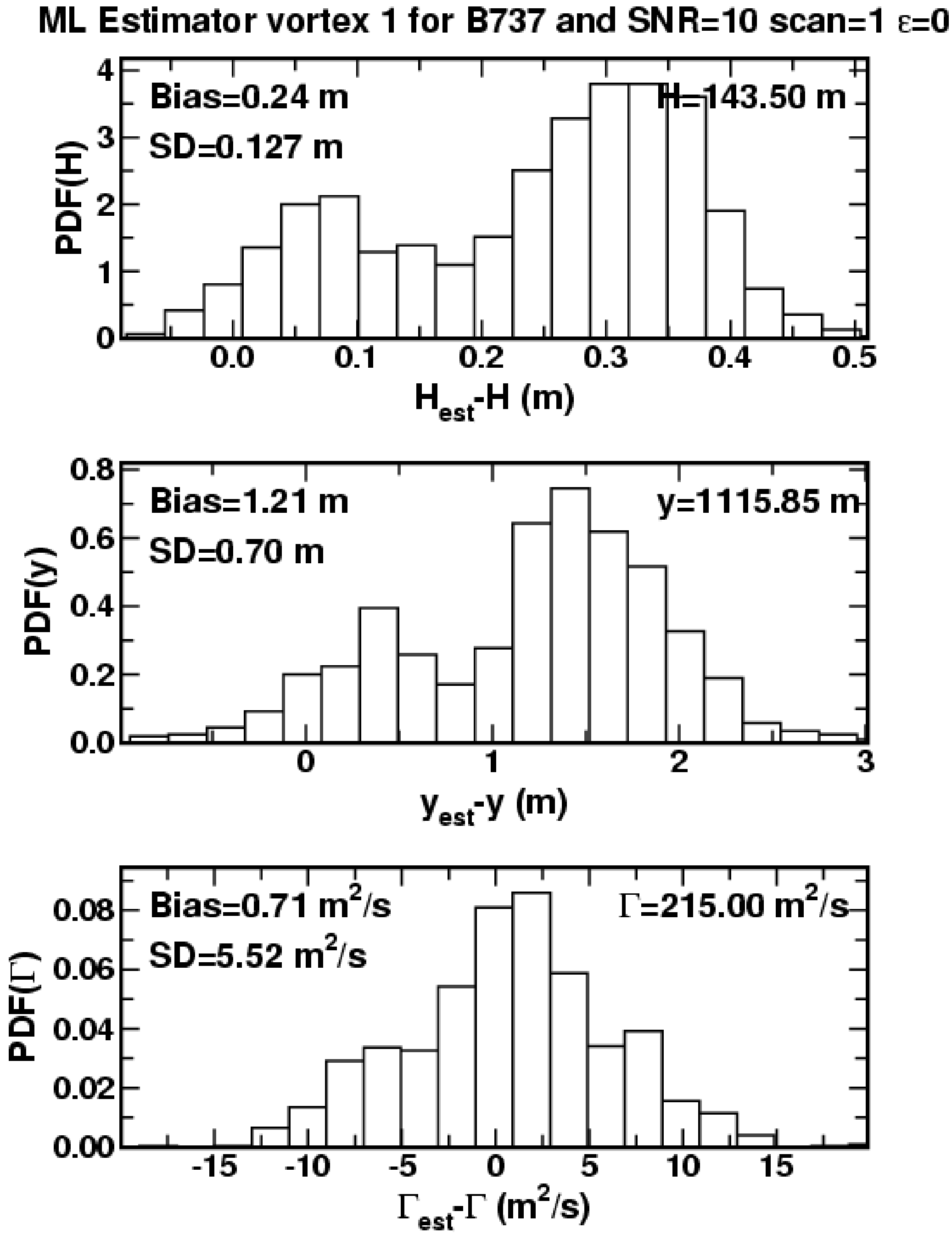

Figure 15. PDF of ML estimates of the parameters of frozen vortex 1. The bias and standard deviation (SD) are shown on the left and the correct values are shown on the right.

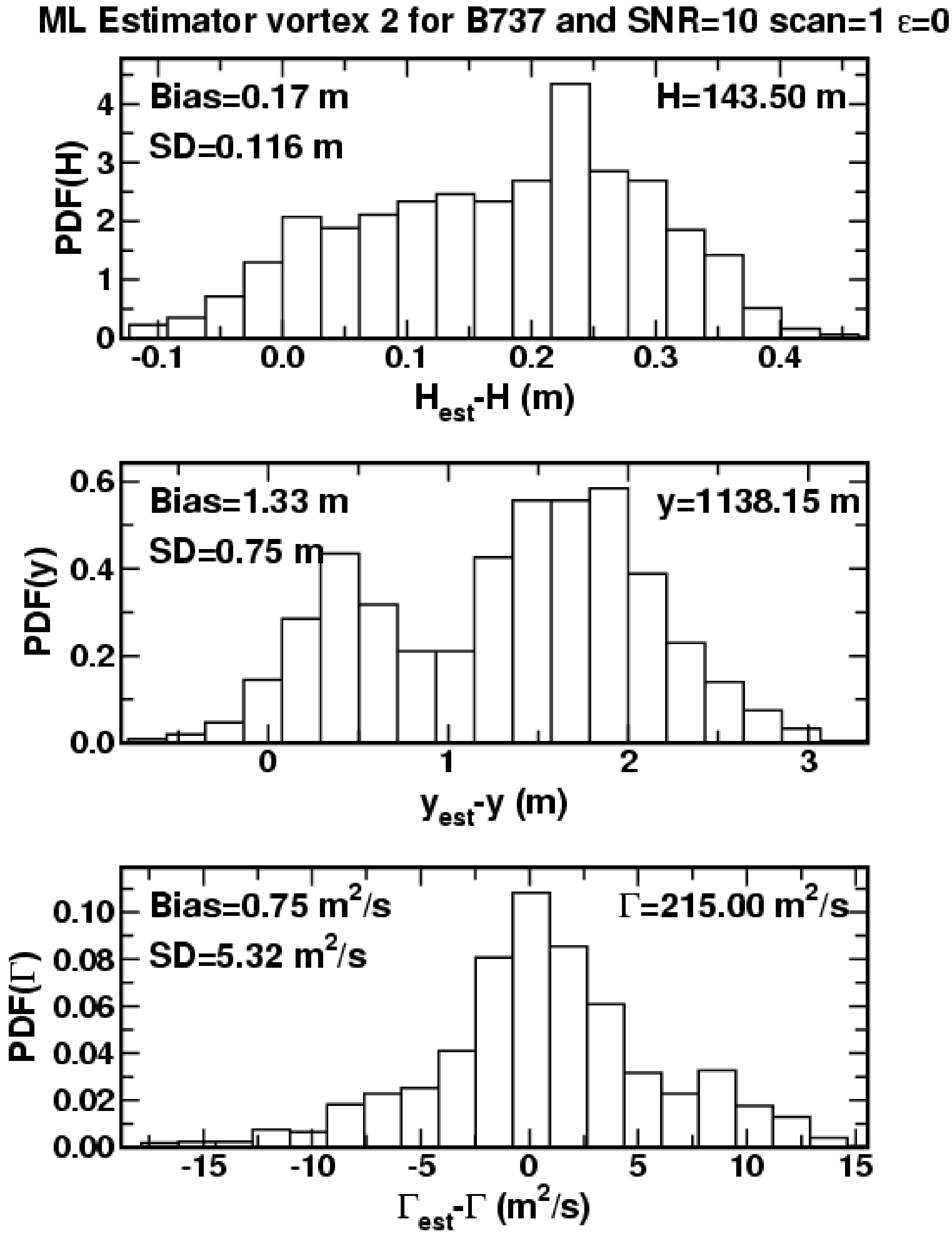

Figure 16. PDF of ML estimates of the parameters of frozen vortex 2. The bias and standard deviation (SD) are shown on the left and the correct values are shown on the right.

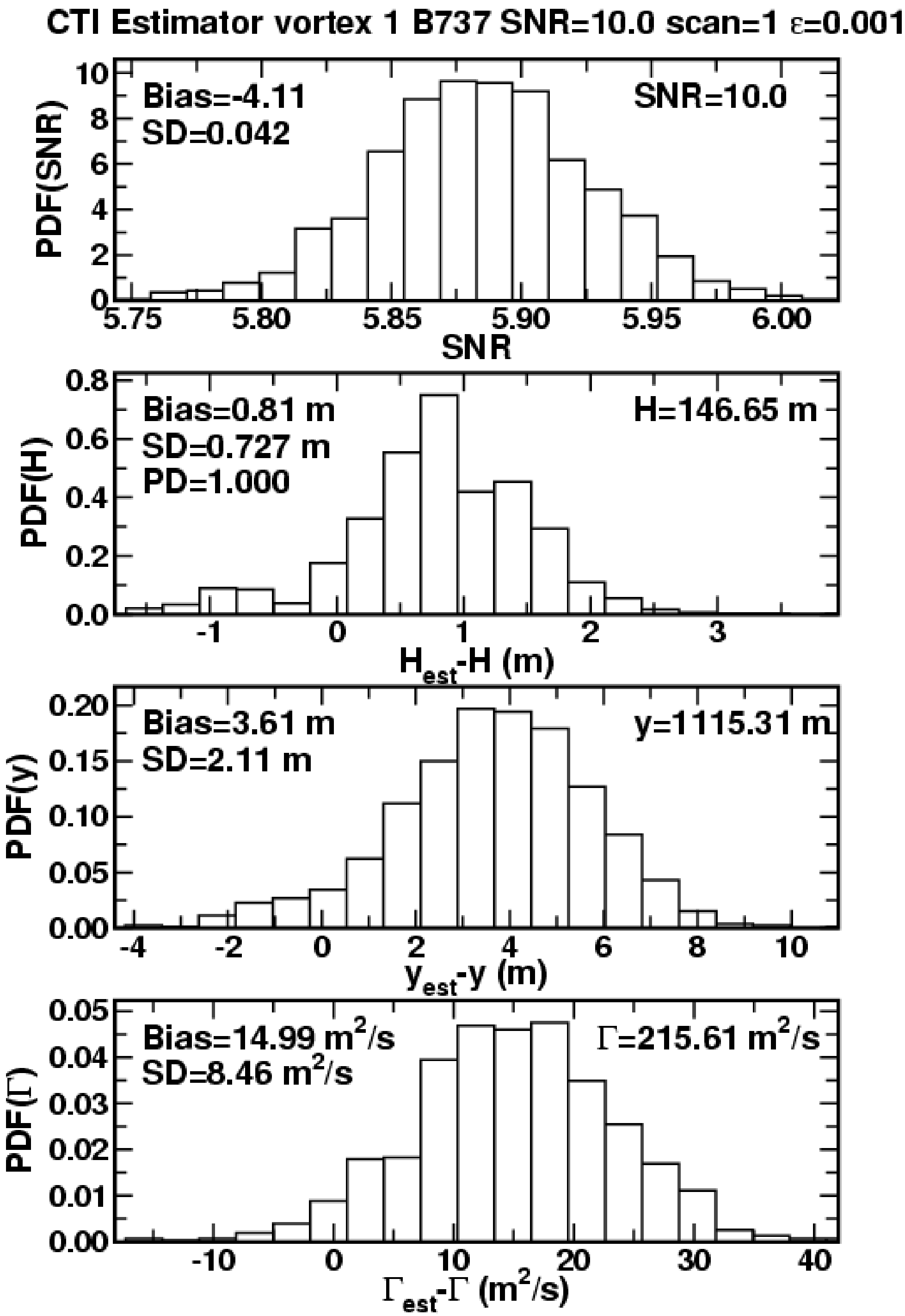

Figure 17. PDF of CTI estimates of the parameters of vortex 1 with added turbulence. The bias and standard deviation (SD) are shown on the left and the correct values are shown on the right. The detection probability PD is also shown.

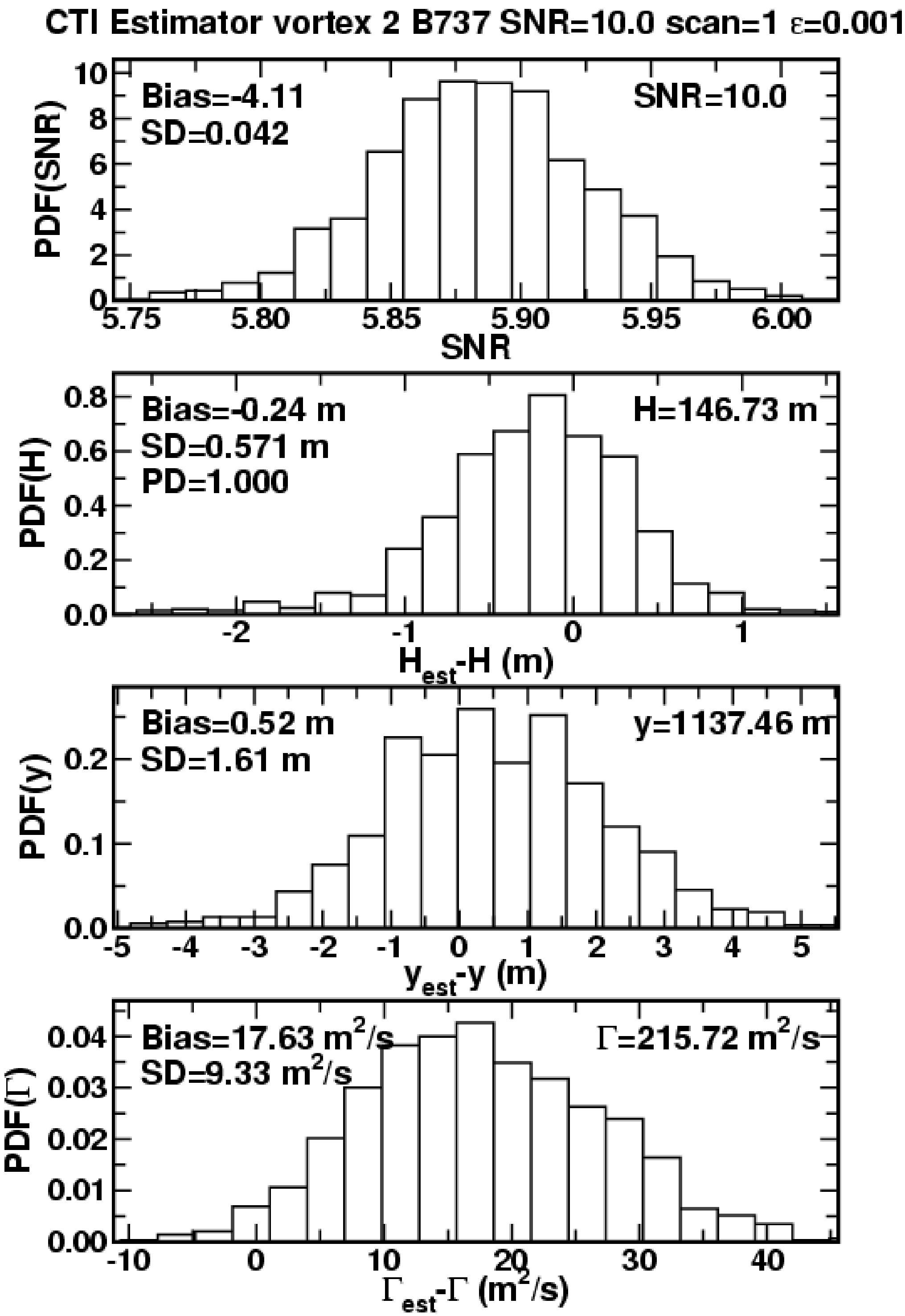

Figure 18. PDF of CTI estimates of the parameters of vortex 2 with added turbulence. The bias and standard deviation (SD) are shown on the left and the correct values are shown on the right. The detection probability PD is also shown.

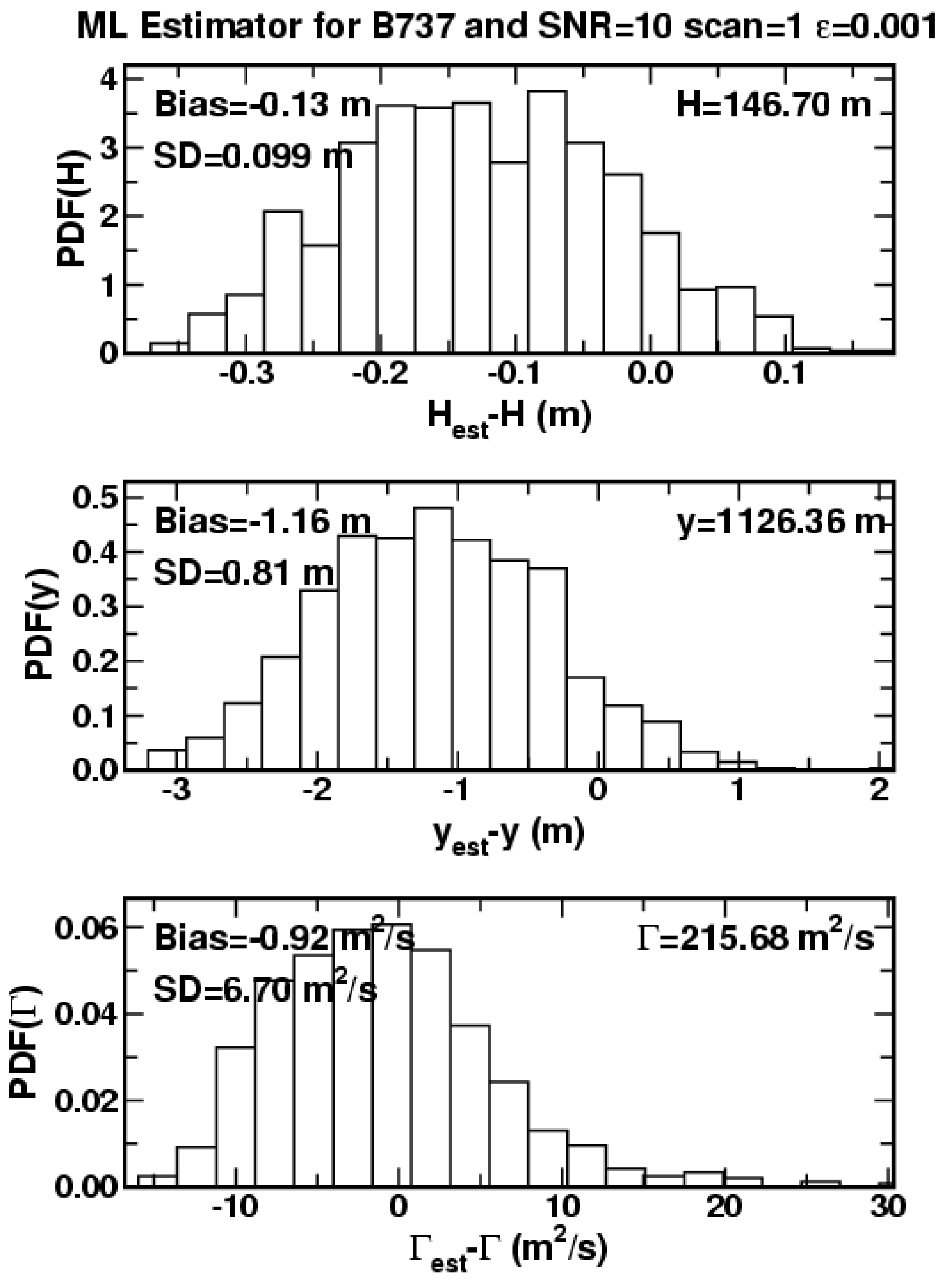

Figure 19. PDF of ML estimates of the vortex parameters with added turbulence assuming each vortex has the same parameters and the spacing between the vortices is known. The bias and standard deviation (SD) are shown on the left and the correct values are shown on the right.

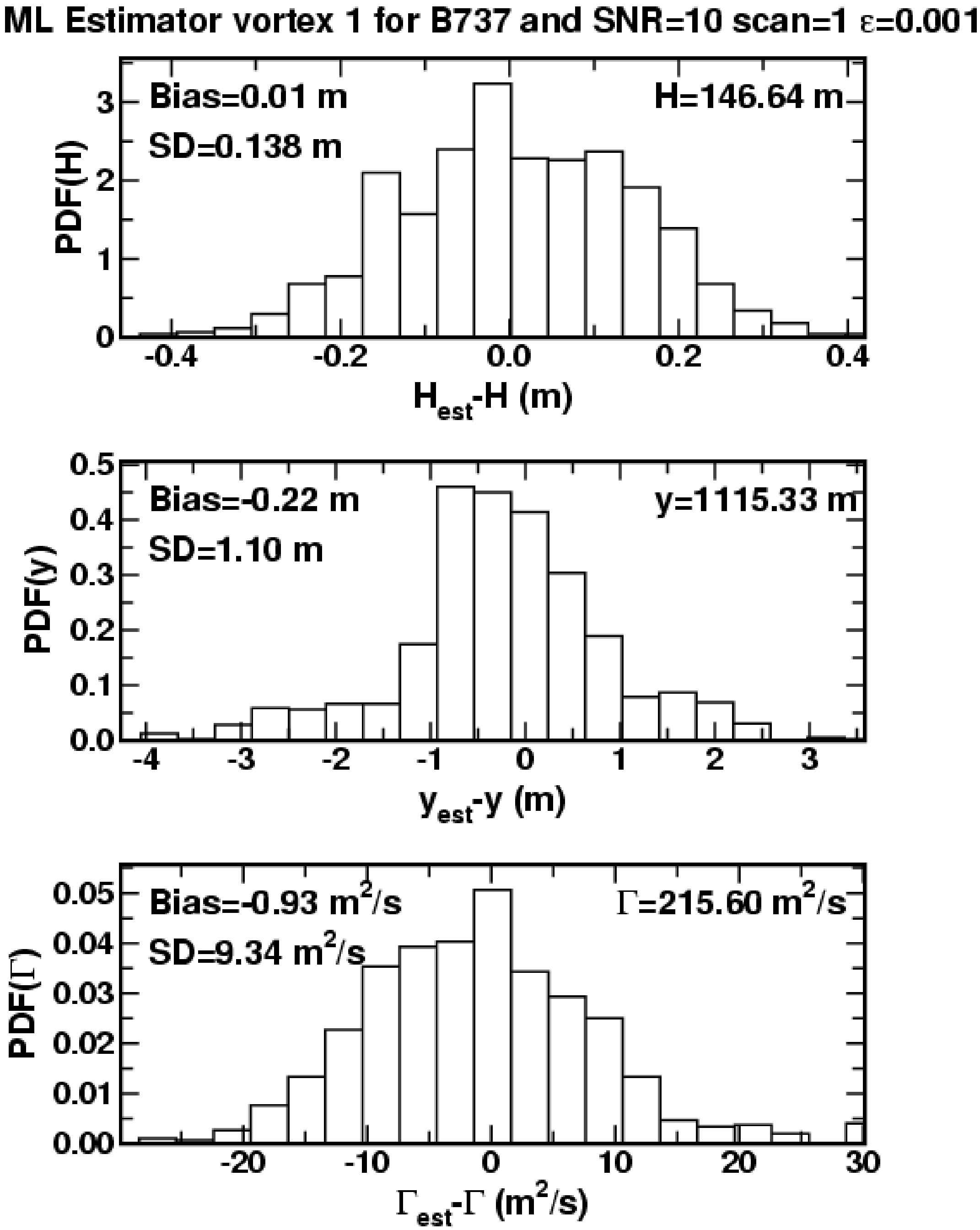

Figure 20. PDF of ML estimates of the parameters of vortex 1 with added turbulence. The bias and standard deviation (SD) are shown on the left and the correct values are shown on the right.

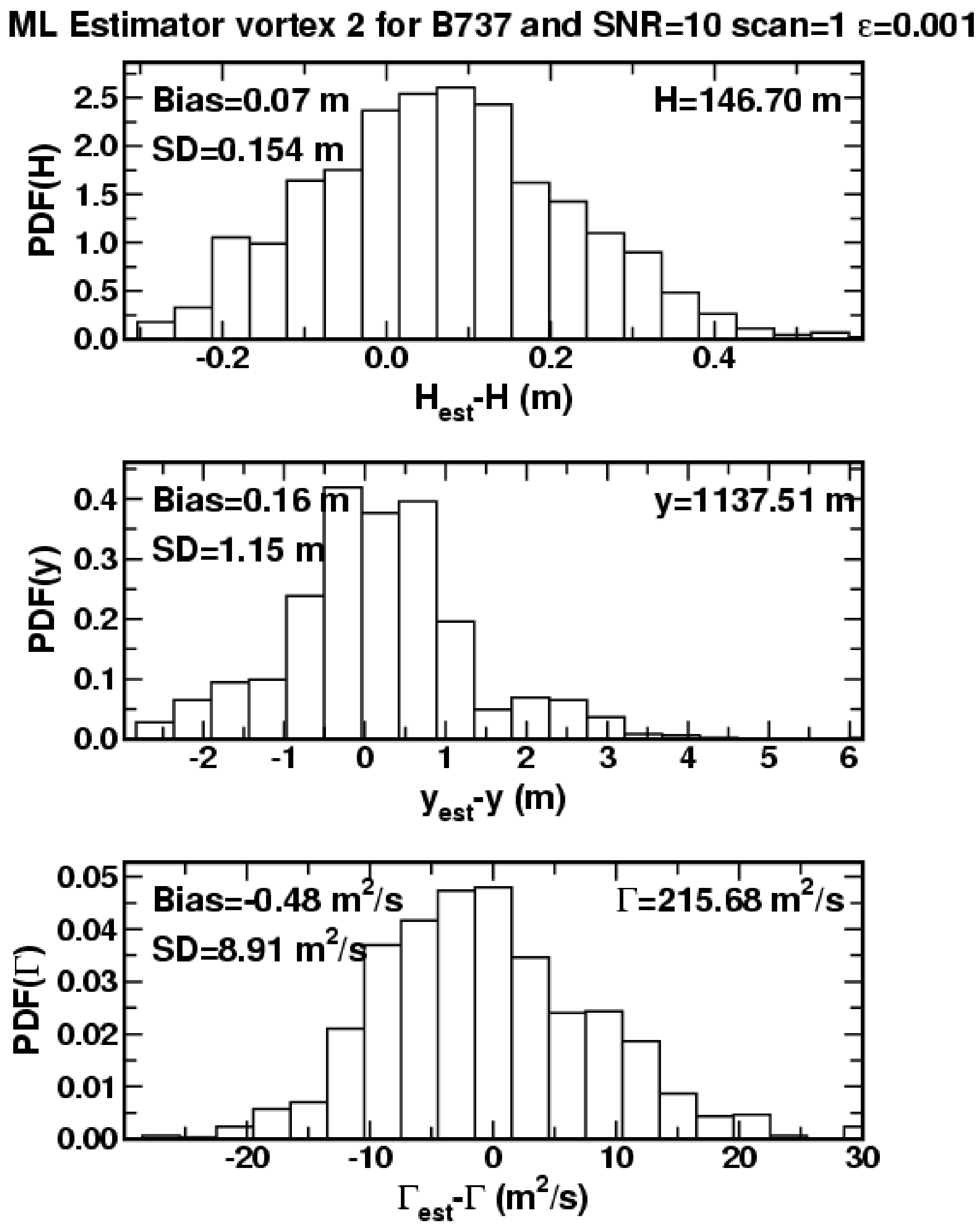

Figure 21. PDF of ML estimates of the parameters of vortex 2 with added turbulence. The bias and standard deviation (SD) are shown on the left and the correct values are shown on the right.

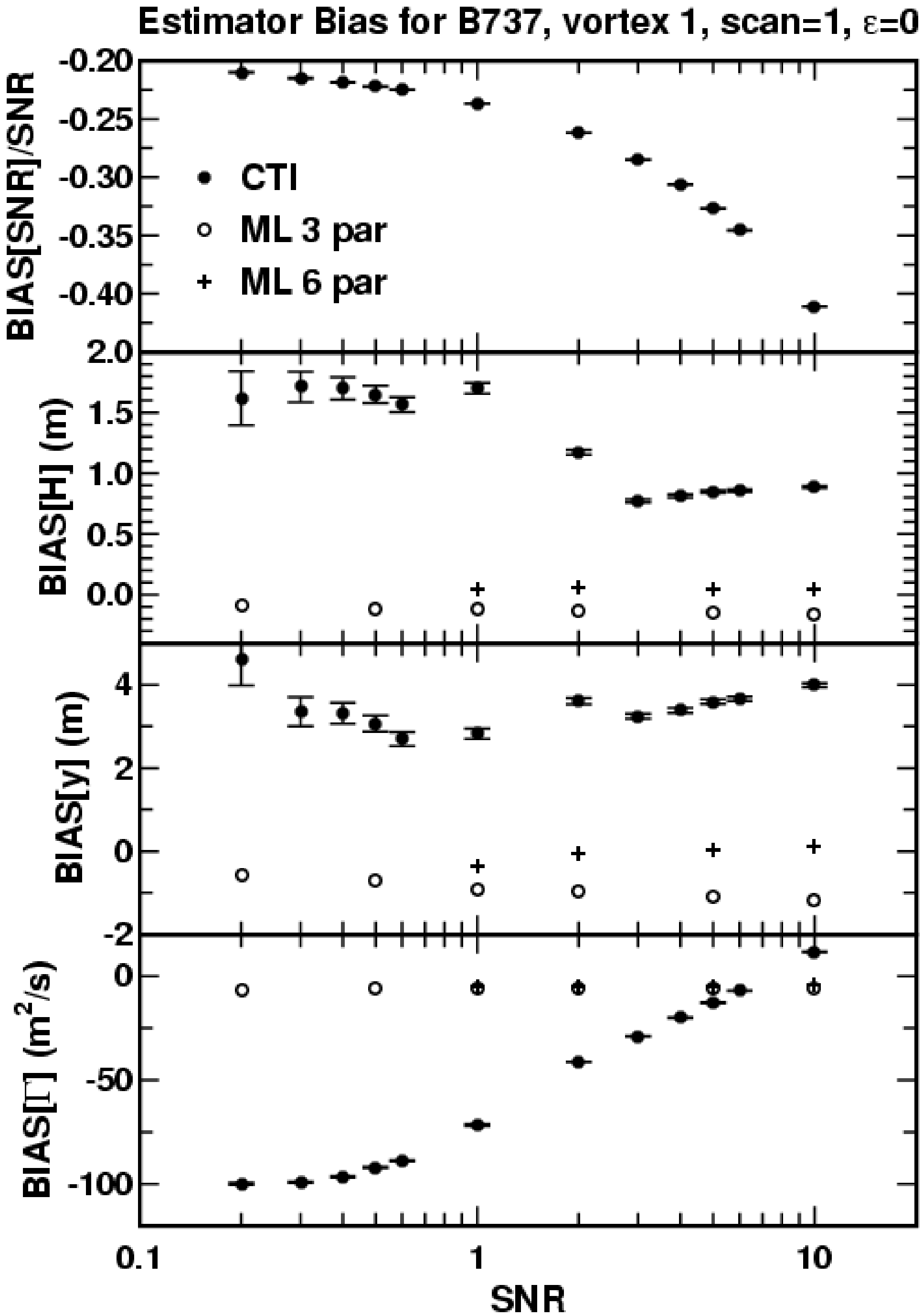

Figure 22. The bias of estimates of vortex parameters as a function of SNR for vortex 1 of the Boeing 737 and no turbulence. The correct values are H=146.65 m, y=1115.31 m, and Γ=215.61 m^2/s.

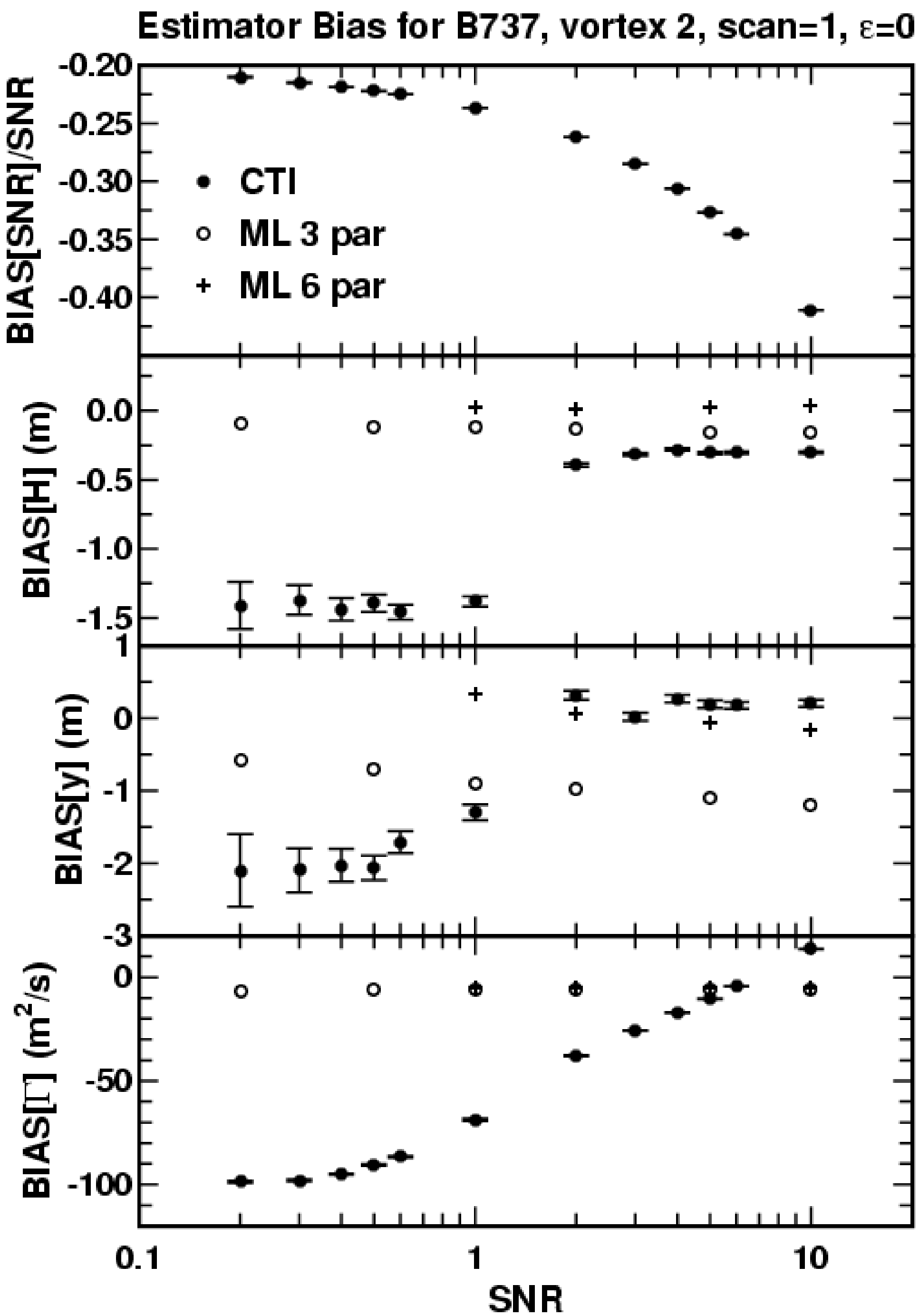

Figure 23. The bias of estimates of vortex parameters as a function of SNR for vortex 2 of the Boeing 737 and no turbulence. The correct values are H=146.73 m, y=1137.46 m, and Γ=215.72 m^2/s.

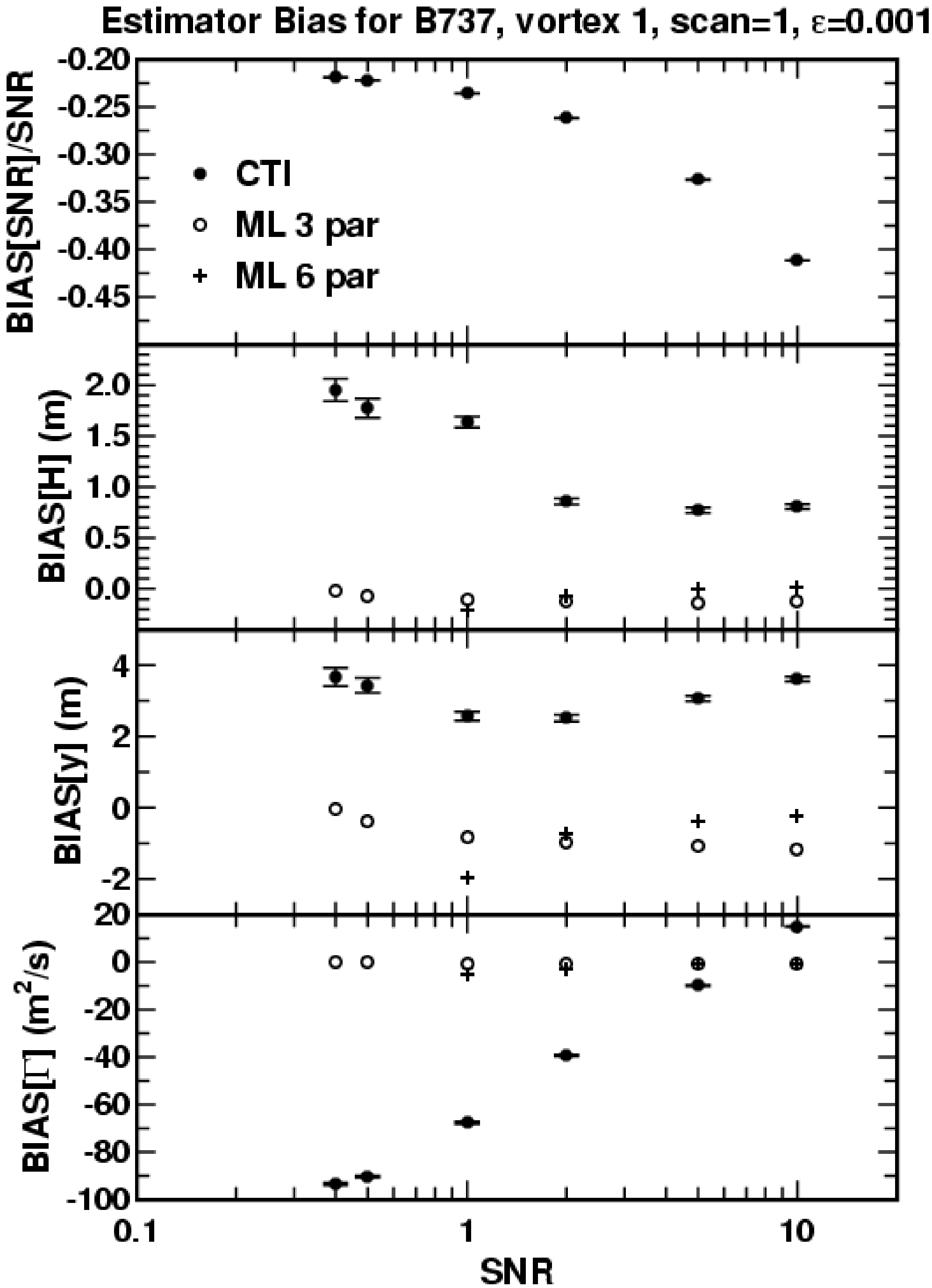

Figure 24. The bias of estimates of vortex parameters as a function of SNR for vortex 1 of the Boeing 737 with added turbulence. The correct values are H=146.65 m, y=1115.31 m, and Γ=215.61 m^2/s.

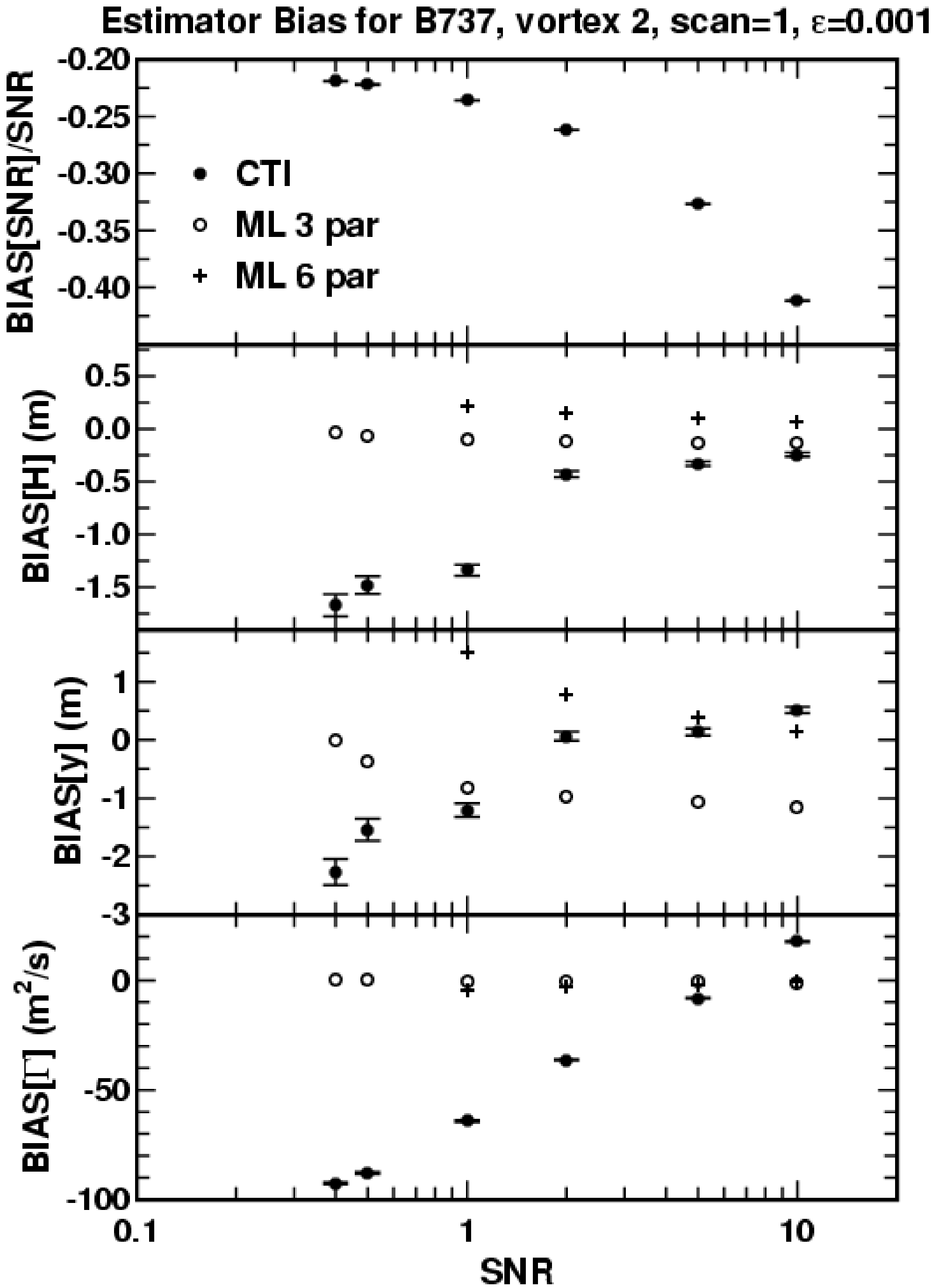

Figure 25. The bias of estimates of vortex parameters as a function of SNR for vortex 2 of the Boeing 737 with added turbulence. The correct values are H=146.73 m, y=1137.46 m, and Γ=215.72 m^2/s.

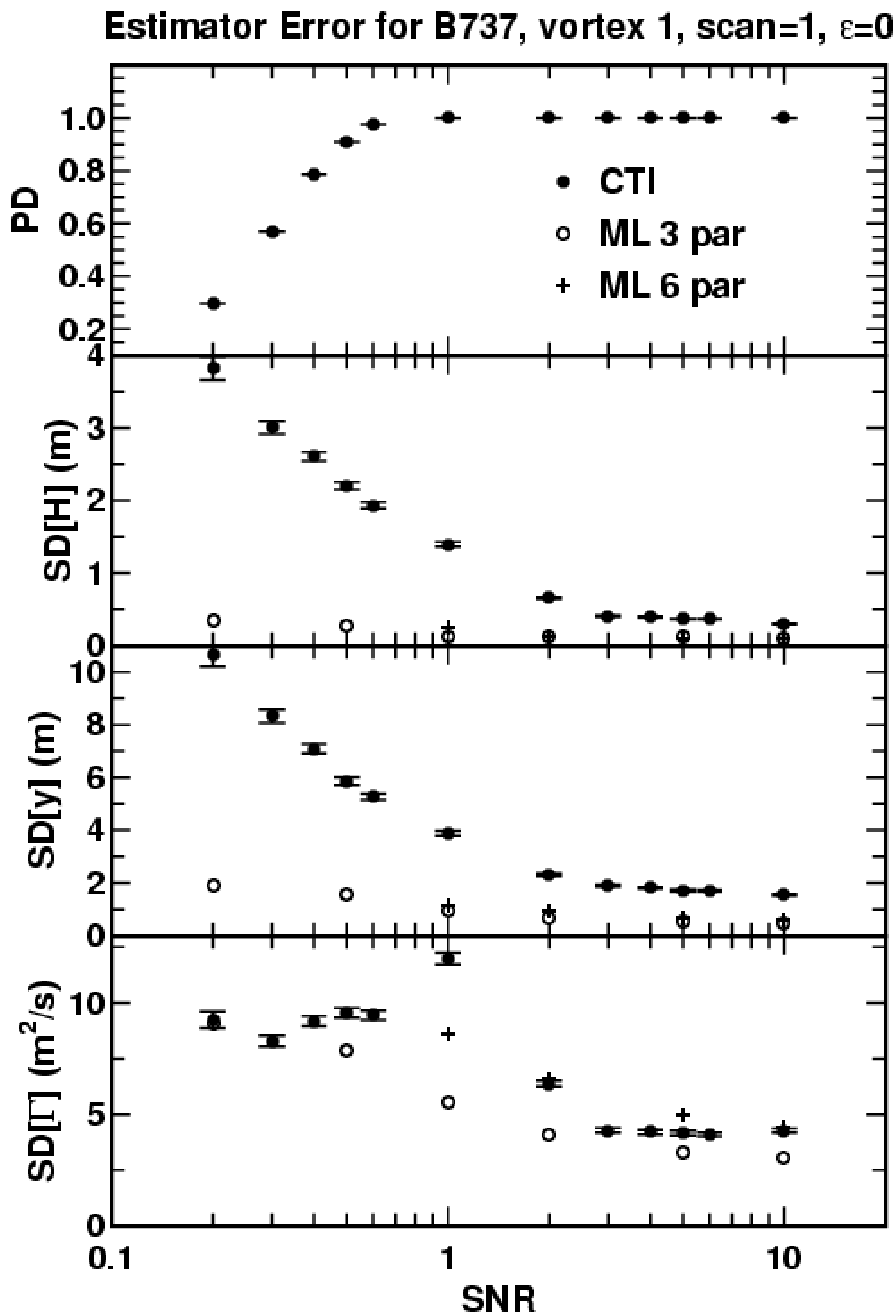

Figure 26. The detection probability (PD) of the CTI algorithm and the standard deviation (SD) of estimates of vortex parameters as a function of SNR for vortex 1 of the Boeing 737 an no turbulence. The correct values are H=146.65 m, y=1115.31 m, and Γ=215.61 m^2/s.

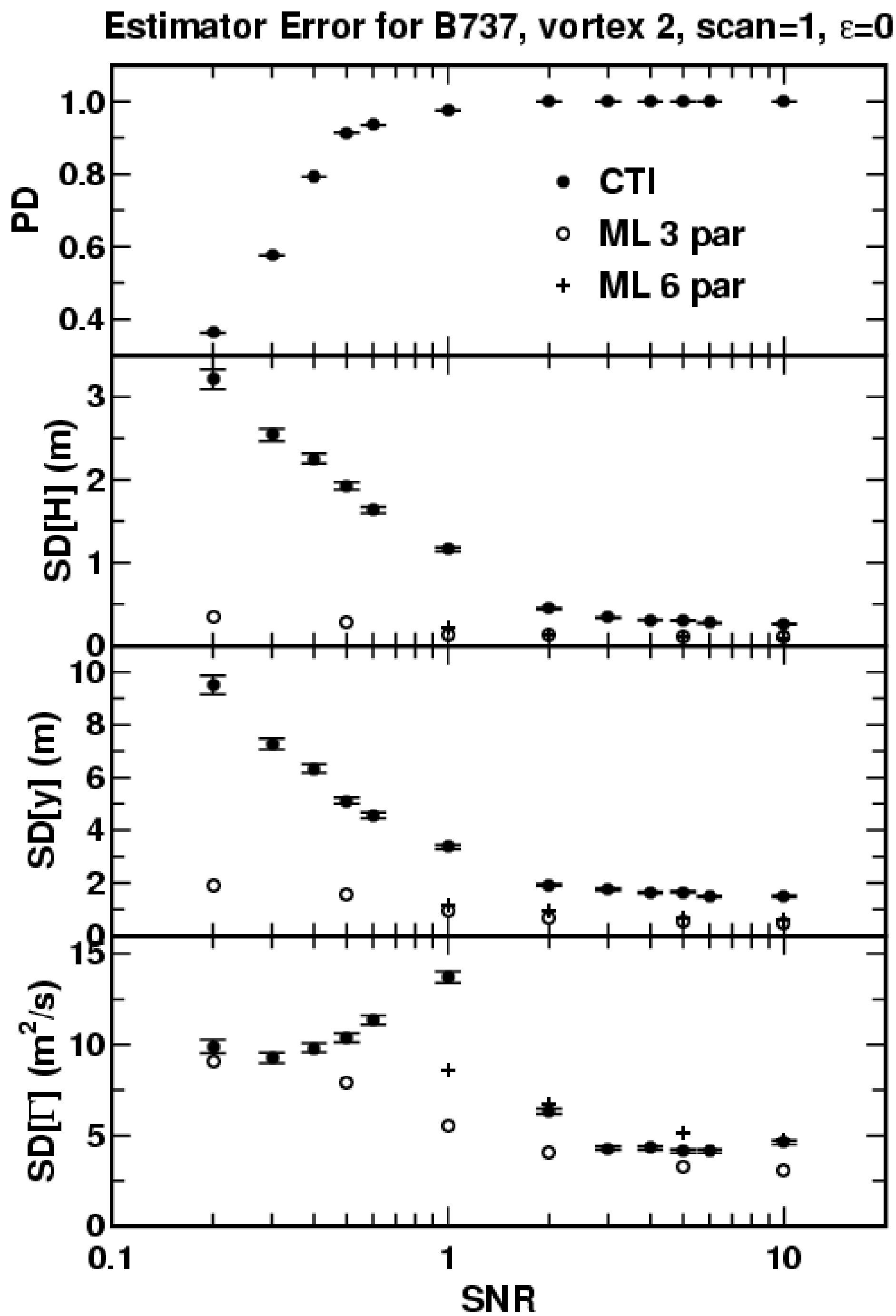

Figure 27. The detection probability (PD) of the CTI algorithm and the standard deviation (SD) of estimates of vortex parameters as a function of SNR for vortex 2 of the Boeing 737 an no turbulence. The correct values are H=146.73 m, y=1137.46 m, and Γ=215.72 m^2/s.

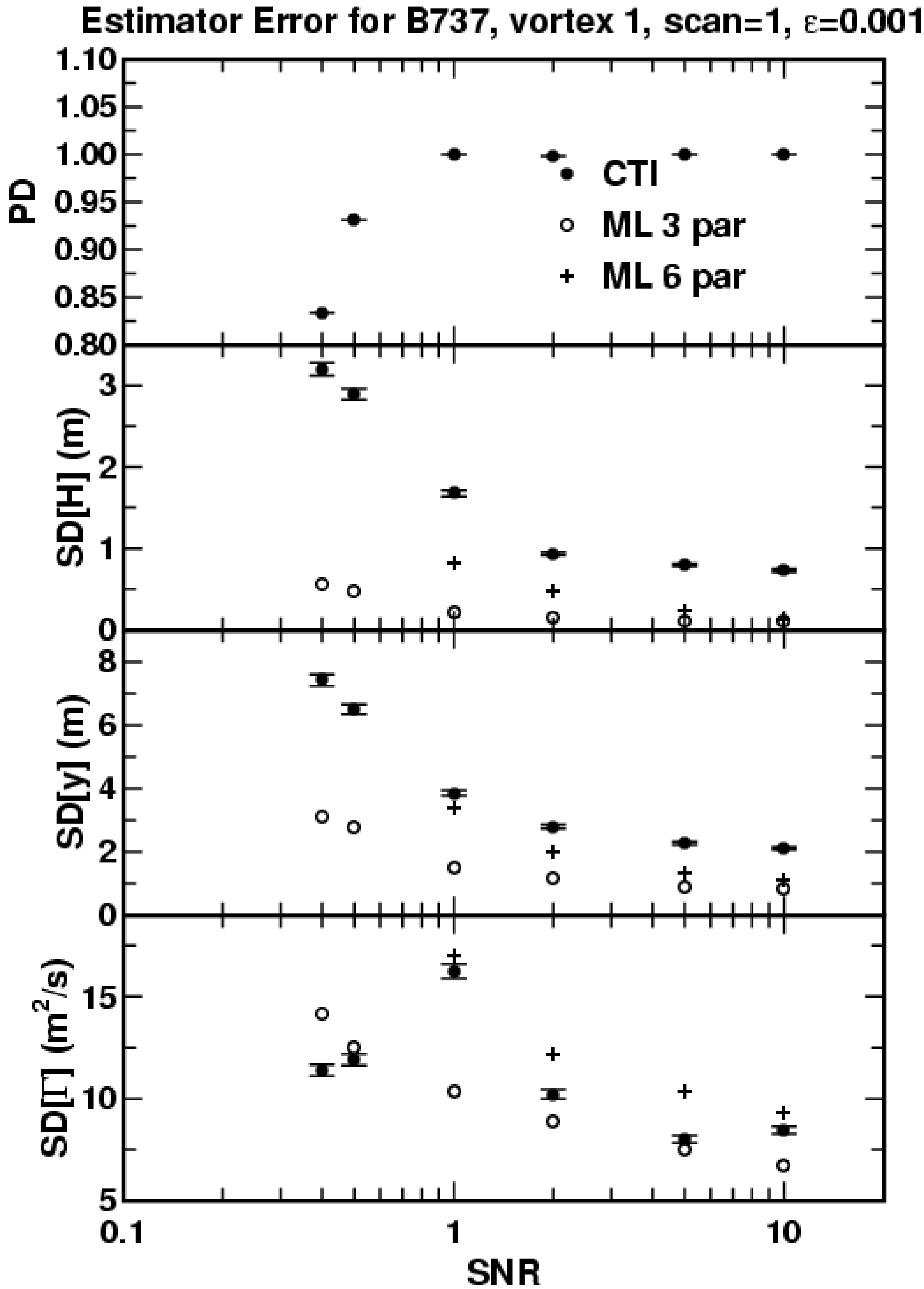

Figure 28. The detection probability (PD) of the CTI algorithm and the standard deviation (SD) of estimates of vortex parameters as a function of SNR for vortex 1 of the Boeing 737 with added turbulence. The correct values are H=146.65 m, y=1115.31 m, and Γ=215.61 m^2/s.

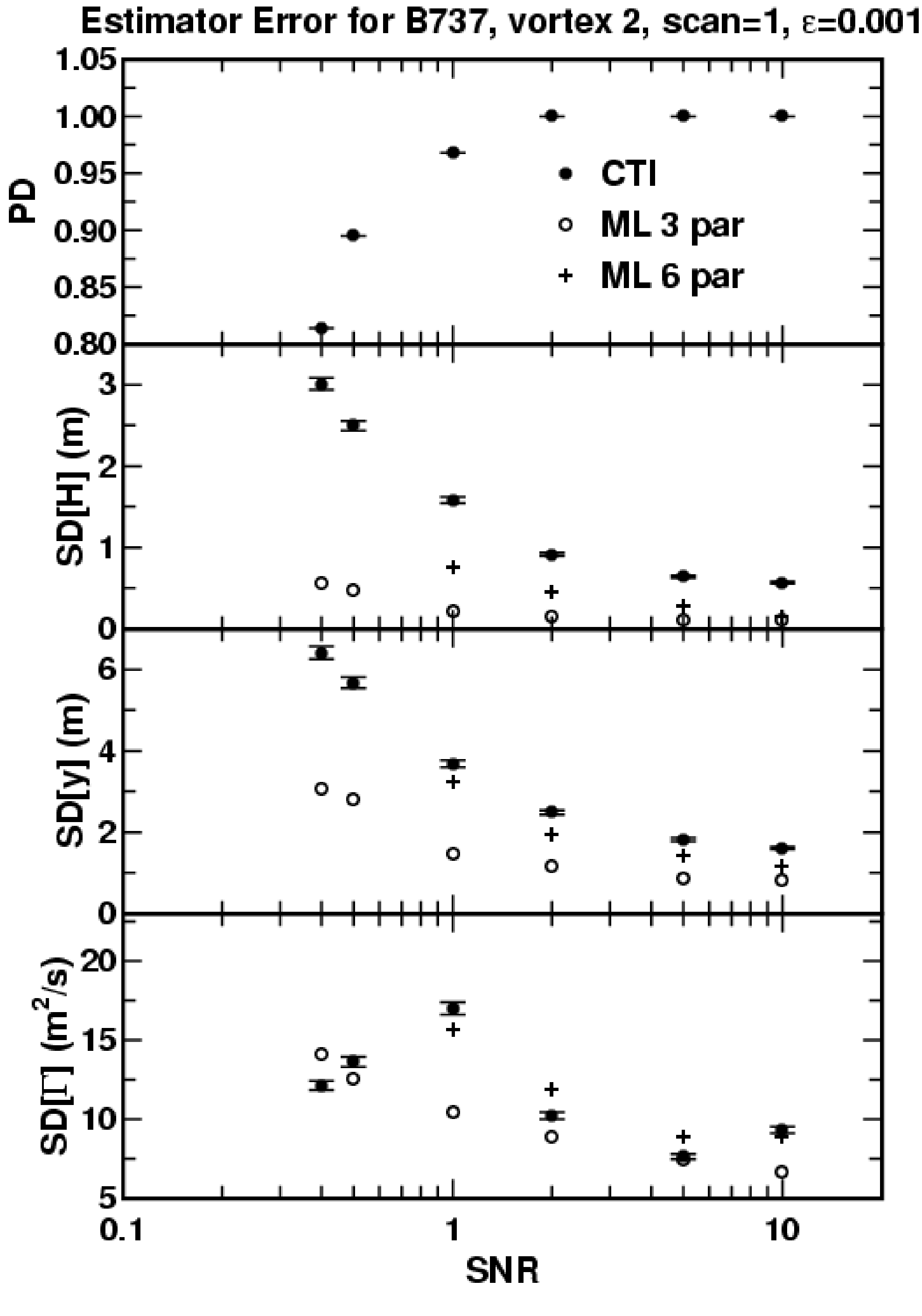

Figure 29. The detection probability (PD) of the CTI algorithm and the standard deviation (SD) of estimates of vortex parameters as a function of SNR for vortex 2 of the Boeing 737 with added turbulence. The correct values are H=146.73 m, y=1137.46 m, and Γ=215.72 m^2/s

3.9 Results for Detection of Boeing 747 Vortex

The same analysis described in the previous section was performed for the detection of the Boeing 747 vortex. The evolution of the vortex parameters and the CTI estimates for one realization in high SNR is shown in Figure 30. The Boeing 747 generates a larger and stronger vortex, which is easier to identify in the lidar data.

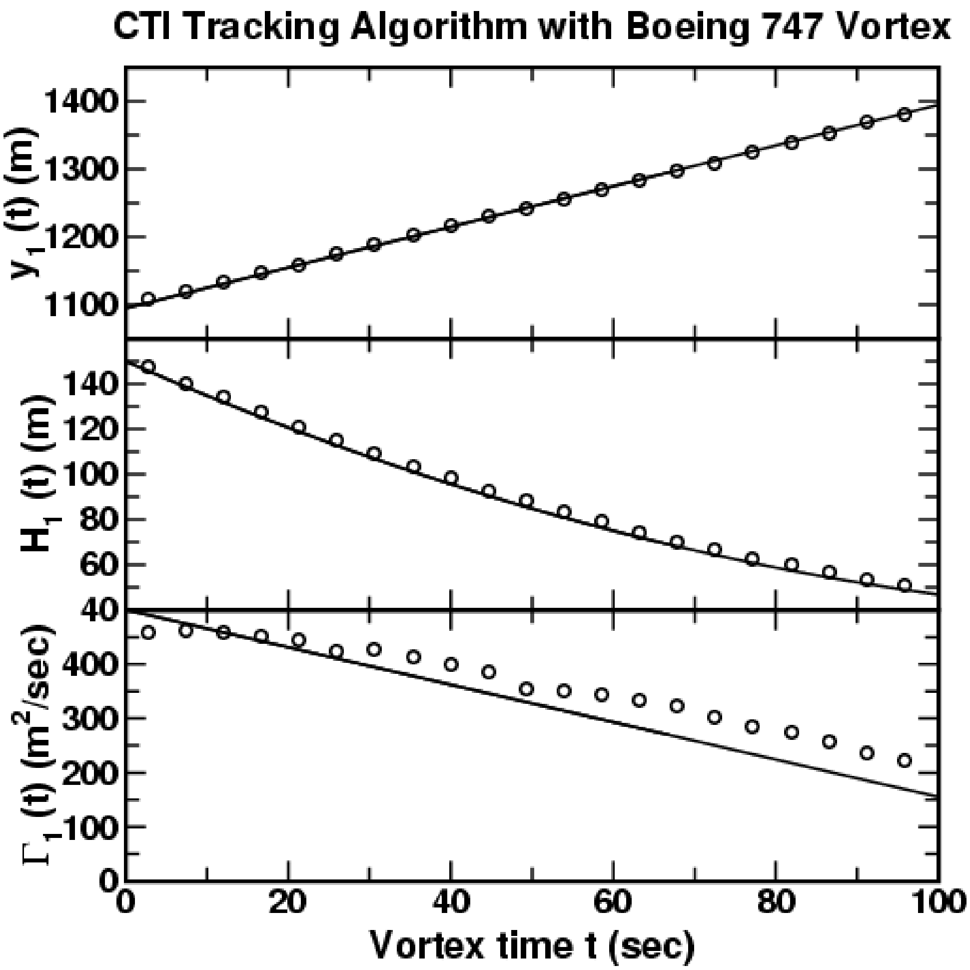

Figure 30. Temporal evolution of the Boeing 747 vortex parameters (solid line) and CTI estimates from simulated data (circle) of distance y_1, altitude H_1, and strength Γ_1 for vortex 1 and SNR=10.

The PDF of the CTI estimates of the closest vortex, vortex 1, the farthest vortex, vortex 2, and three different ML estimates of the vortex parameters for the first lidar scan of the Boeing 747 case are shown in Figure 31 to Figure 35, for a high SNR case and no background turbulence (ε=0). The bias of the ML estimates is small and the random error is very low. The bias of the CTI estimates is small except for the vortex strength Γ, which is larger than for the ML estimators. This is probably due to the approximations used to increase the numerical efficiency of the CTI algorithm. The random error for vortex location is very small, especially compared with the dimensions of the vortex and the CTI estimator has slightly larger error than the ML estimators. The effects of the additive turbulence for the high SNR case are shown in Figure 36 to Figure 40. The standard deviation of all the estimates has increased. However, there is little effect on the bias of the estimates. Some of the PDF's of vortex altitude from the CTI algorithm (Figure

31 and Figure 32) have zero values in the center of the PDF's indicating a discrete nature of the estimates.

The performance of the CTI algorithm is summarized by plotting the detection probability, PD, the bias, and the standard deviation of the estimates of the vortex parameters and the estimates of SNR as a function of the true SNR. The results for the Boeing 747 vortex simulations are shown in Figure 41 to Figure 48. The CTI estimator has a small bias except for the estimates of vortex strength Γ in lower SNR. There is a consistent bias in the CTI estimates of the SNR, i.e., -20% bias at low SNR to –40% bias at high SNR. As expected, for the ML estimates, the estimation of more independent parameters increase the standard deviation or estimation error of the estimates and the added turbulence produces an additional increase in the estimation error. However, there is only a small impact on the bias of the estimates reflecting the robust nature of the ML estimator.

Table 4 summarizes the simulations that were performed in order to evaluate the performance of the detection algorithms for the Boeing 747. The results are shown in Figure 31 through Figure 48.

Table 4. **Performance Simulations of Detection Algorithms - 747**

ε	Estimator	Vortex	Figure No.
PDFs – SNR, H, Y, Γ. SNR = 10			
0	CTI	1	31
0	CTI	2	32
0	ML 3	Both	33
0	ML 6	1	34
0	ML 6	2	35
With turbulence			
0.001	CTI	1	36
0.001	CTI	2	37
0.001	ML 3	Both	38
0.001	ML 6	1	39
0.001	ML 6	2	40
Bias vs. SNR – SNR, H, Y, Γ			
0	All	1	41
0	All	2	42
0.001	All	1	43
0.001	All	2	44
PD, SD(H), SD(Y), SD(Γ)			
0	All	1	45
0	All	2	46
0.001	All	1	47
0.001	All	2	48

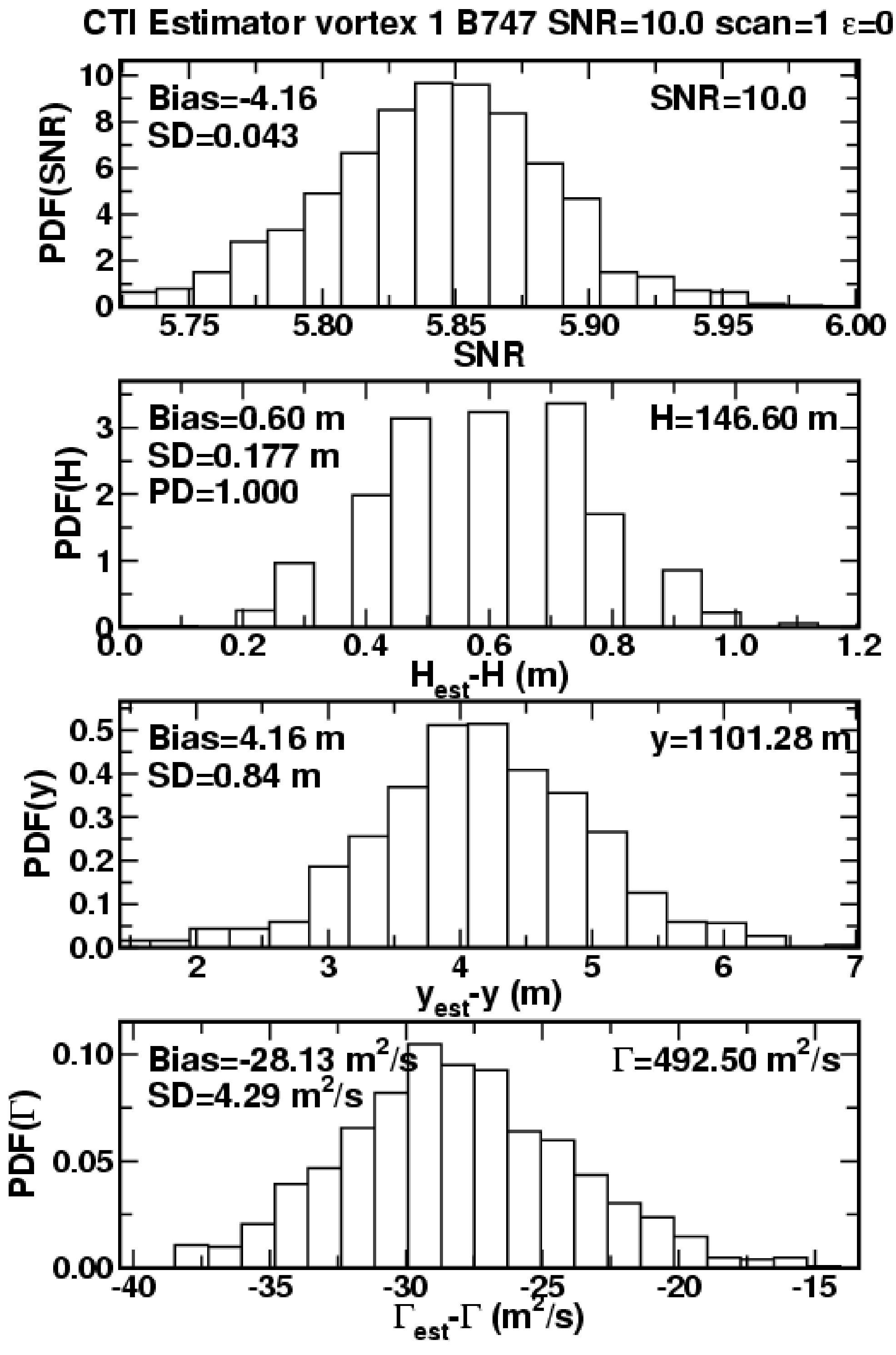

Figure 31. PDF of CTI estimates of the parameters of vortex 1. The bias and standard deviation (SD) are shown on the left and the correct values are shown on the right. The detection probability PD is also shown.

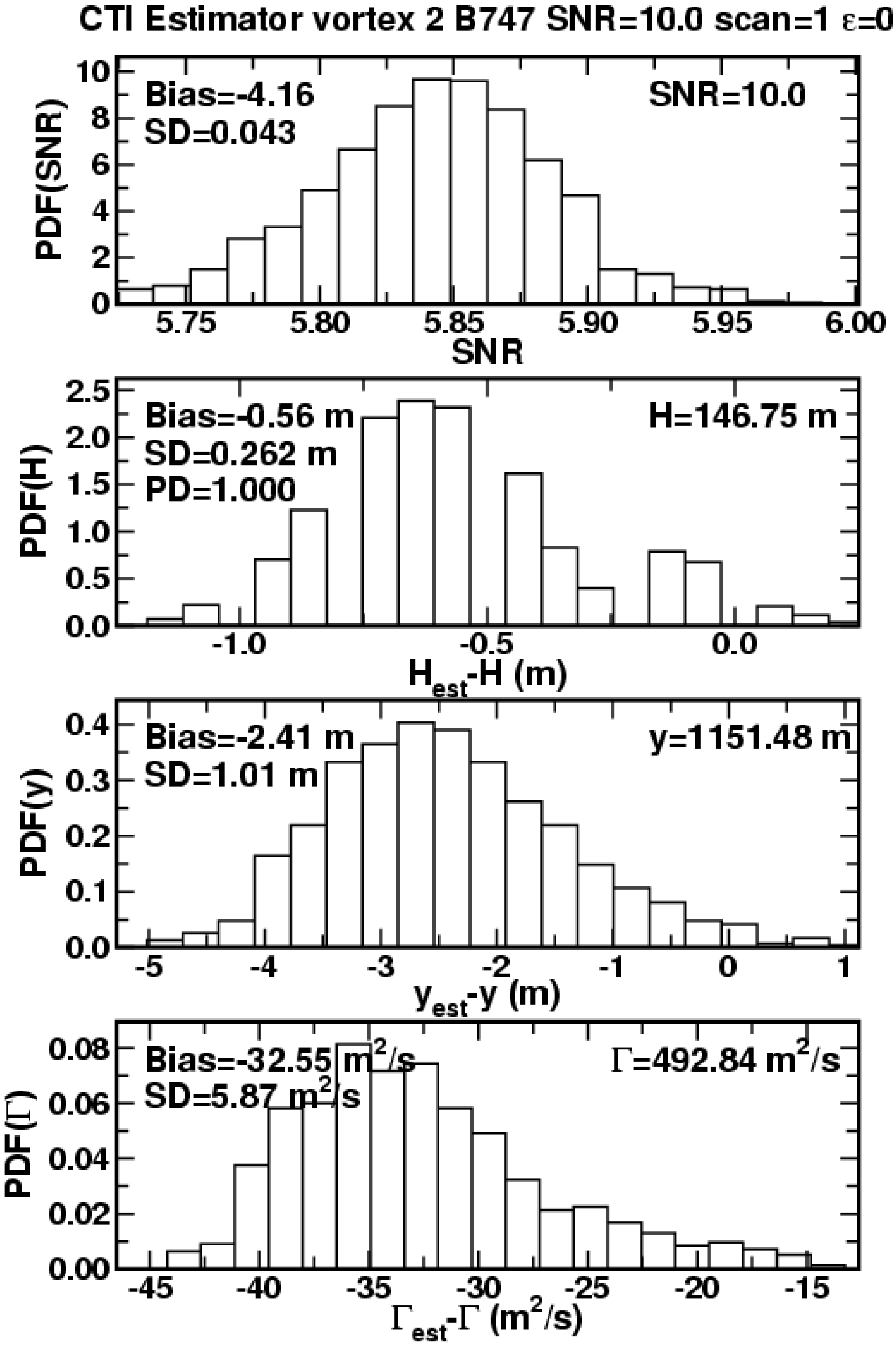

Figure 32. PDF of CTI estimates of the parameters of vortex 2. The bias and standard deviation (SD) are shown on the left and the correct values are shown on the right. The detection probability PD is also shown.

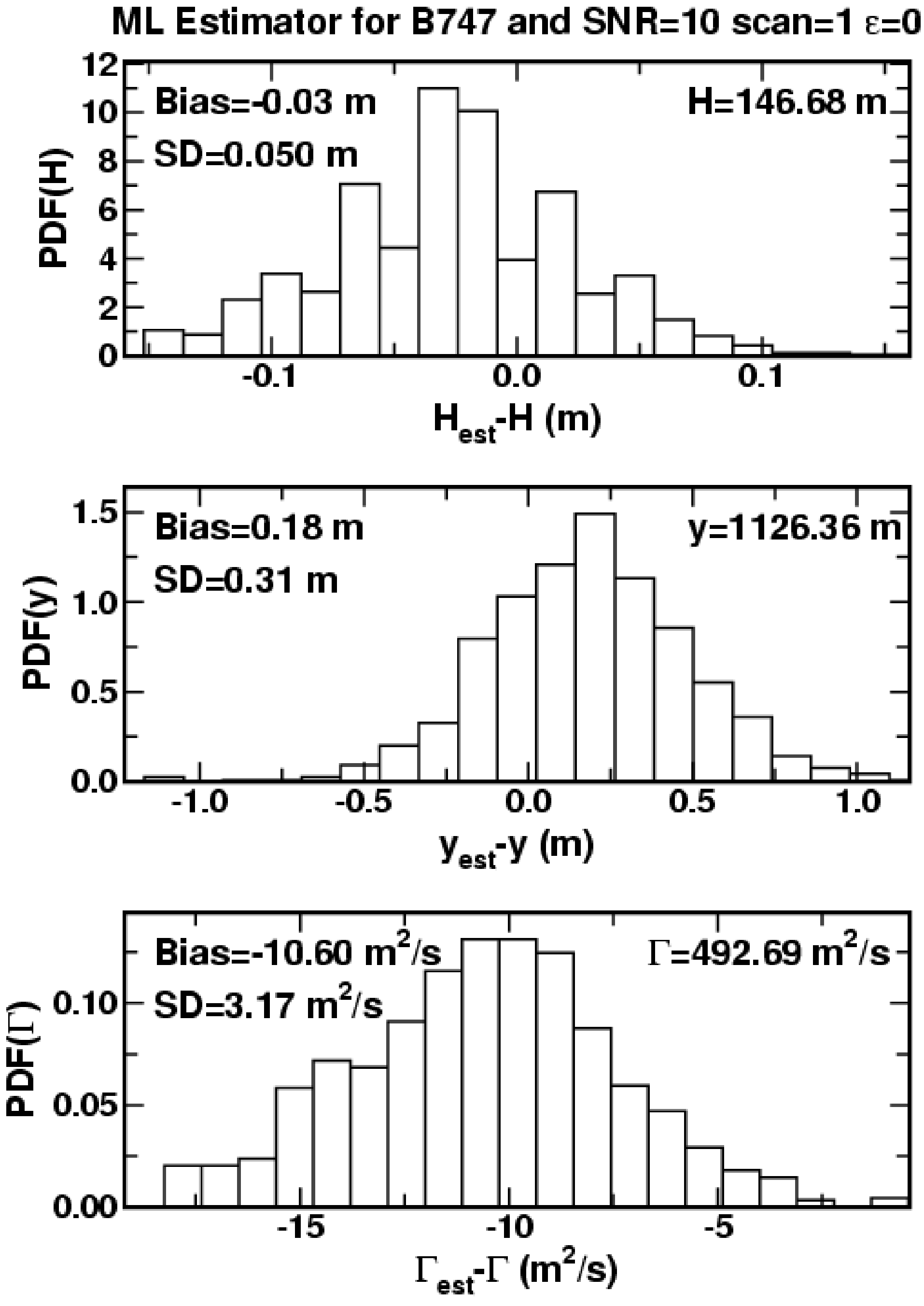

Figure 33. PDF of ML estimates of the vortex parameters assuming each vortex has the same parameters and the spacing between the vortices is known. The bias and standard deviation (SD) are shown on the left and the correct values are shown on the right.

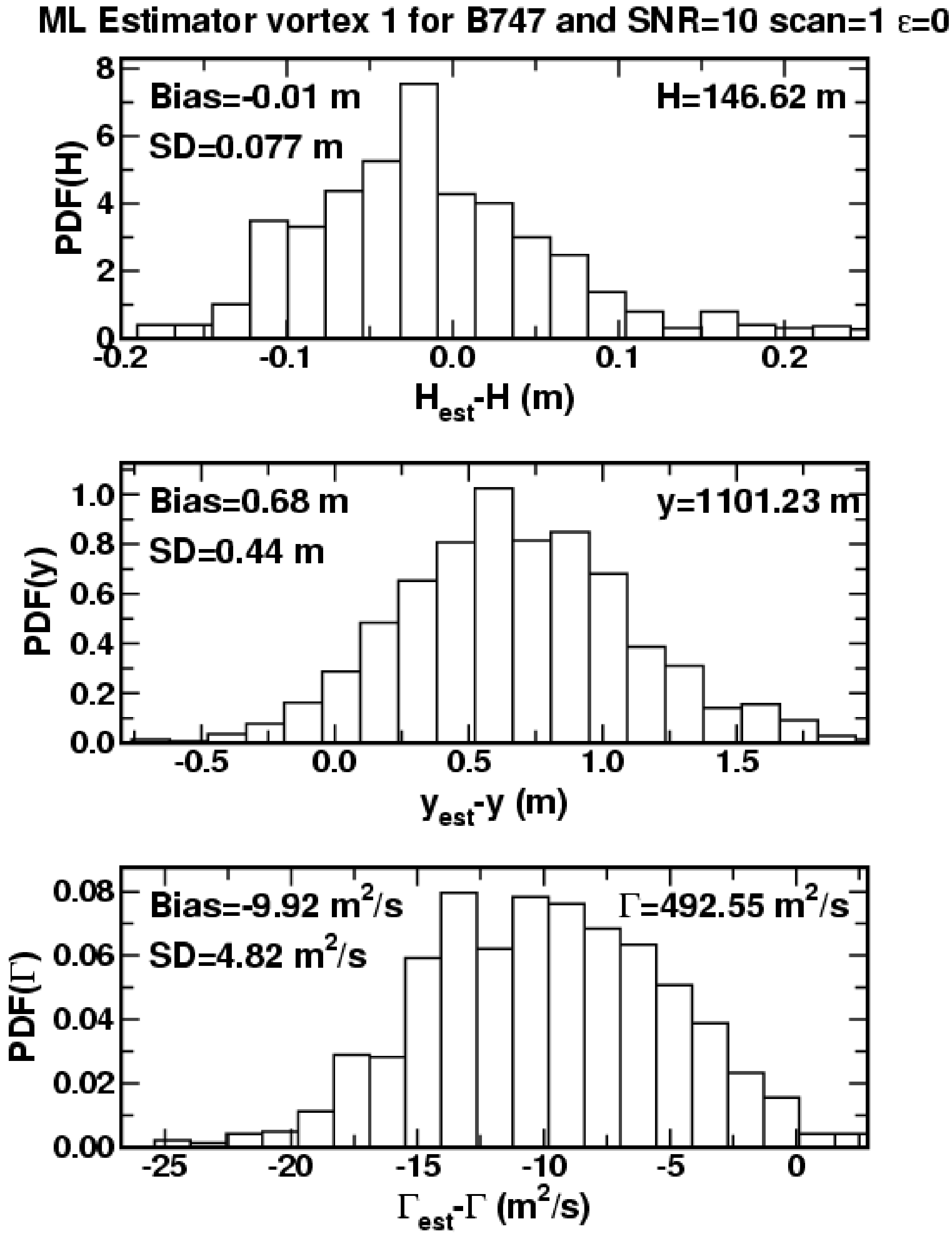

Figure 34. PDF of ML estimates of the parameters of vortex 1. The bias and standard deviation (SD) are shown on the left and the correct values are shown on the right.

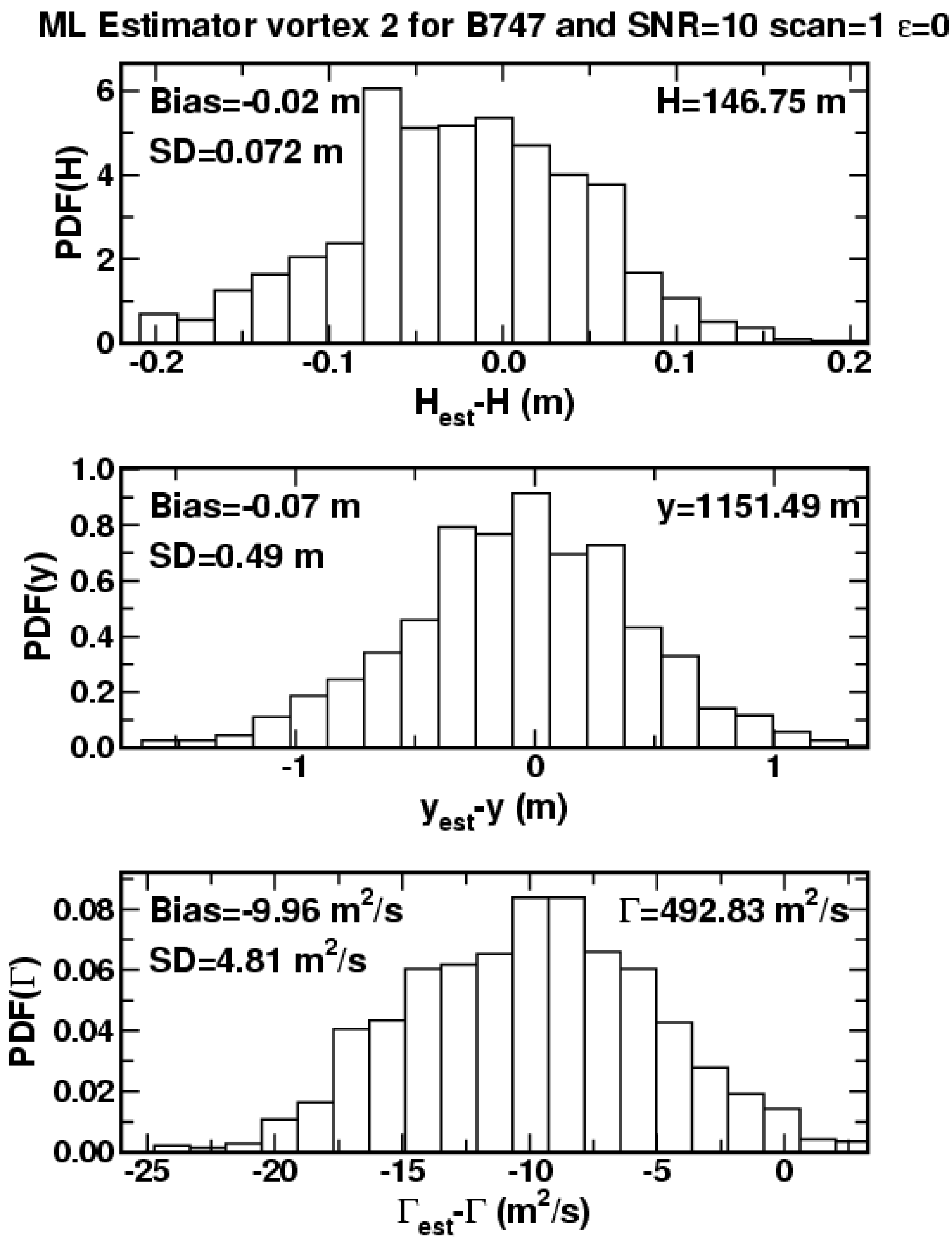

Figure 35. PDF of ML estimates of the parameters of vortex 2. The bias and standard deviation (SD) are shown on the left and the correct values are shown on the right.

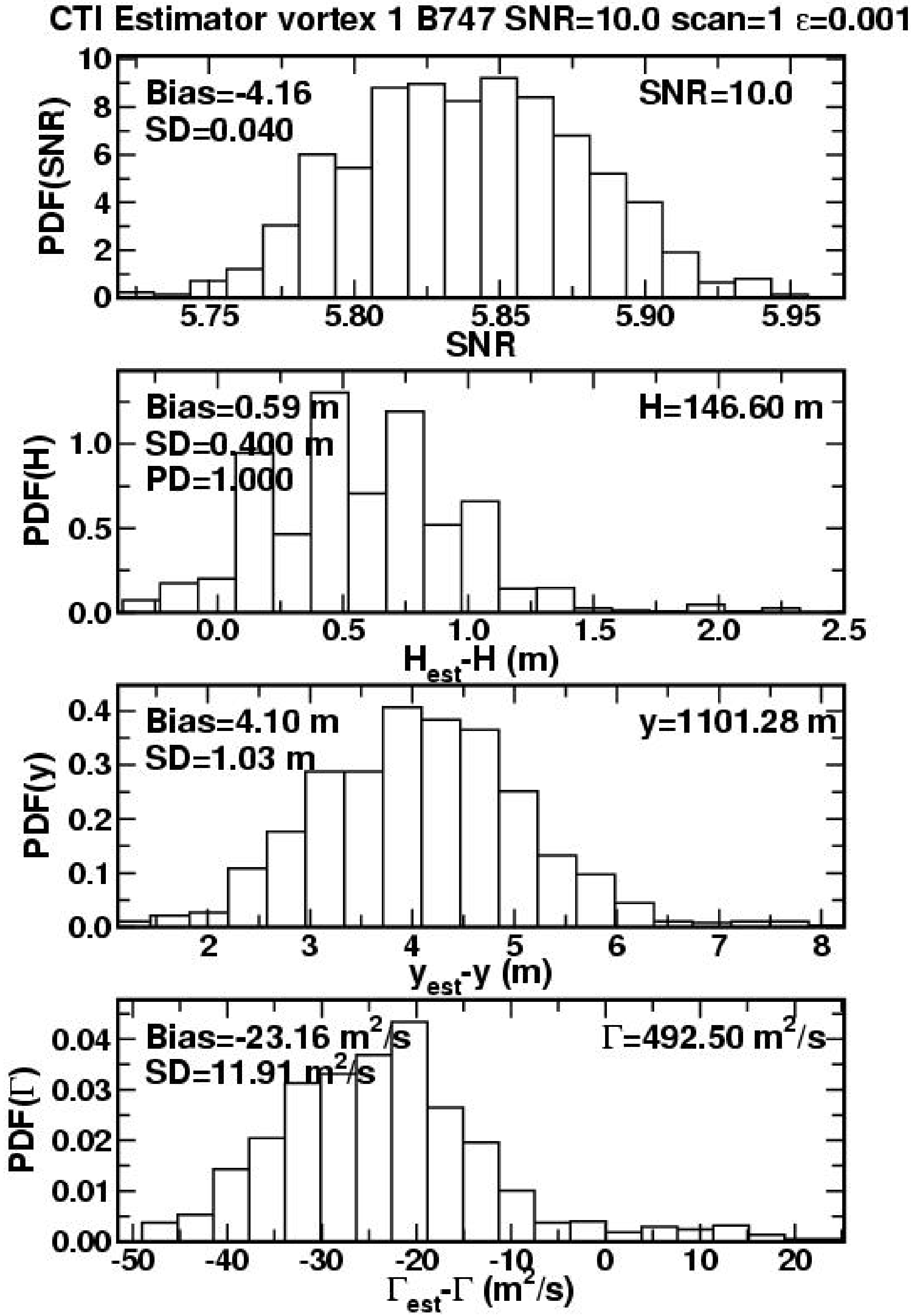

Figure 36. PDF of CTI estimates of the parameters of vortex 1 with added turbulence. The bias and standard deviation (SD) are shown on the left and the correct values are shown on the right. The detection probability PD is also shown.

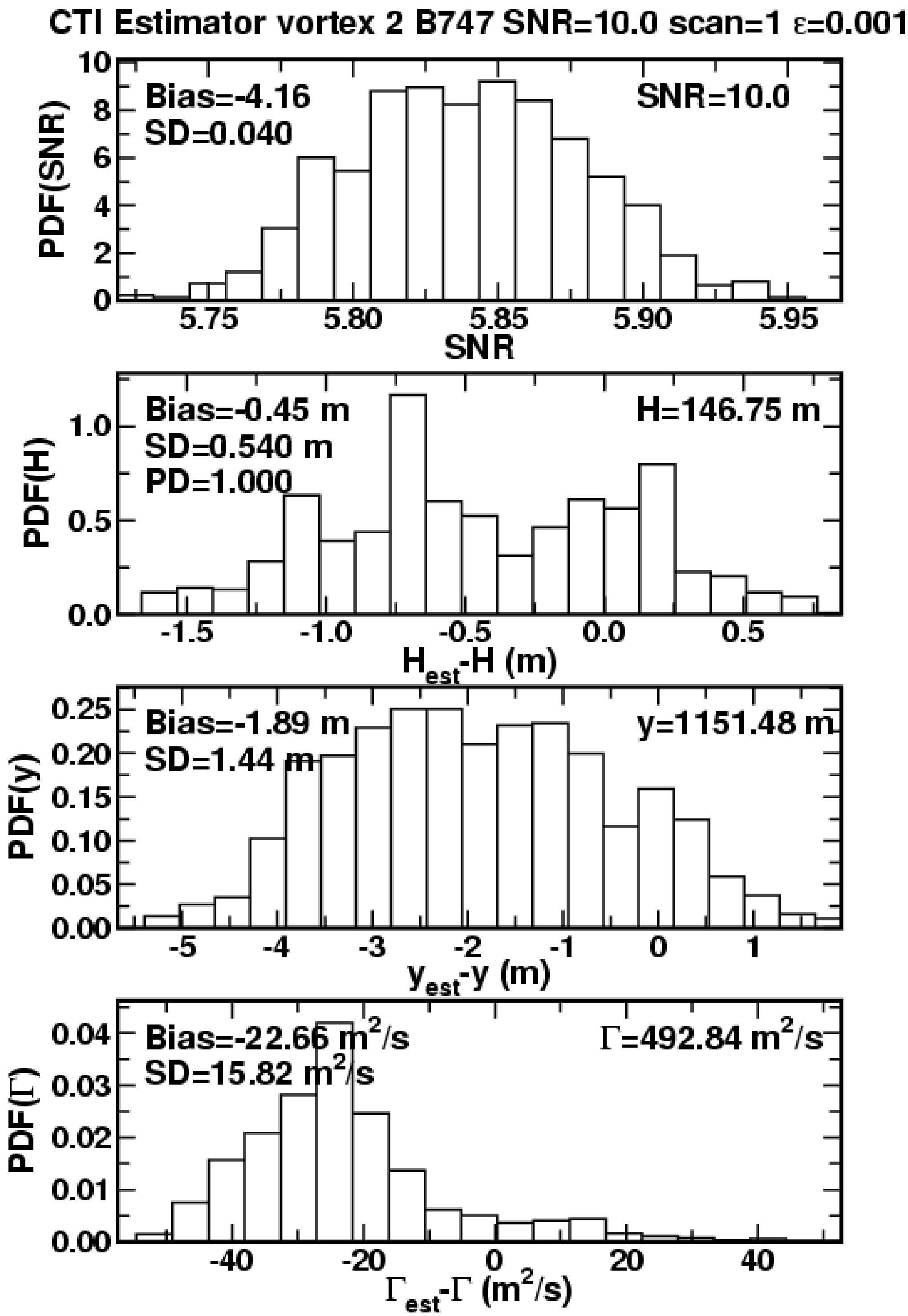

Figure 37. PDF of CTI estimates of the parameters of vortex 2 with added turbulence. The bias and standard deviation (SD) are shown on the left and the correct values are shown on the right. The detection probability PD is also shown.

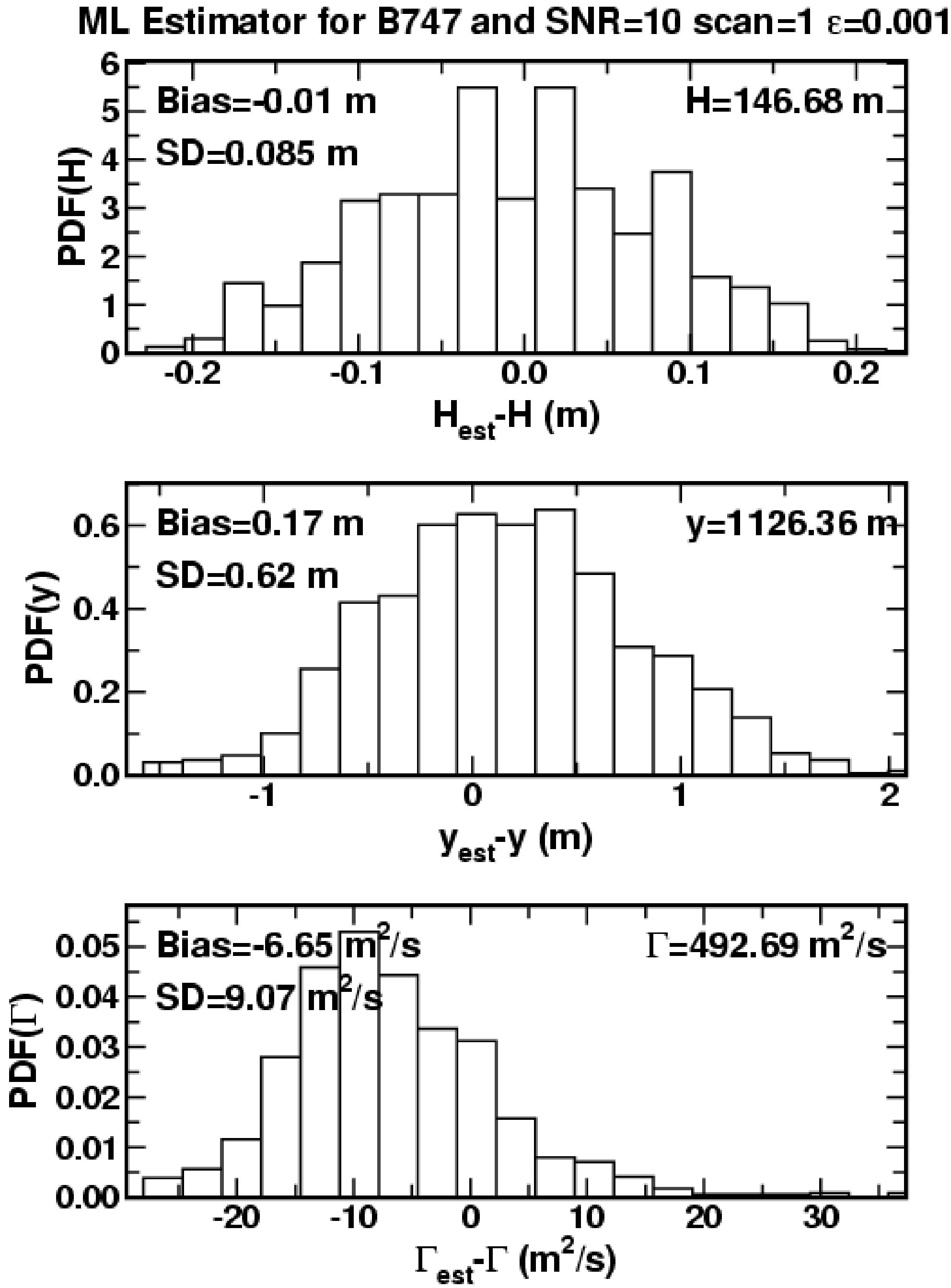

Figure 38. PDF of ML estimates of the vortex parameters with added turbulence assuming each vortex has the same parameters and the spacing between the vortices is known. The bias and standard deviation (SD) are shown on the left and the correct values are shown on the right.

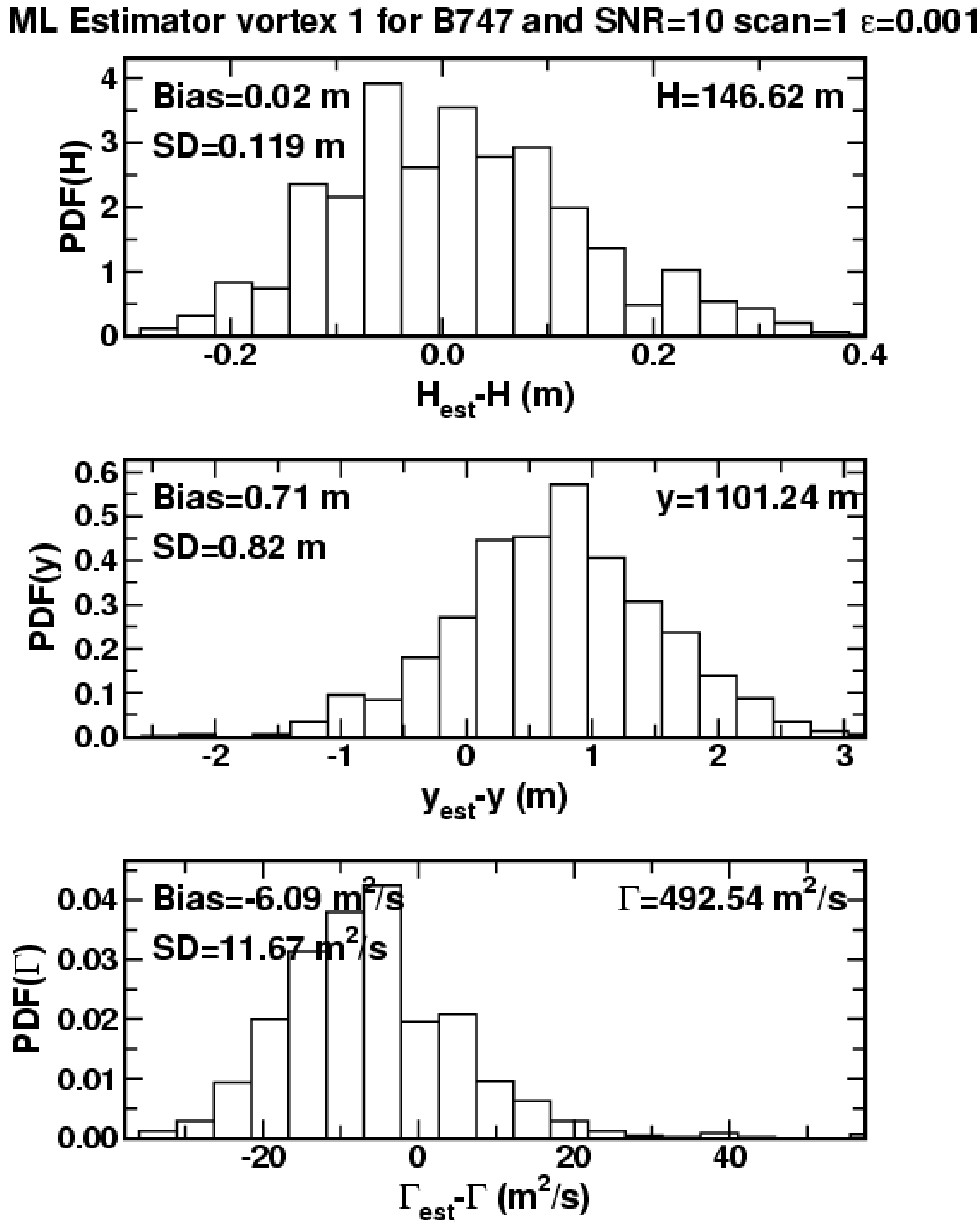

Figure 39. PDF of ML estimates of the parameters of vortex 1 with added turbulence. The bias and standard deviation (SD) are shown on the left and the correct values are shown on the right.

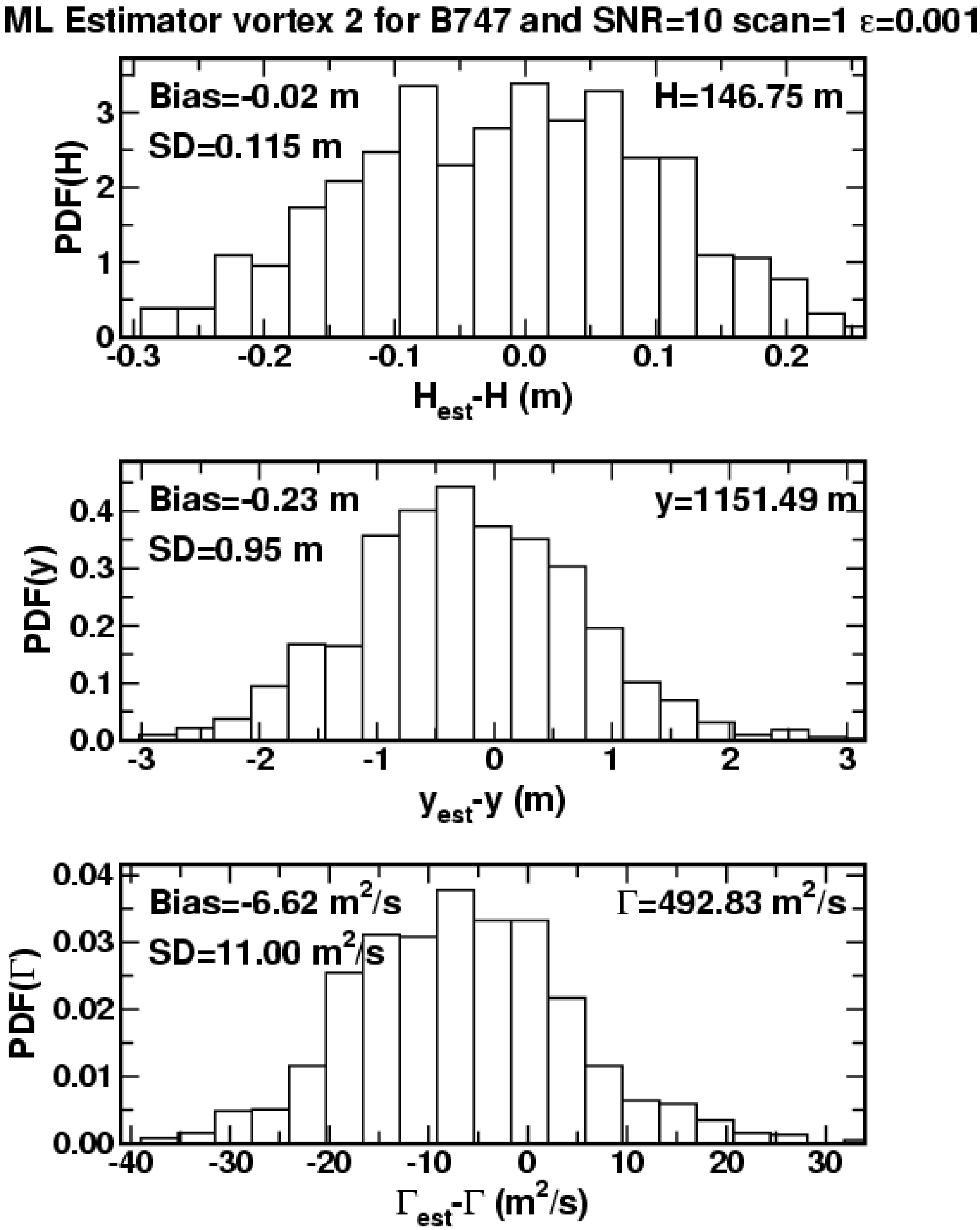

Figure 40. PDF of ML estimates of the vortex parameters with added turbulence assuming each vortex has the same parameters and the spacing between the vortices is known. The bias and standard deviation (SD) are shown on the left and the correct values are shown on the right.

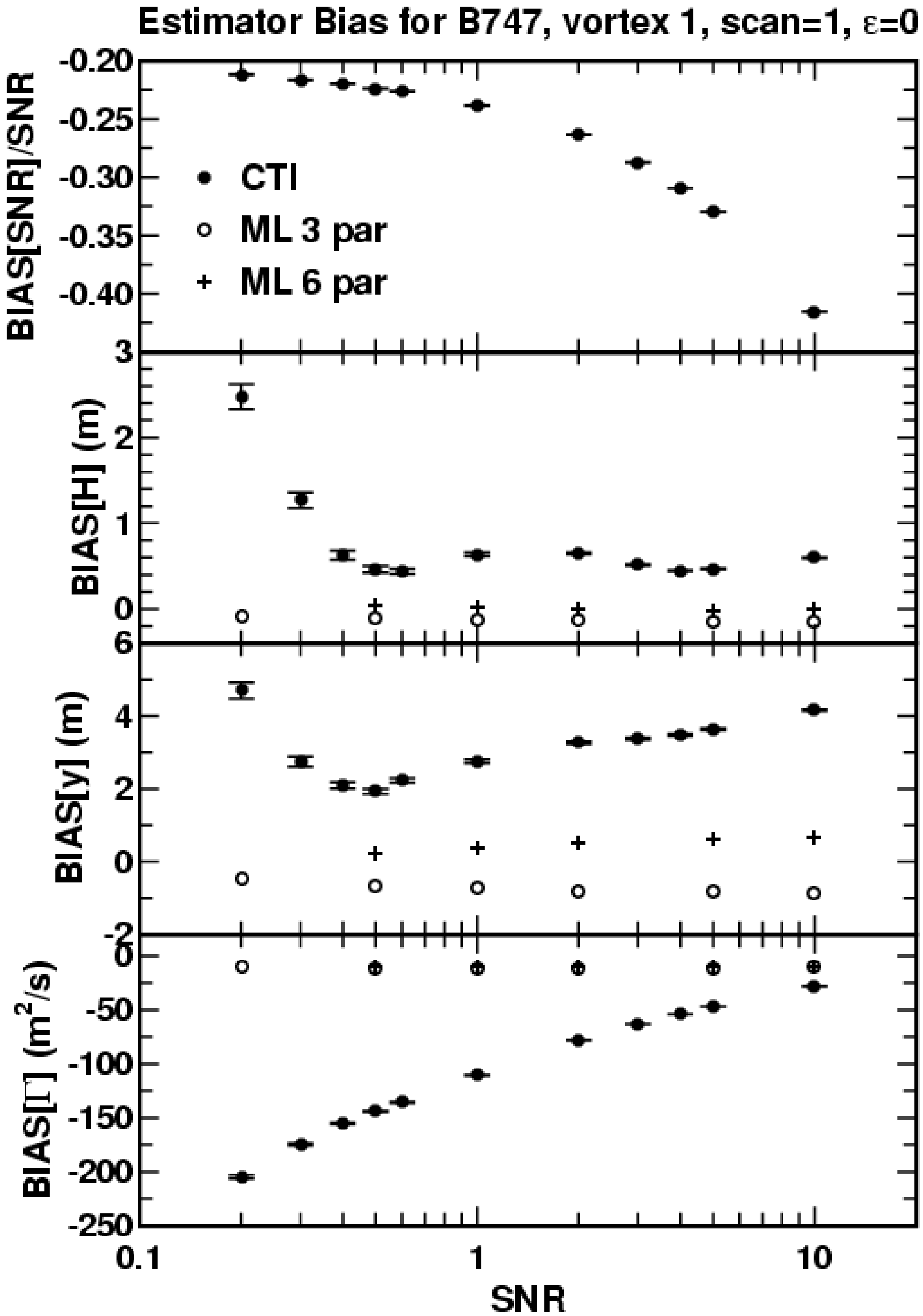

Figure 41. The bias of estimates of vortex parameters as a function of SNR for vortex 1 of the Boeing 747 and no turbulence. The correct values are H=146.60 m, y=1101.28 m, and Γ=492.50 m^2/s.

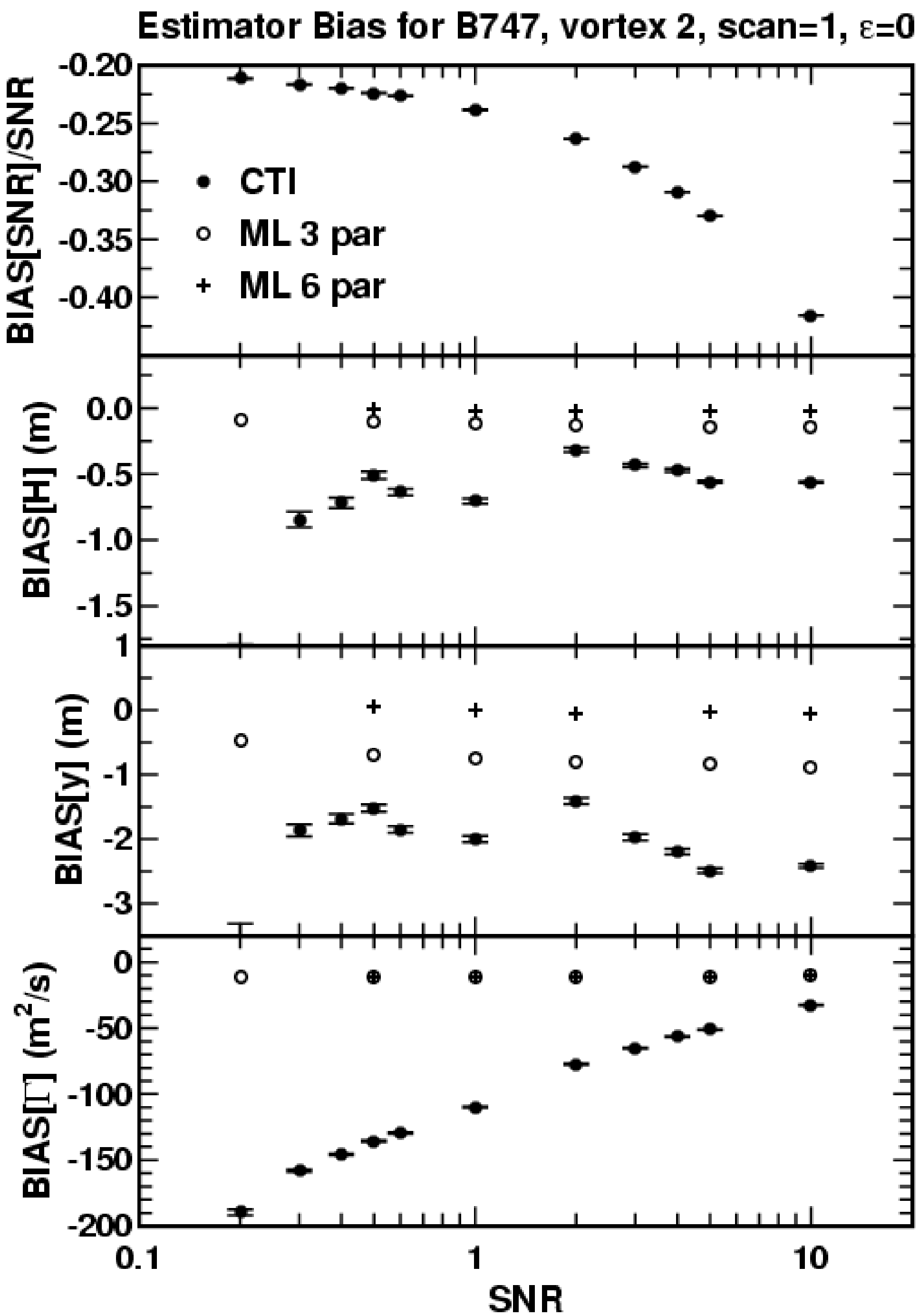

Figure 42. The bias of estimates of vortex parameters as a function of SNR for vortex 2 of the Boeing 747 and no turbulence. The correct values are H=146.75 m, y=1151.48 m, and Γ=492.84 m^2/s.

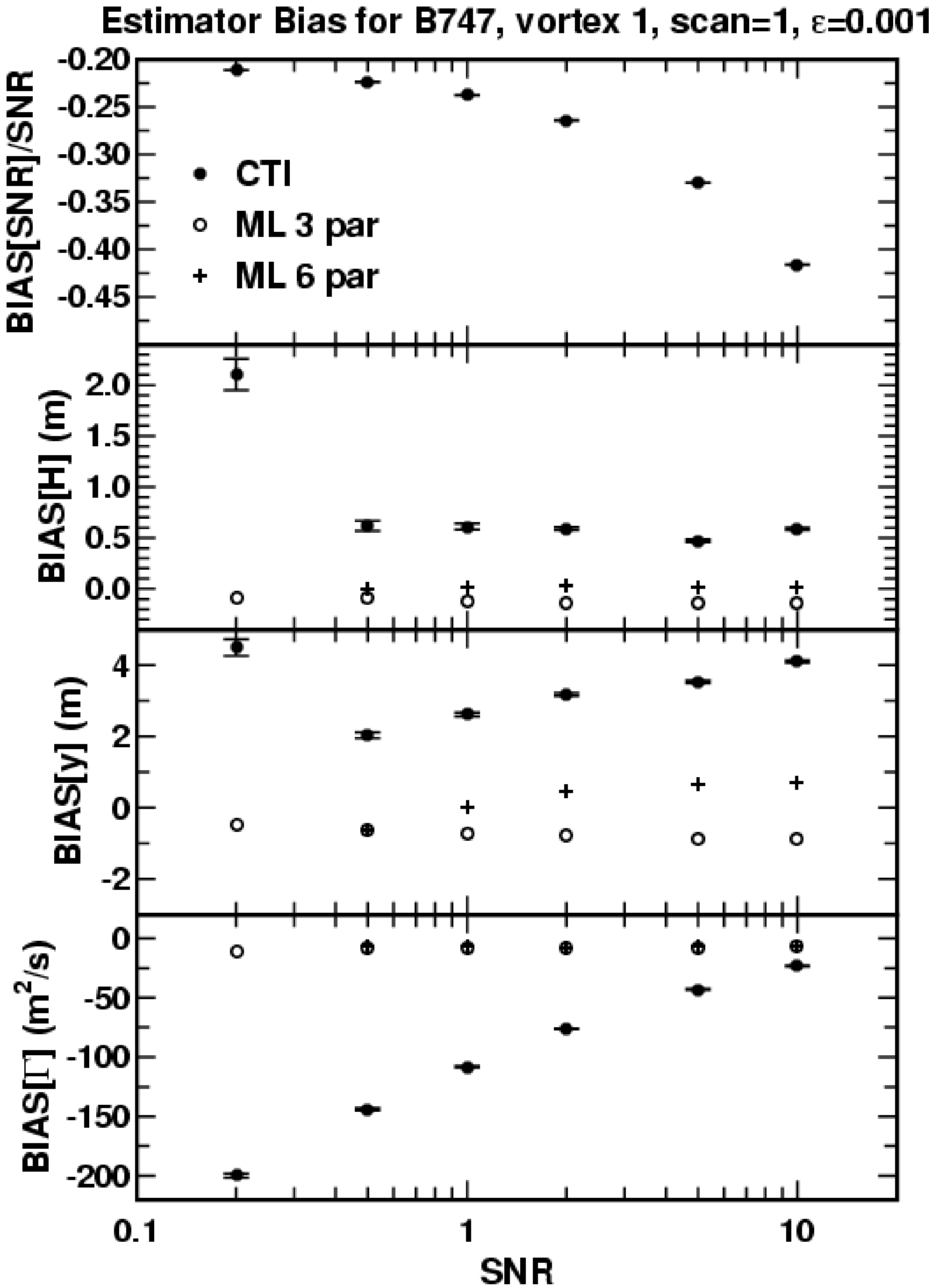

Figure 43. The bias of estimates of vortex parameters as a function of SNR for vortex 1 of the Boeing 747 with added turbulence. The correct values are H=146.60 m, y=1101.28 m, and Γ=492.50 m^2/s.

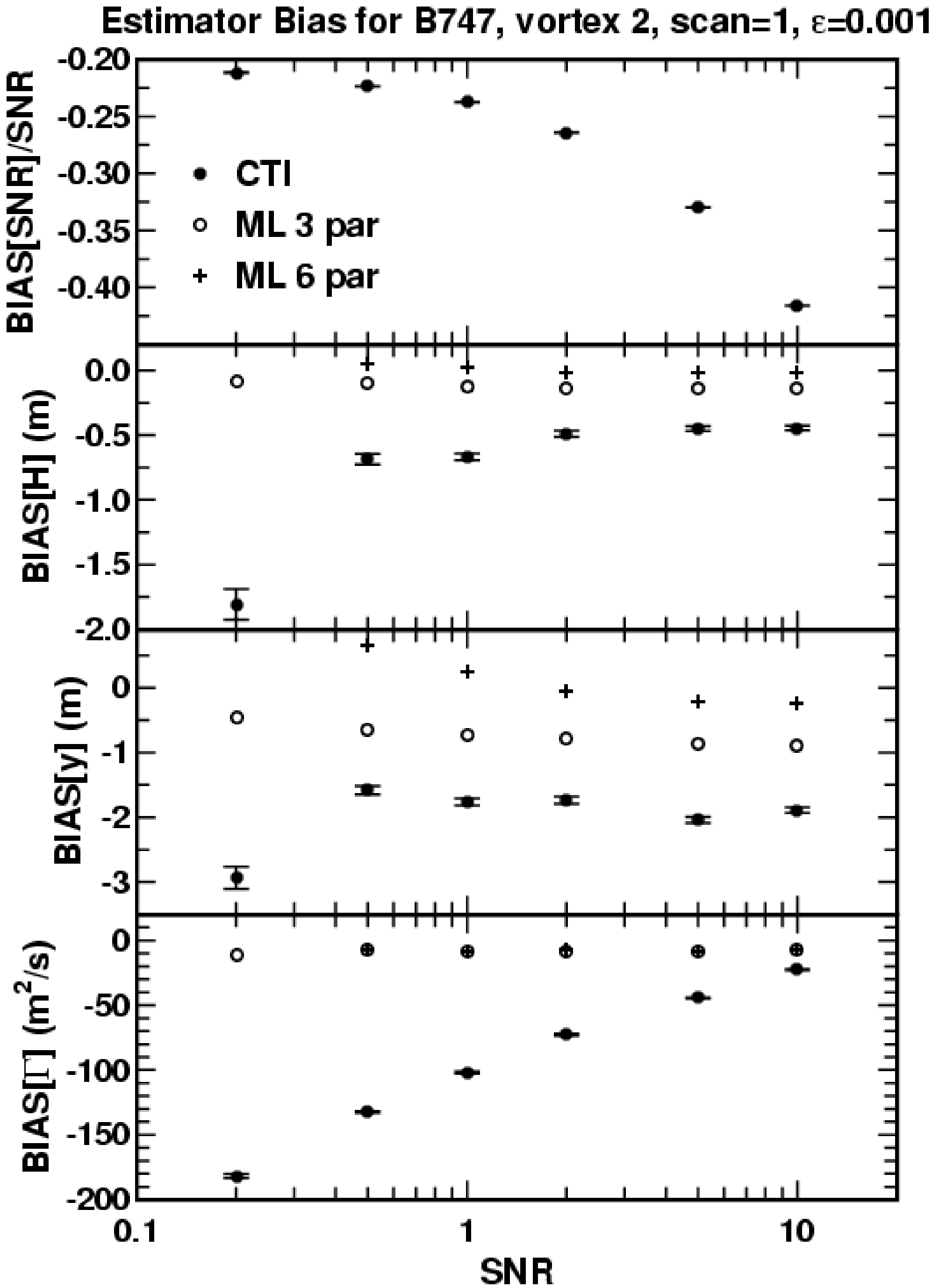

Figure 44. The bias of estimates of vortex parameters as a function of SNR for vortex 2 of the Boeing 747 with added turbulence. The correct values are H=146.75 m, y=1151.48 m, and Γ=492.84 m^2/s.

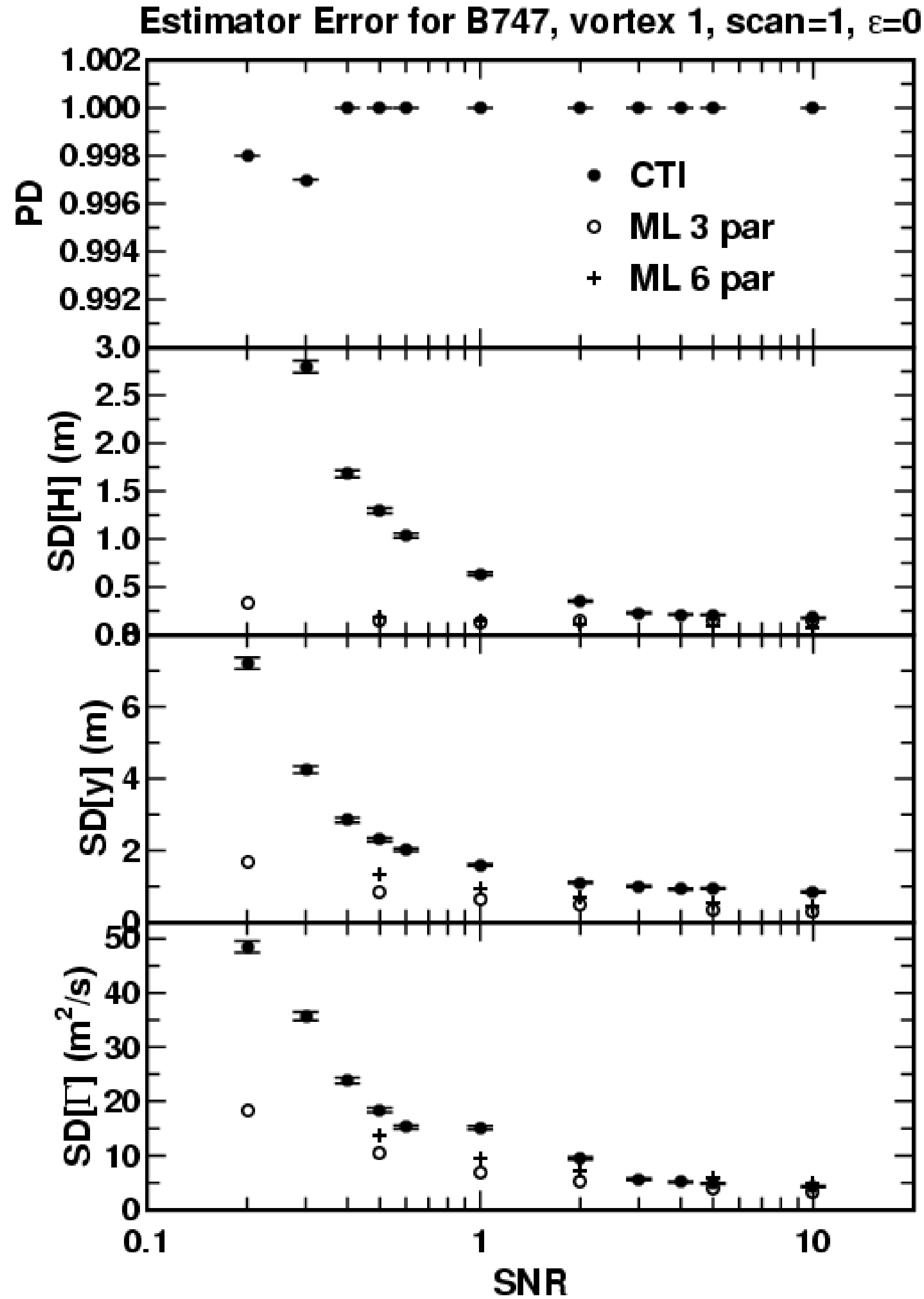

Figure 45. The detection probability (PD) of the CTI algorithm and the standard deviation (SD) of estimates of vortex parameters as a function of SNR for vortex 2 of the Boeing 747 and no turbulence. The correct values are H=146.75 m, y=1151.48 m, and Γ=492.84 m^2/s.

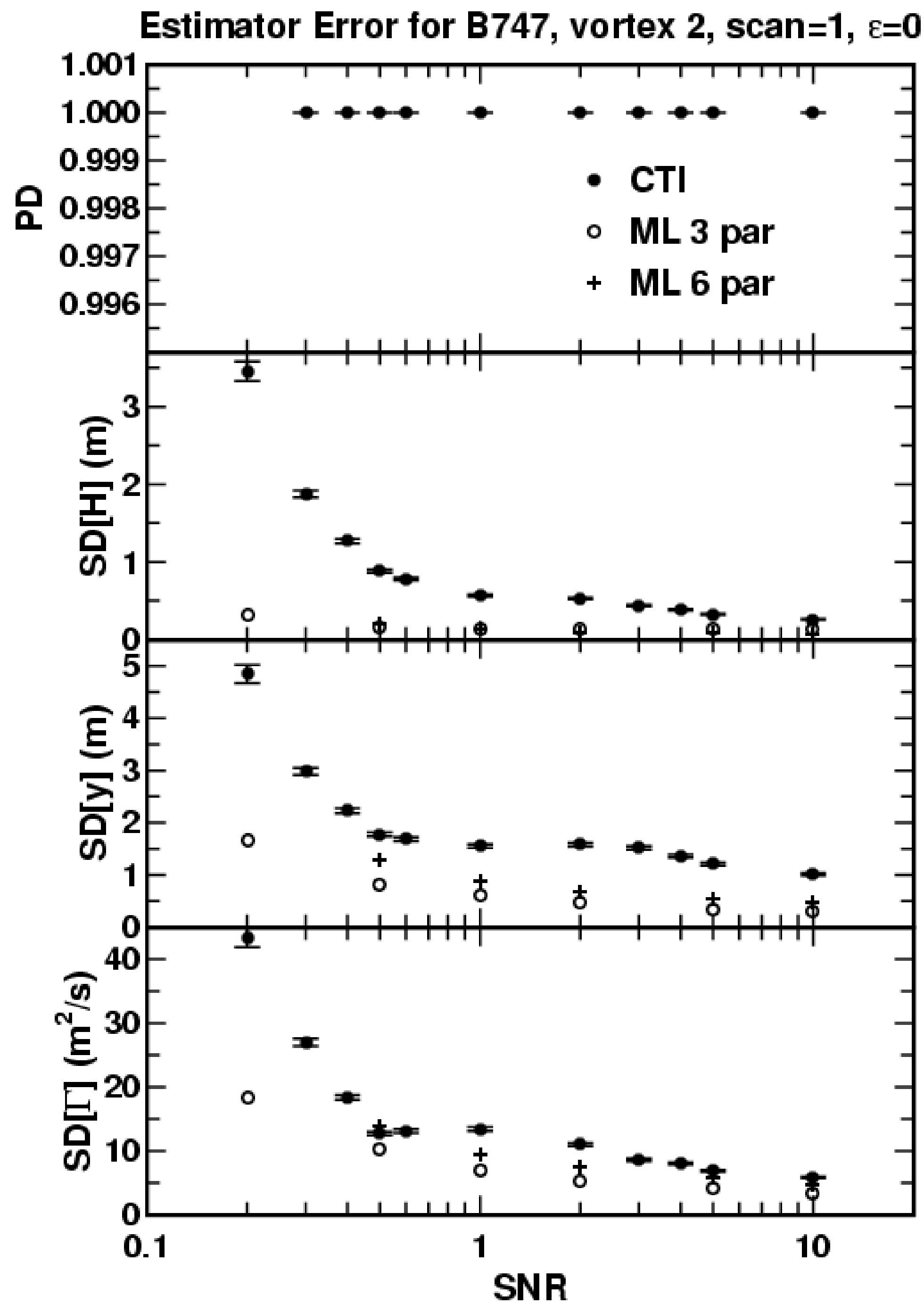

Figure 46. The detection probability (PD) of the CTI algorithm and the standard deviation (SD) of estimates of vortex parameters as a function of SNR for vortex 2 of the Boeing 747 and no turbulence. The correct values are H=146.75 m, y=1151.48 m, and Γ=492.84 m^2/s.

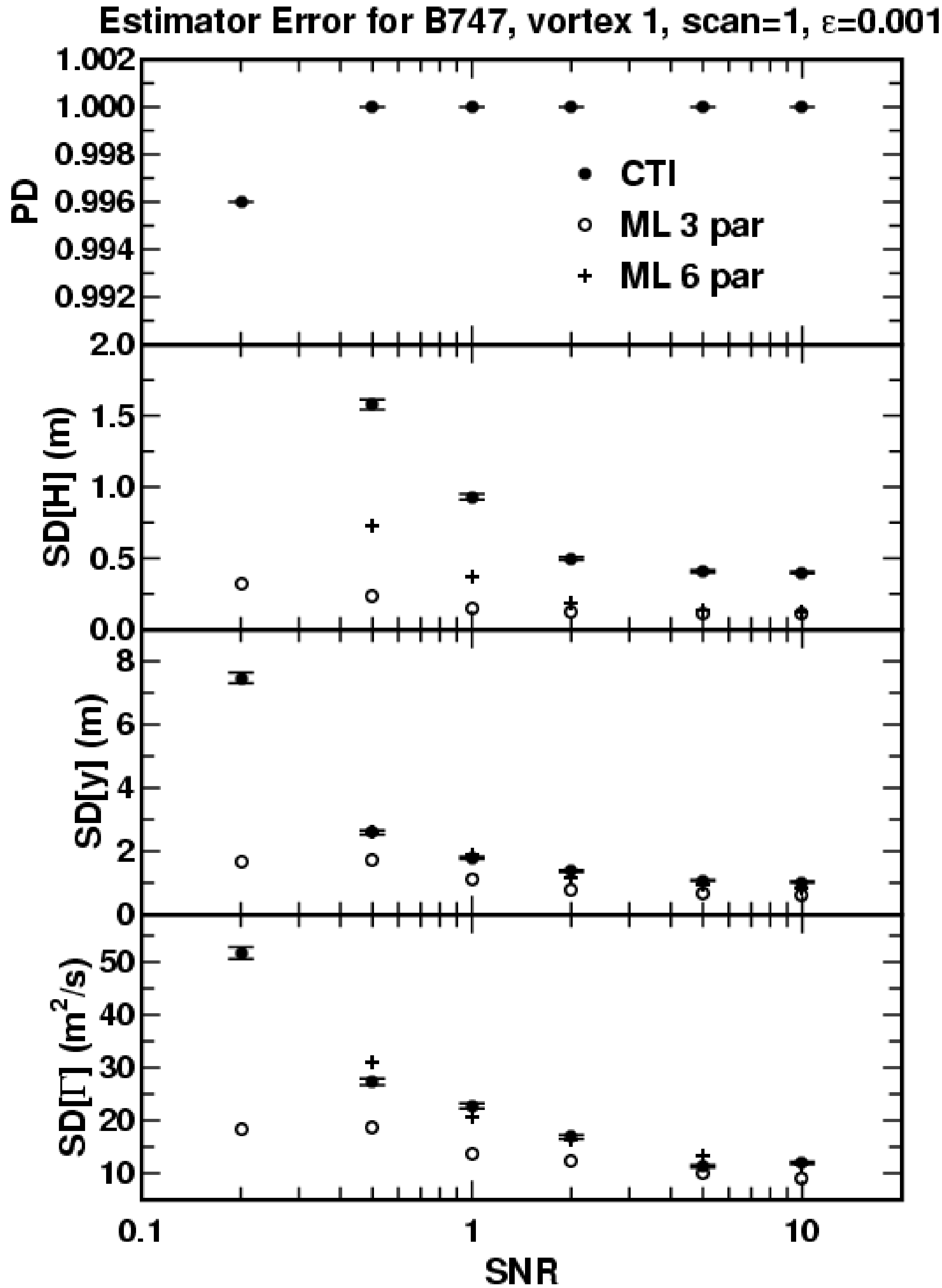

Figure 47. The detection probability (PD) of the CTI algorithm and the standard deviation (SD) of estimates of vortex parameters as a function of SNR for vortex 2 of the Boeing 747 with added turbulence. The correct values are H=146.75 m, y=1151.48 m, and Γ=492.84 m^2/s.

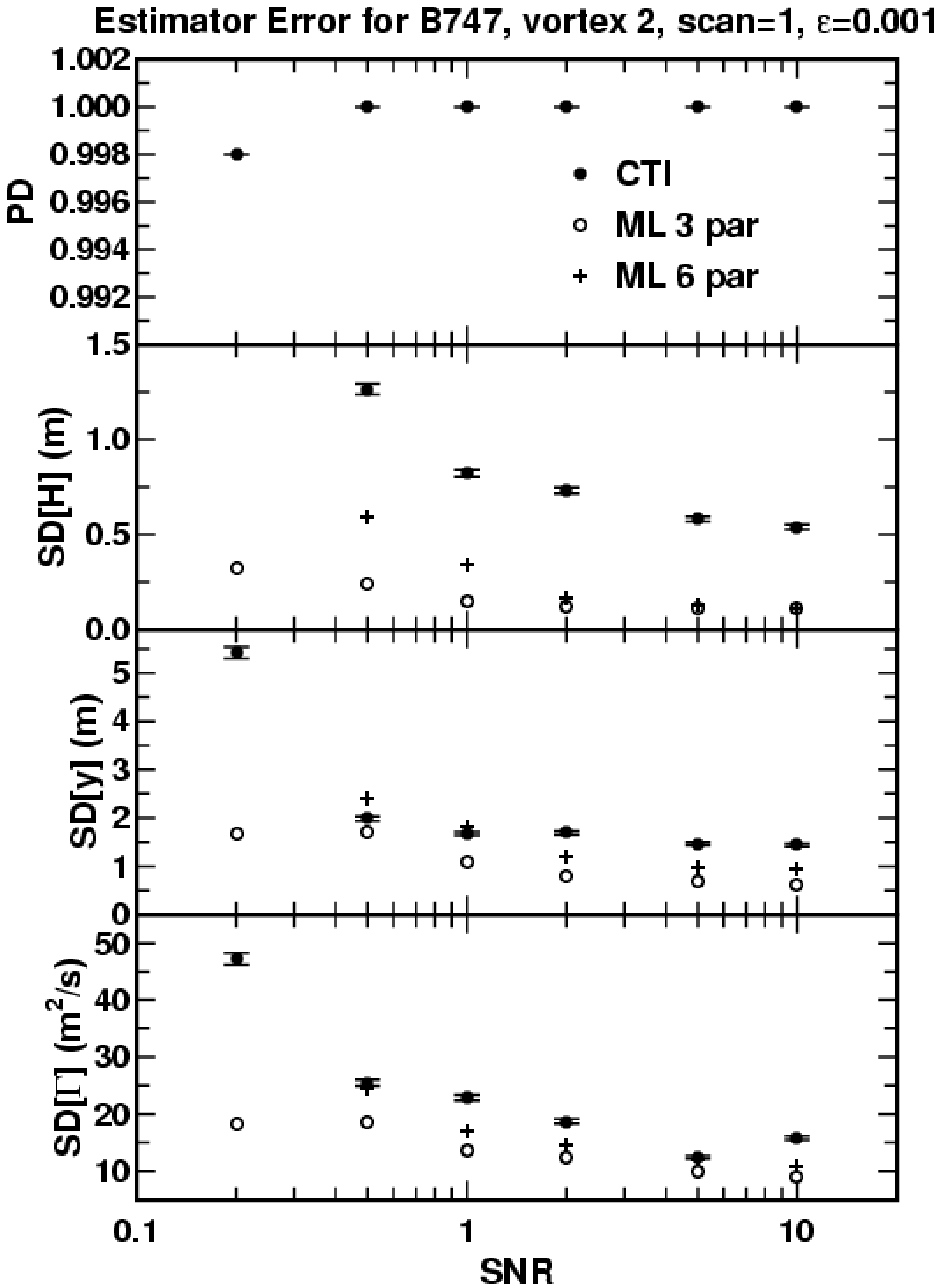

Figure 48. The detection probability (PD) of the CTI algorithm and the standard deviation (SD) of estimates of vortex parameters as a function of SNR for vortex 2 of the Boeing 747 with added turbulence. The correct values are H=146.75 m, y=1151.48 m, and Γ=492.84 m^2/s.

3.10 CTI Tracking Performance for Boeing 737 Vortex

The performance of the CTI algorithm of the vortex estimates after first detection is described by the PDF of the estimates, the bias, and the standard deviation (SD) or random estimation error. The PDF's have similar behavior to the detection case. The bias and SD are shown in Figure 49 to Figure 56 for lidar scan 4 and the two cases of no turbulence (ε=0.0) and the turbulence case (ε=0.001). The bias for vortex location is small however; the bias in vortex strength Γ is a function of SNR. The detection probability PD is very high for SNR greater than 0.5. The SD of the estimates for vortex location (H,y) is small over the regime where the vortex is clearly detected, i.e., PD=1. The performance of the CTI estimates for the no turbulence case and lidar scan 16 is shown in Figure 57 to Figure 60. Since the vortex strength Γ=76.2 m^2/s, the bias in the estimates of Γ is large and the SNR required for a detection is larger. However, the estimates of vortex location are still reasonably accurate. Table 5 summarizes the simulations that were performed in order to evaluate the performance of the CTI tracking algorithms for the Boeing 737. The results are shown in Figure 49 through Figure 60.

Table 5. Performance Simulations of CTI Tracking Algorithms - 737

ε	Vortex	Scan No.	Figure No.
Bias - SNR, H, Y, Γ			
0	1	4	49
0	2	4	50
0.001	1	4	51
0.001	2	4	52
PD, SD(H), SD(Y), SD(Γ)			
0	1	4	53
0	2	4	54
0.001	1	4	55
0.001	2	4	56
Bias - SNR, H, Y, Γ			
0	1	16	57
0	2	16	58
PD, SD(H), SD(Y), SD(Γ)			
0	1	16	59
0	2	16	60

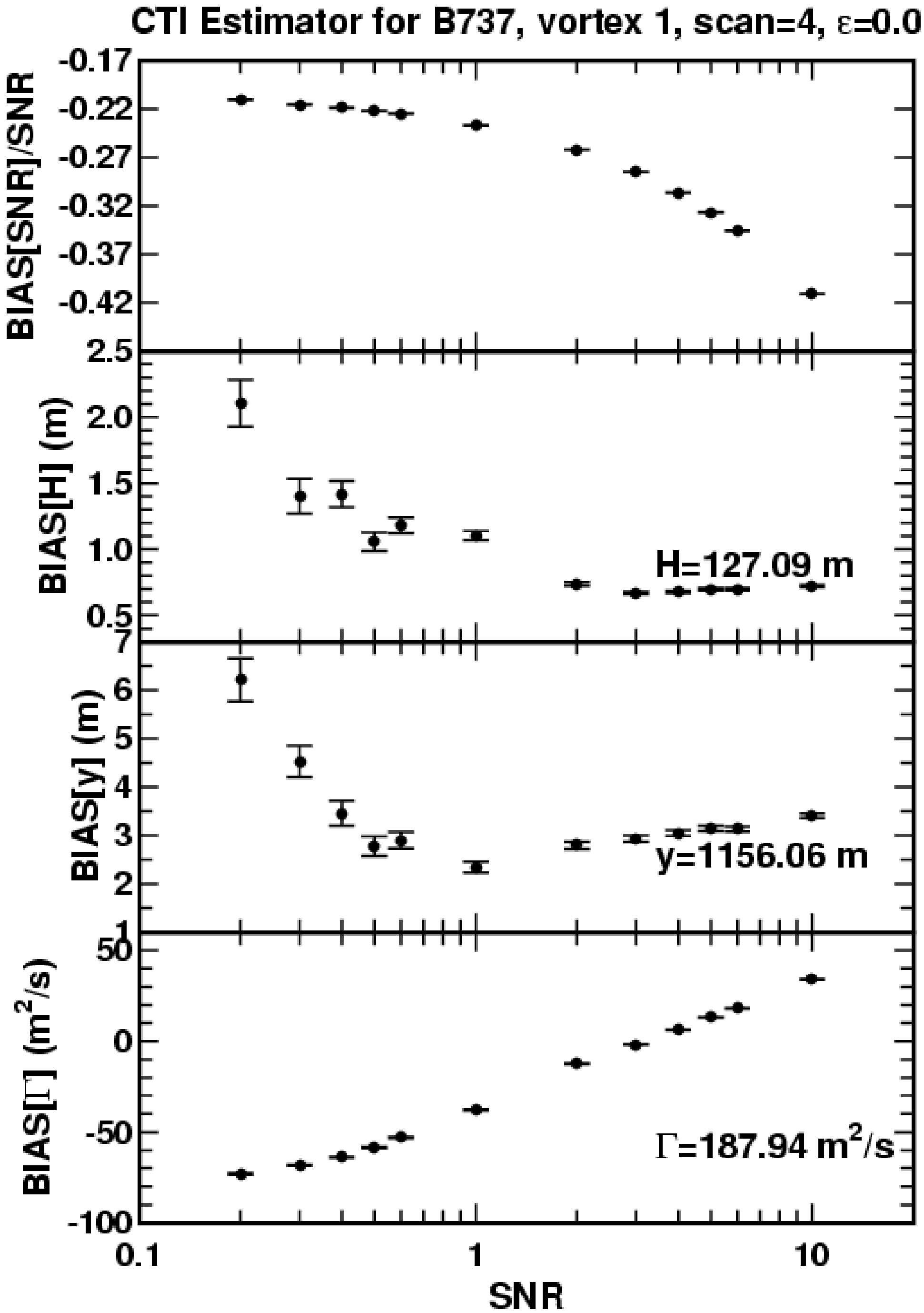

Figure 49. Bias of CTI estimates of the Boeing 737 vortex parameters for vortex 1 of lidar scan 4 as a function of SNR for no added turbulence (ε=0.0). The correct values are indicated.

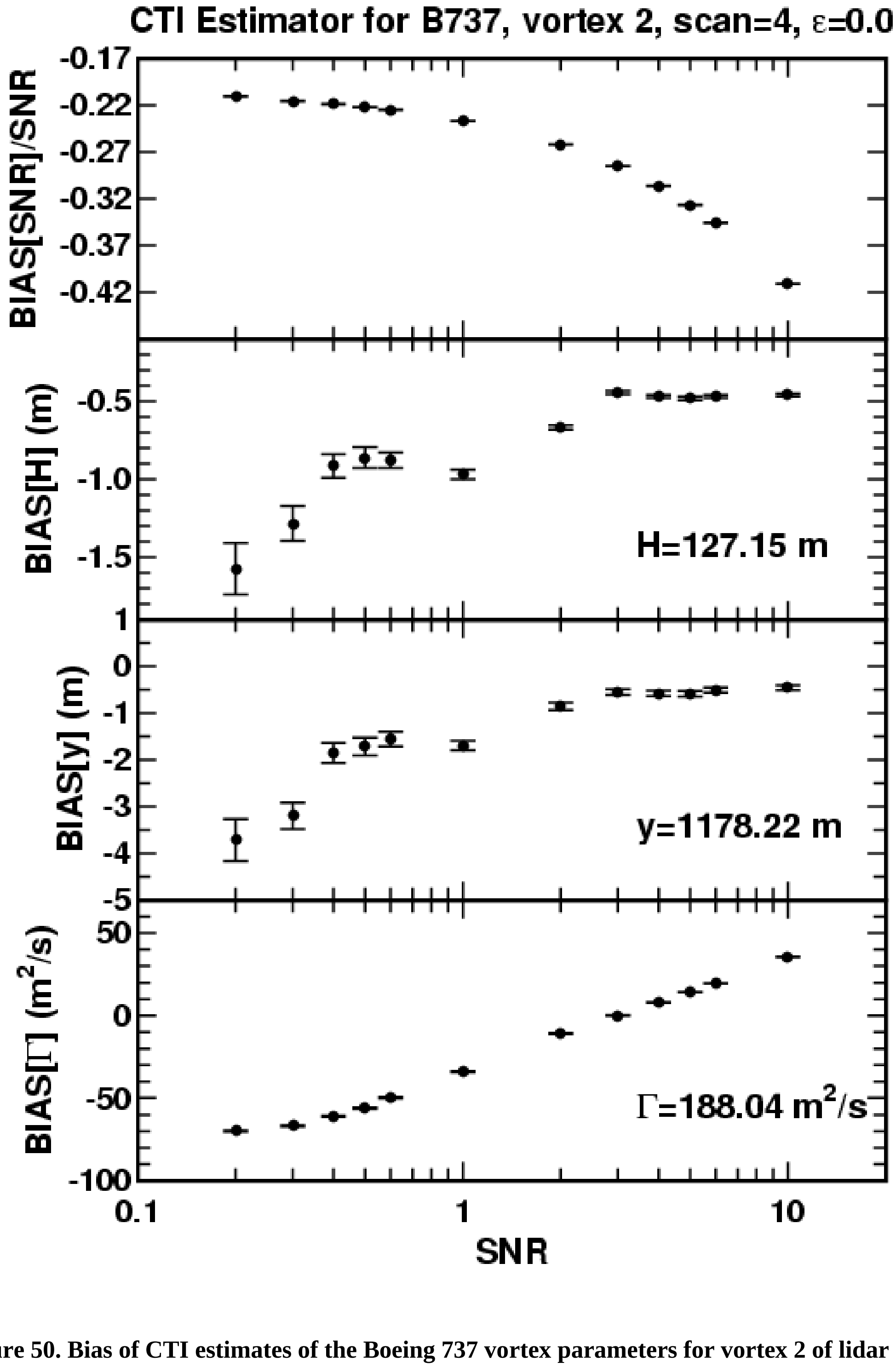

Figure 50. Bias of CTI estimates of the Boeing 737 vortex parameters for vortex 2 of lidar scan 4 as a function of SNR for no added turbulence (ε=0.0). The correct values are indicated.

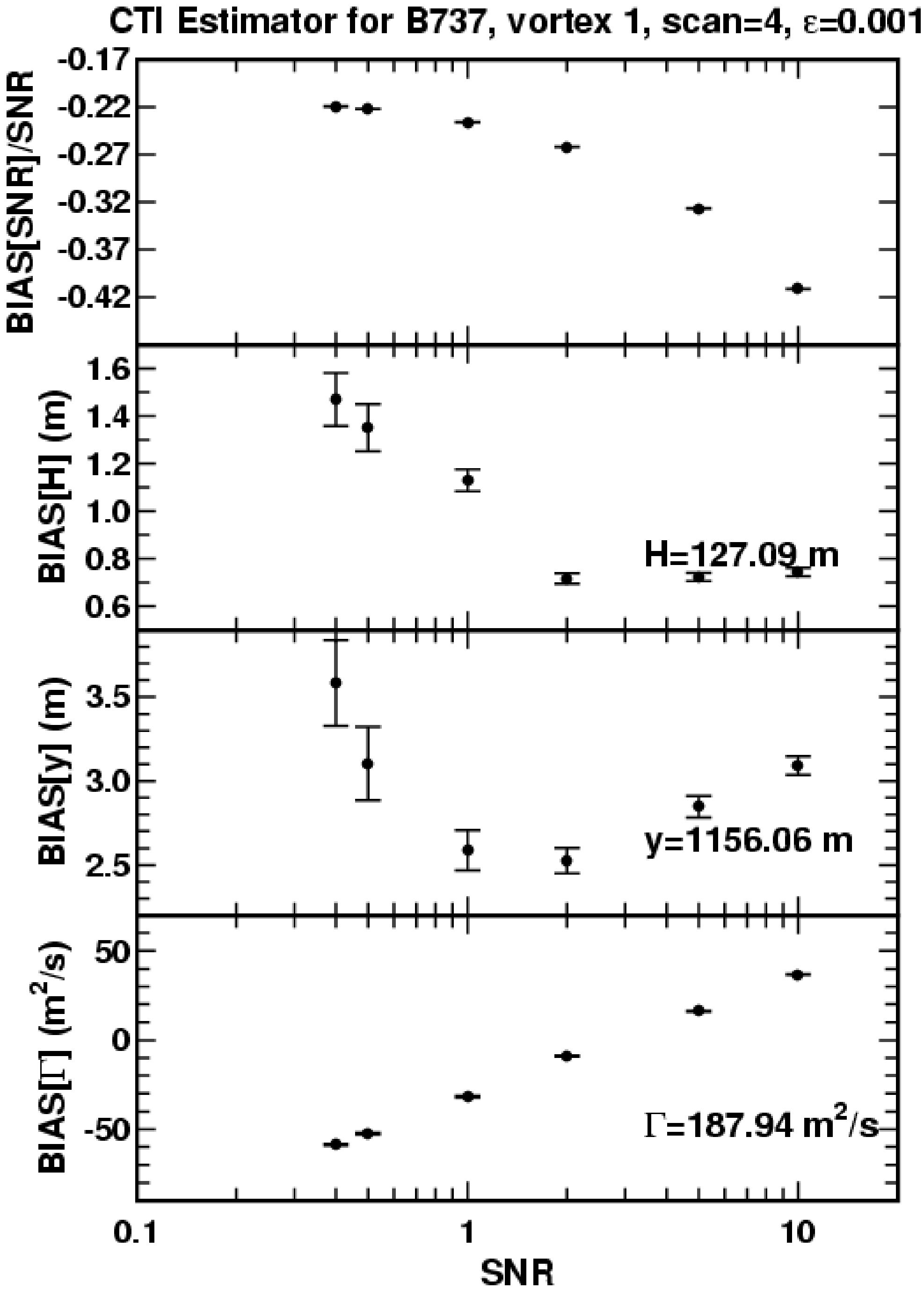

Figure 51. Bias of CTI estimates of the Boeing 737 vortex parameters for vortex 1 of lidar scan 4 as a function of SNR for added turbulence (ε=0.001). The correct values are indicated.

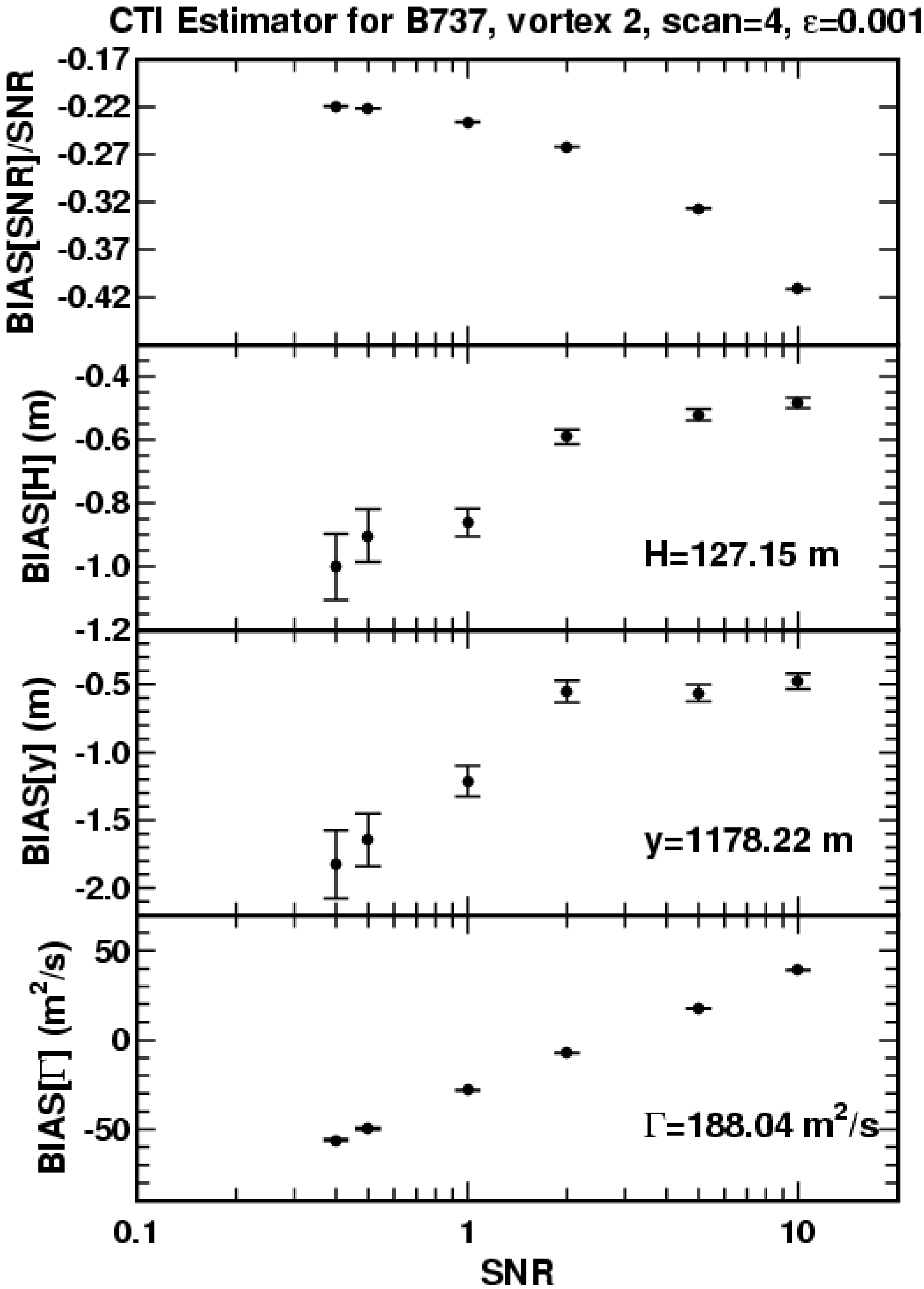

Figure 52. Bias of CTI estimates of the Boeing 737 vortex parameters for vortex 2 of lidar scan 4 as a function of SNR for added turbulence (ε=0.001). The correct values are indicated.

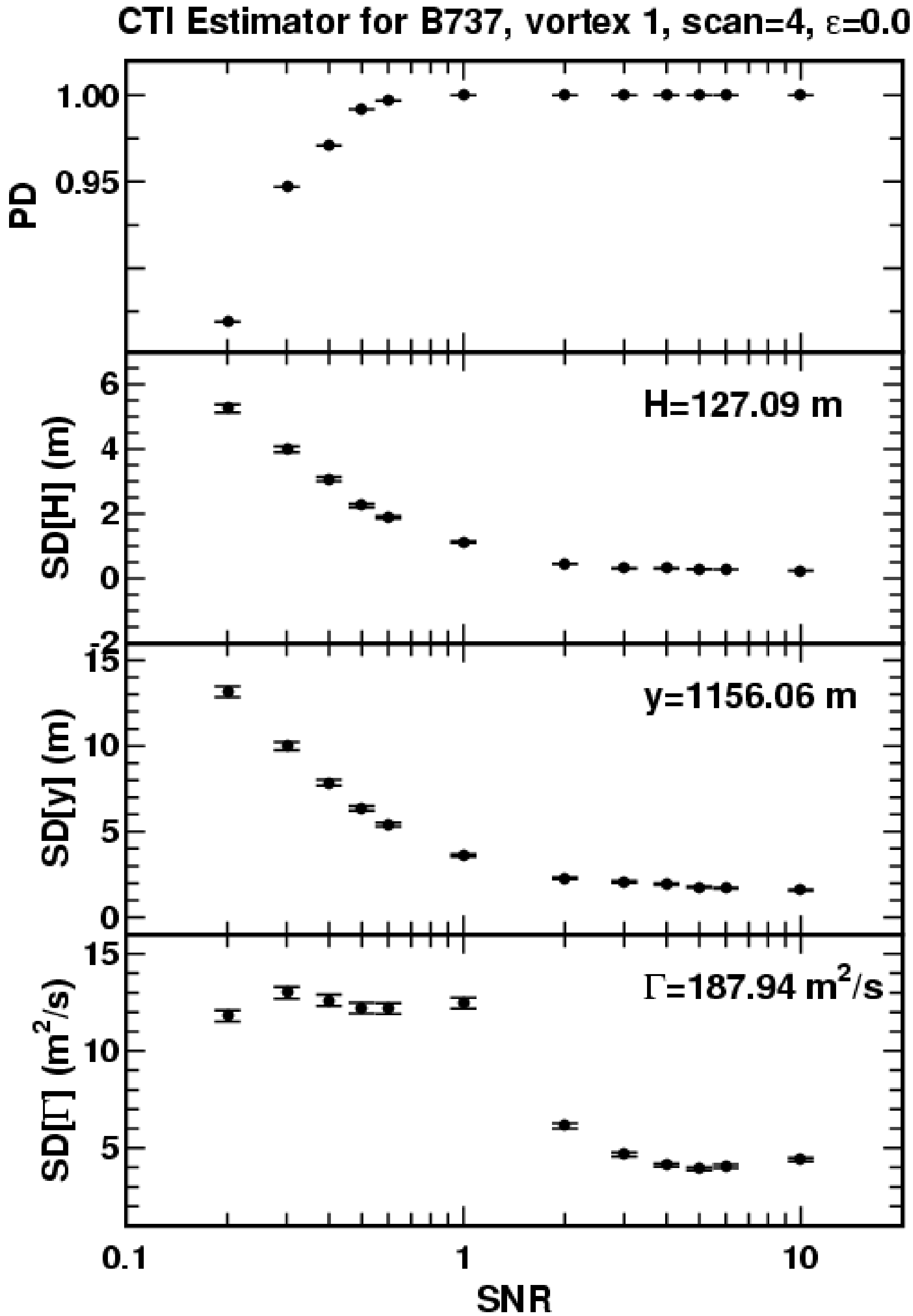

Figure 53. Detection probability (PD) and standard deviation (SD) of CTI estimates of the Boeing 737 vortex parameters for vortex 1 of lidar scan 4 as a function of SNR for no added turbulence (ε=0.0). The correct values are indicated.

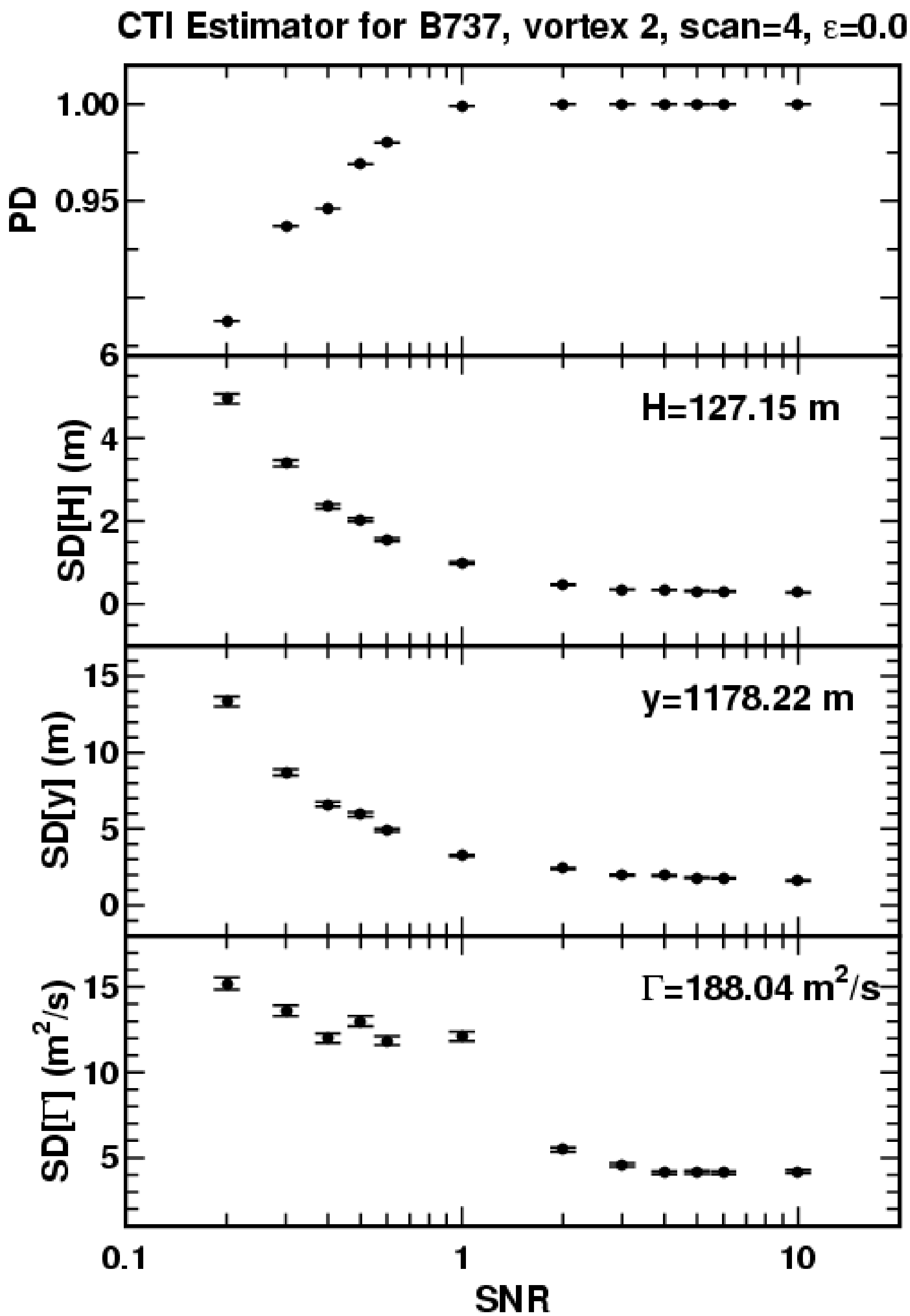

Figure 54. Detection probability (PD) and standard deviation (SD) of CTI estimates of the Boeing 737 vortex parameters for vortex 2 of lidar scan 4 as a function of SNR for no added turbulence (ε=0.0). The correct values are indicated.

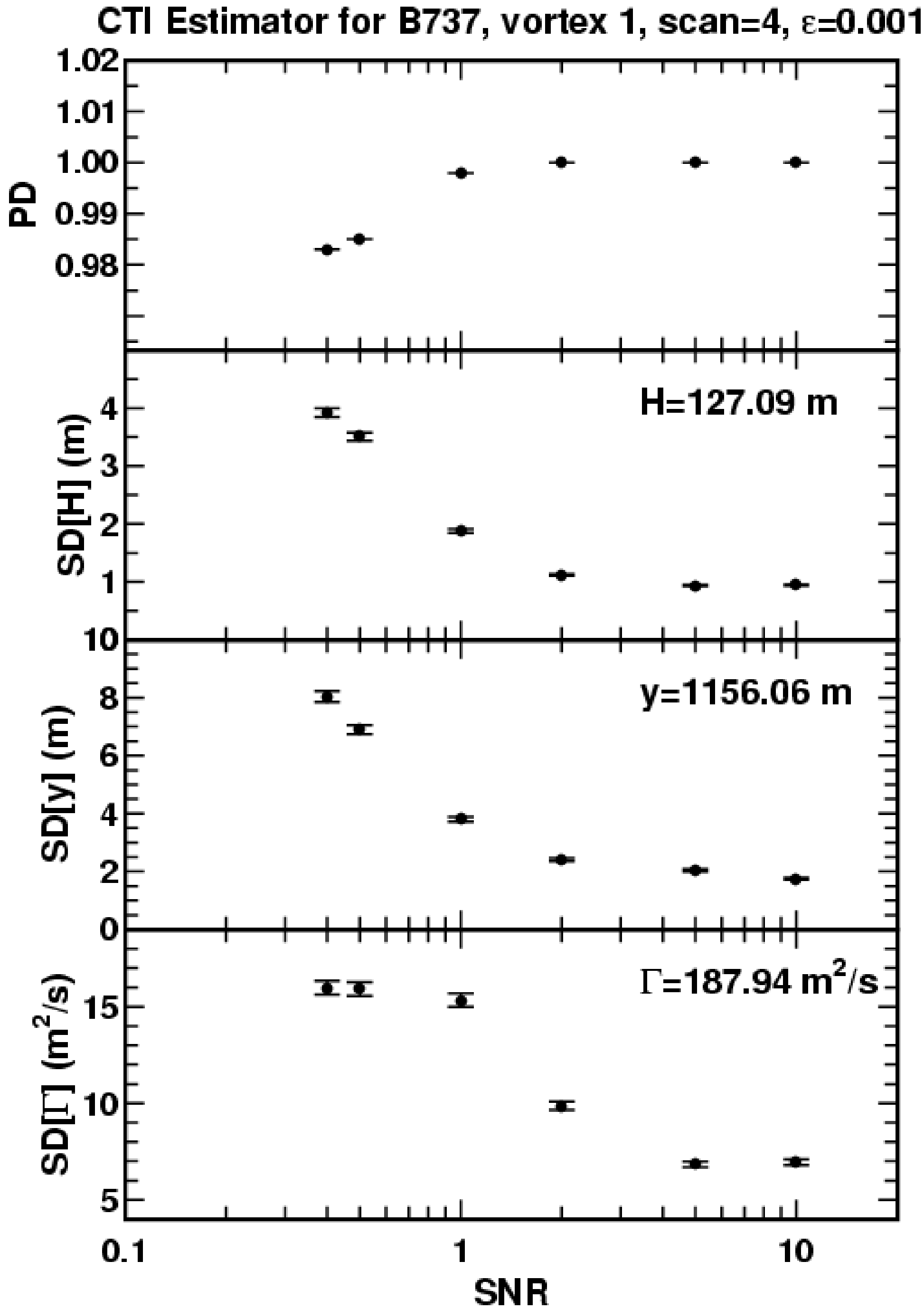

Figure 55. Detection probability (PD) and standard deviation (SD) of CTI estimates of the Boeing 737 vortex parameters for vortex 1 of lidar scan 4 as a function of SNR for added turbulence (ε=0.001). The correct values are indicated.

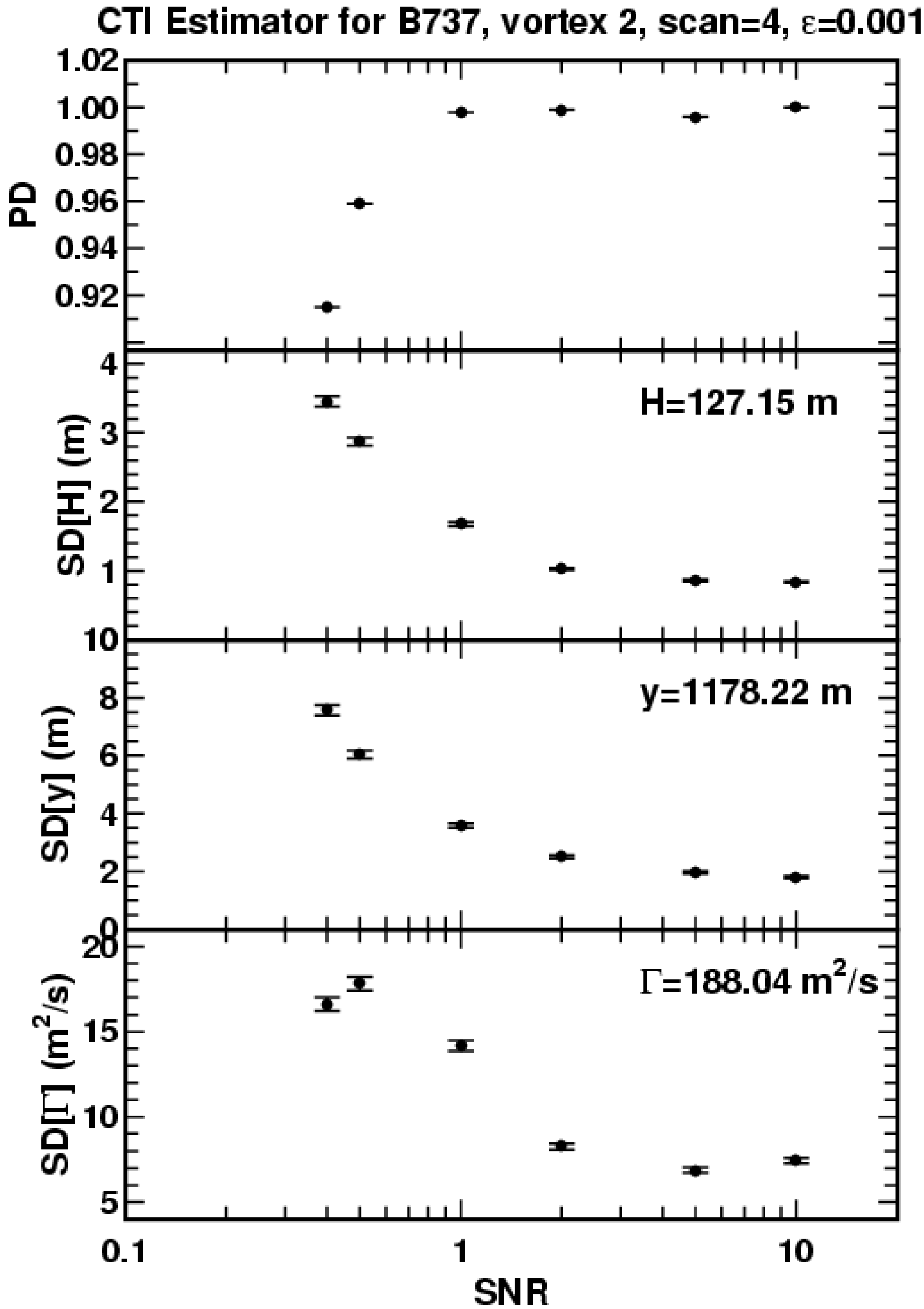

Figure 56. Detection probability (PD) and standard deviation (SD) of CTI estimates of the Boeing 737 vortex parameters for vortex 2 of lidar scan 4 as a function of SNR for added turbulence (ε=0.001). The correct values are indicated.

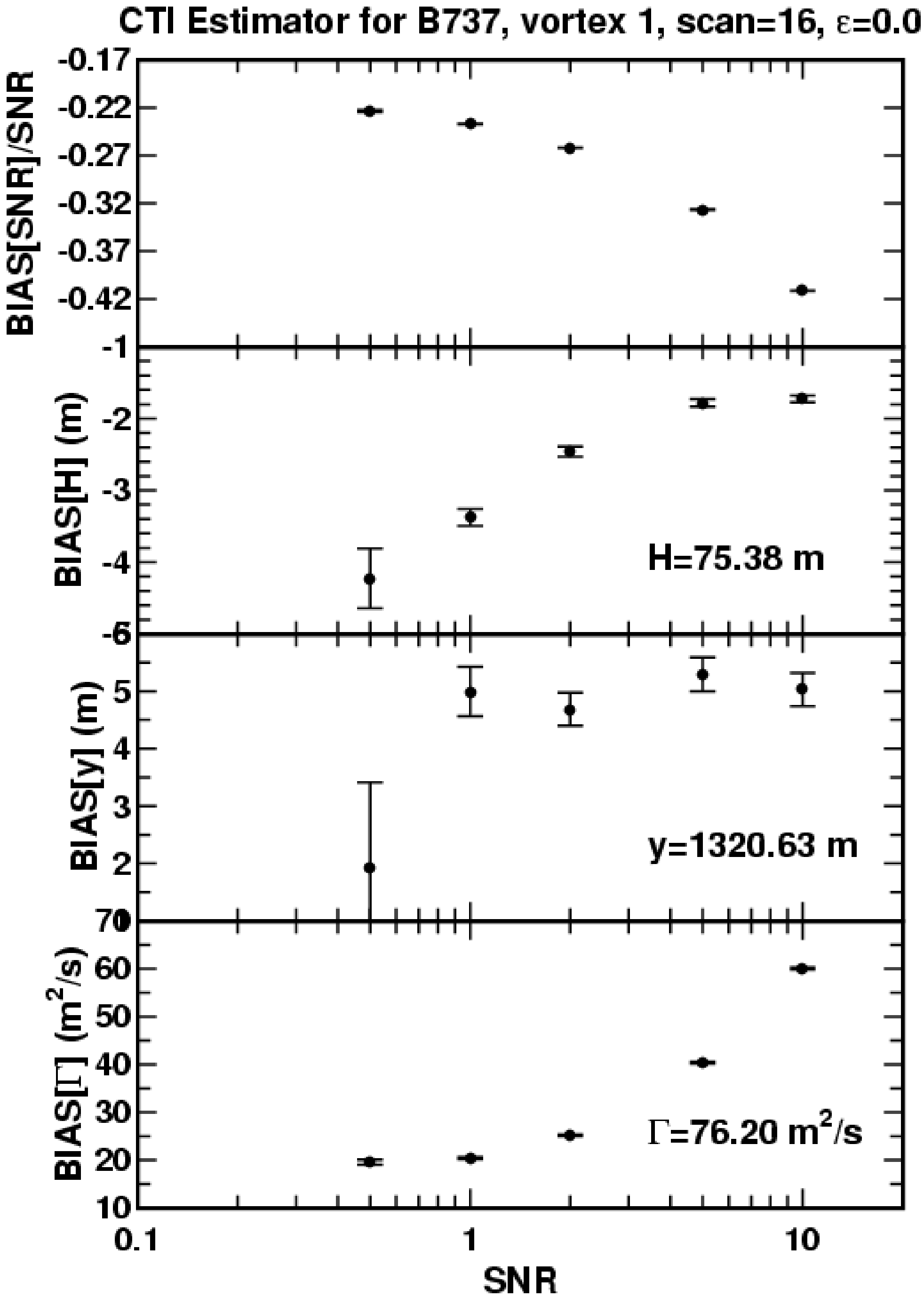

Figure 57. Bias of CTI estimates of the Boeing 737 vortex parameters for vortex 1 of lidar scan 16 as a function of SNR for no added turbulence (ε=0.0). The correct values are indicated.

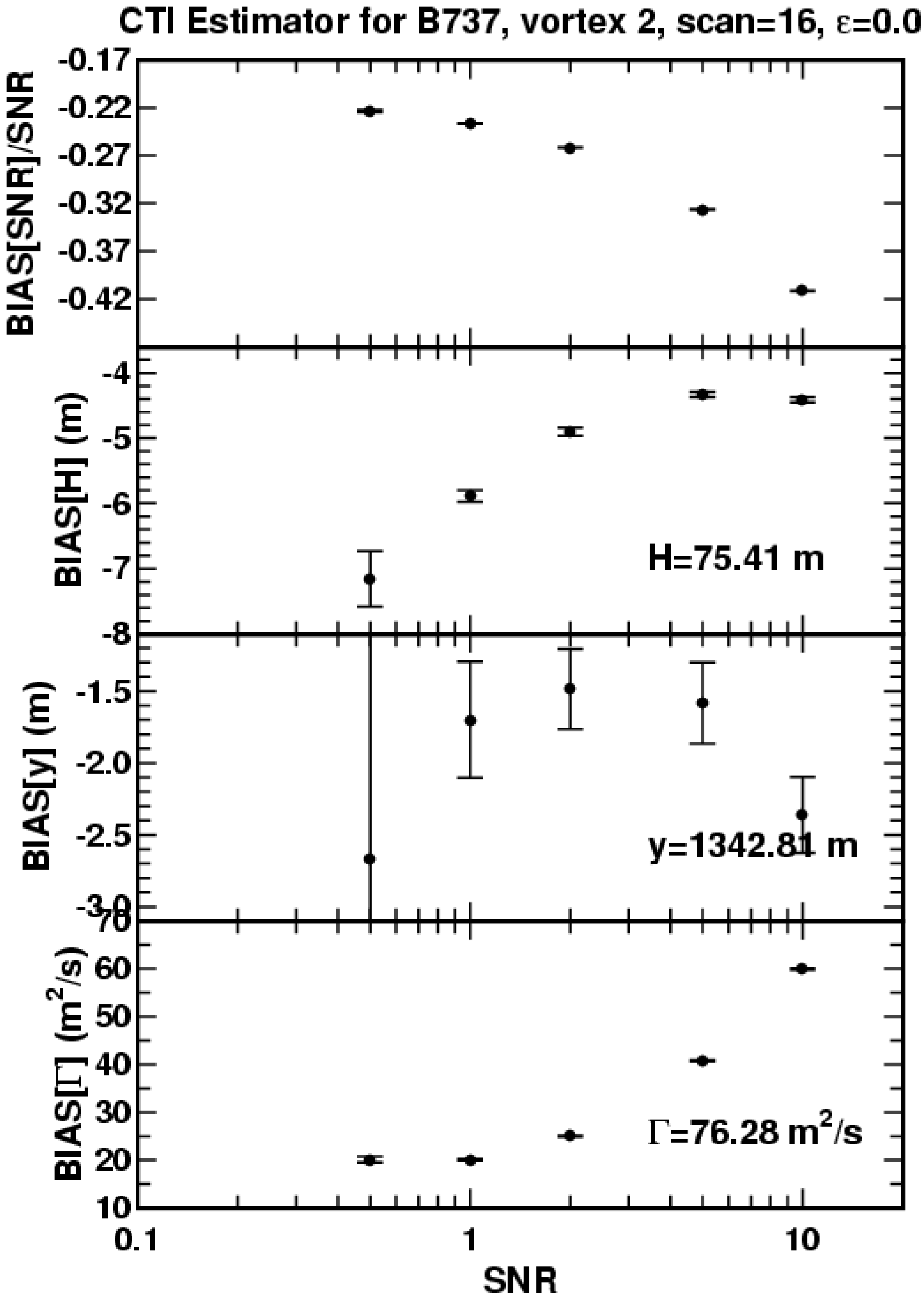

Figure 58. Bias of CTI estimates of the Boeing 737 vortex parameters for vortex 2 of lidar scan 16 as a function of SNR for no added turbulence (ε=0.0). The correct values are indicated.

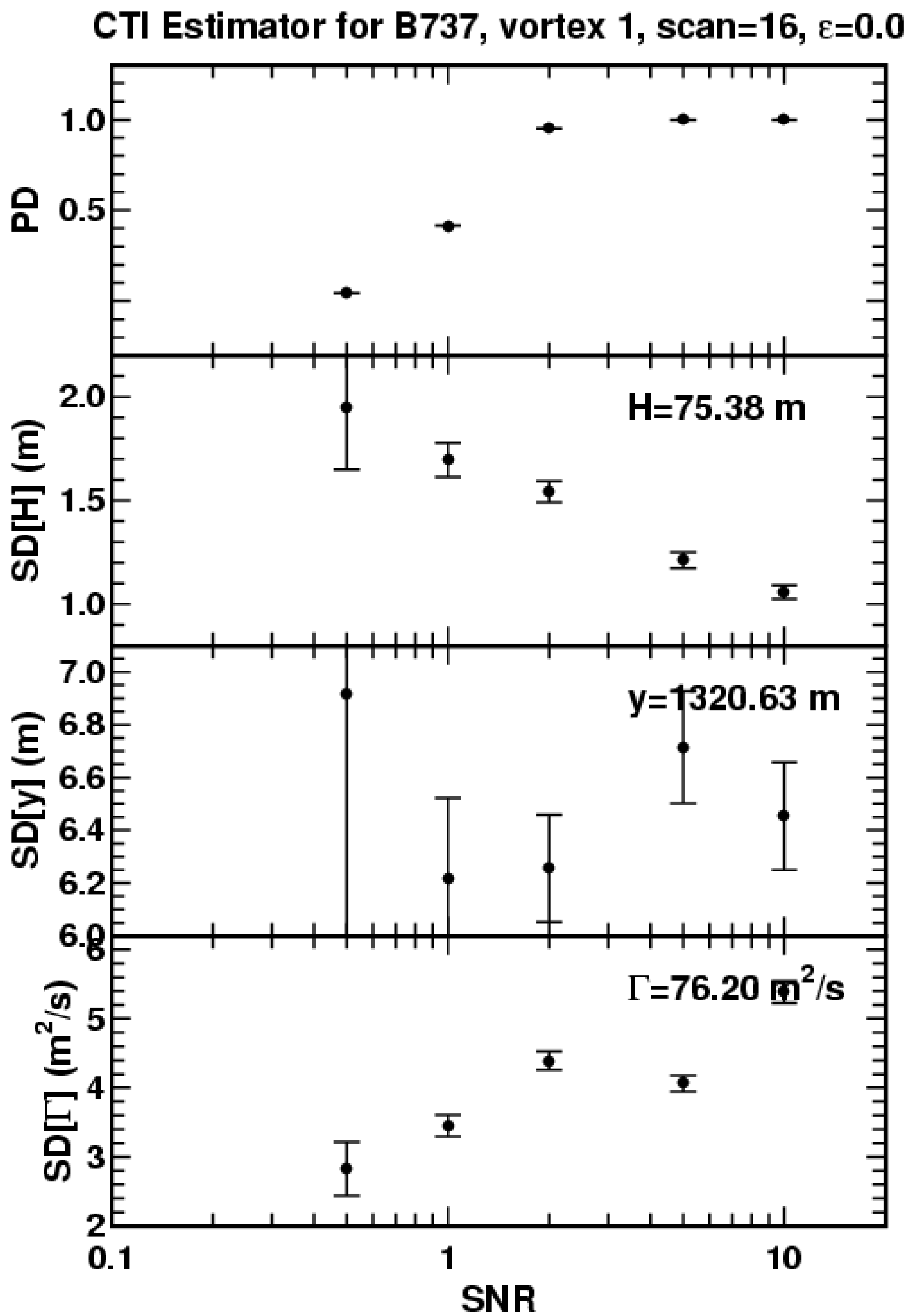

Figure 59. Detection probability (PD) and standard deviation (SD) of CTI estimates of the Boeing 737 vortex parameters for vortex 1 of lidar scan 16 as a function of SNR for no added turbulence (ε=0.0). The correct values are indicated.

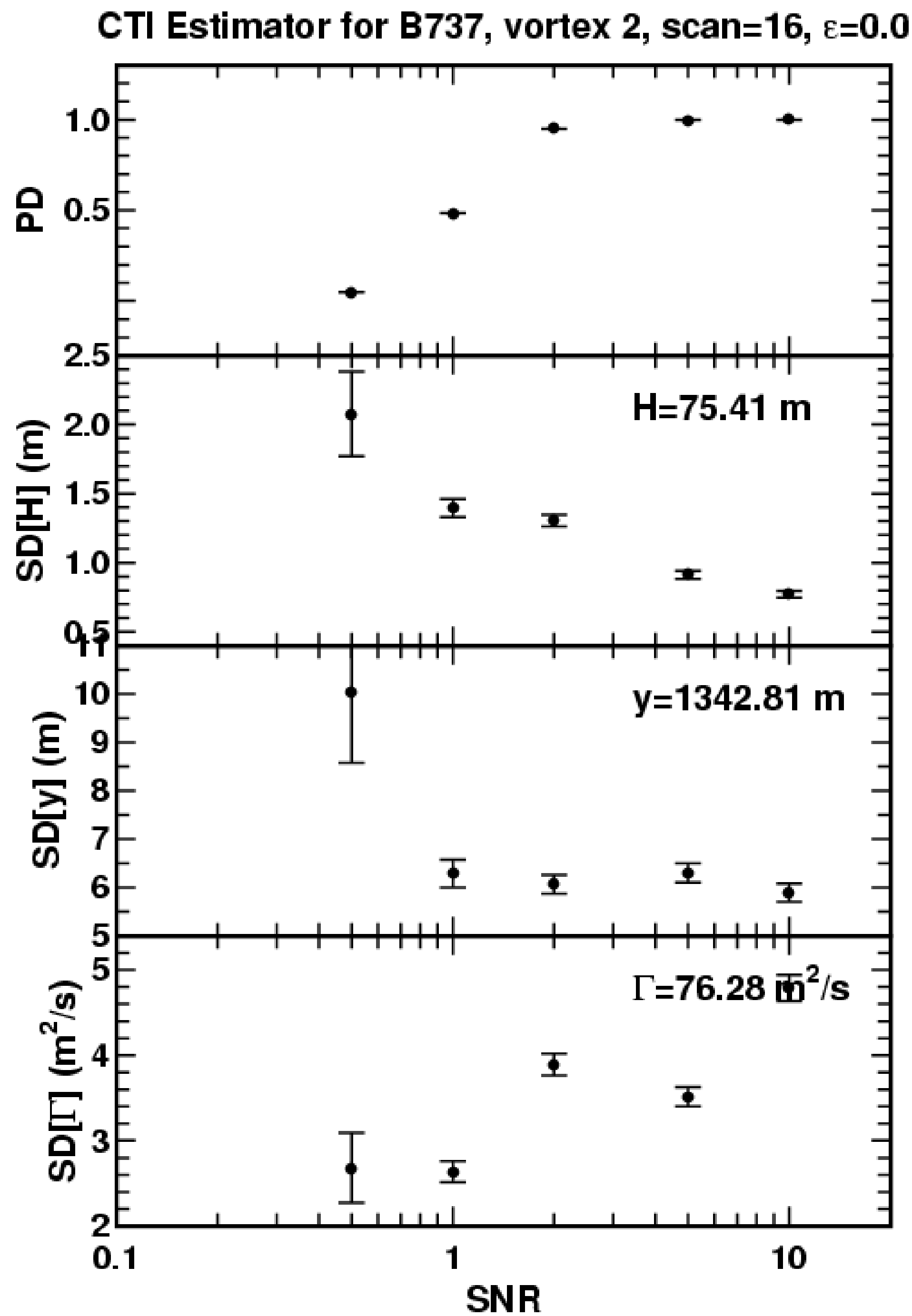

Figure 60. Detection probability (PD) and standard deviation (SD) of CTI estimates of the Boeing 737 vortex parameters for vortex 1 of lidar scan 16 as a function of SNR for no added turbulence (ε=0.0). The correct values are indicated.

3.11 CTI Tracking Performance for Boeing 747 Vortex

The performance of the CTI algorithm of the vortex estimates after first detection is described by the PDF of the estimates, the bias, and the standard deviation (SD) or random estimation error. The PDFs have similar behavior to the detection case and the plots are contained on a CD. The bias and SD are shown in Figure 61 to Figure 68 for lidar scan 4 and the two cases of no turbulence (ε=0.0) and the turbulence case (ε=0.001). The bias for vortex location is small however, the bias in vortex strength Γ is a function of SNR. The detection probability PD is very high for SNR greater than 0.5. The SD of the estimates is small over the regime where there is clearly a detection, i.e., PD=1. The performance of the CTI estimates for the no turbulence case and lidar scan 22 is shown in Figure 69 to Figure 72. Since the vortex strength Γ=162 m^2/s, the bias in the estimates of Γ is large and the SNR required for a detection is larger. However, the estimates of vortex location are still reasonably accurate. Table 6 summarizes the simulations that were performed in order to evaluate the performance of the CTI tracking algorithms for the Boeing 747. The results are shown in Figure 61 through Figure 72.

Table 6. Performance Simulations of CTI Tracking Algorithms - 747

ε	Vortex	Scan No.	Figure No.
Bias - SNR, H, Y, Γ			
0	1	4	61
0	2	4	62
0.001	1	4	63
0.001	2	4	64
PD, SD(H), SD(Y), SD(Γ)			
0	1	4	65
0	2	4	66
0.001	1	4	67
0.001	2	4	68
Bias - SNR, H, Y, Γ			
0	1	22	69
0	2	22	70
PD, SD(H), SD(Y), SD(Γ)			
0	1	22	71
0	2	22	72

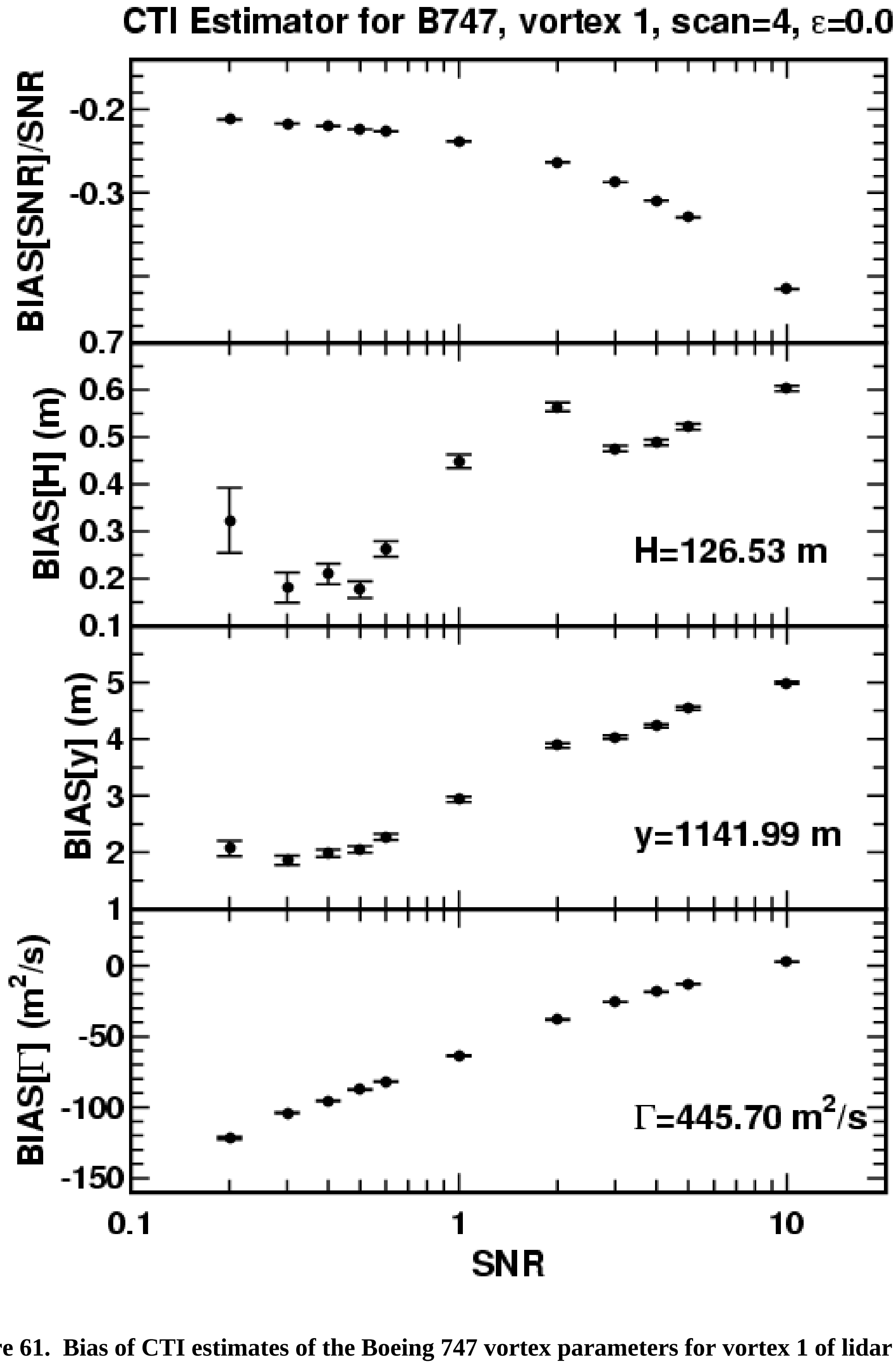

Figure 61. Bias of CTI estimates of the Boeing 747 vortex parameters for vortex 1 of lidar scan 4 as a function of SNR for no added turbulence (ε=0.0). The correct values are indicated.

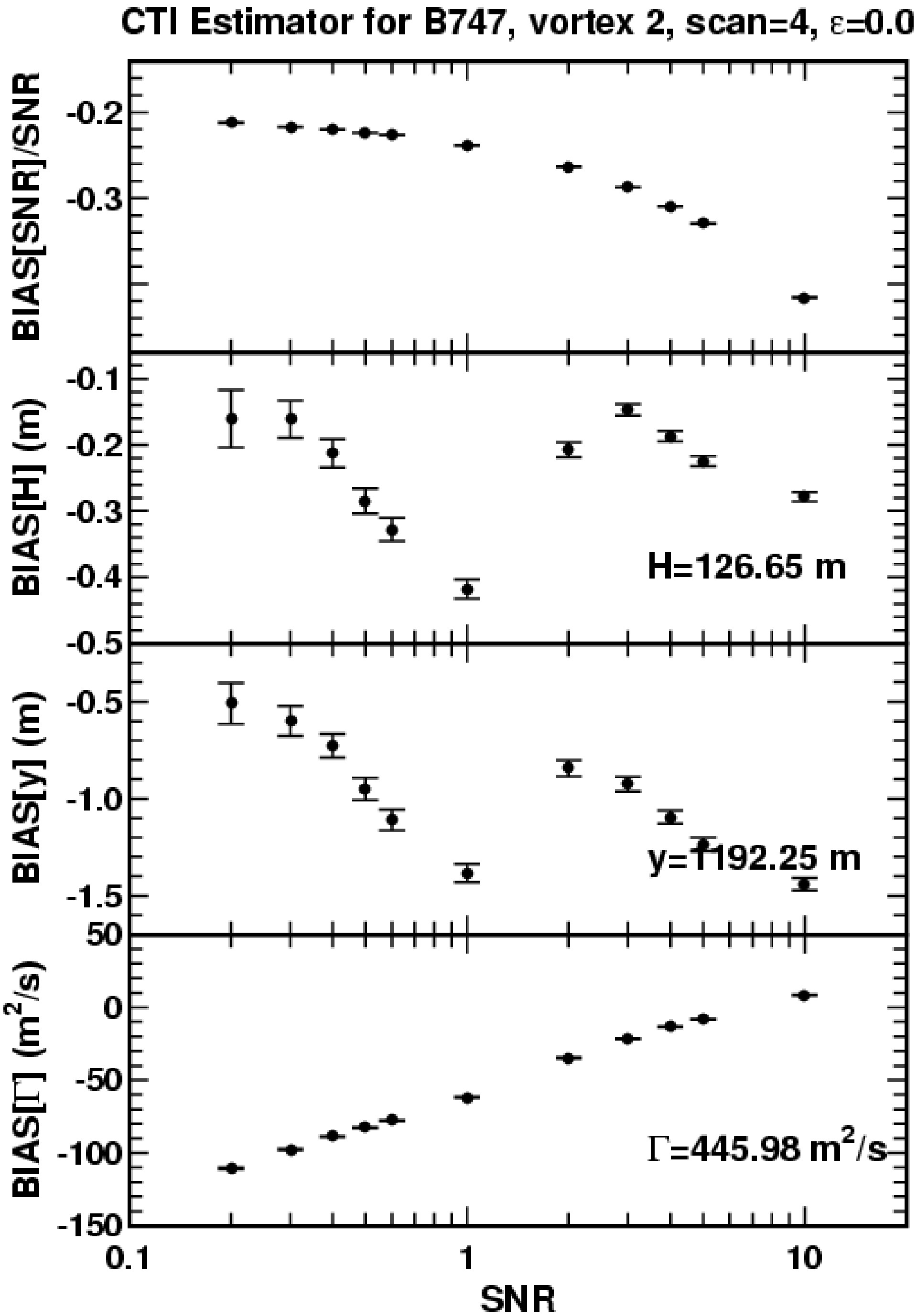

Figure 62. Bias of CTI estimates of the Boeing 747 vortex parameters for vortex 2 of lidar scan 4 as a function of SNR for no added turbulence (ε=0.0). The correct values are indicated.

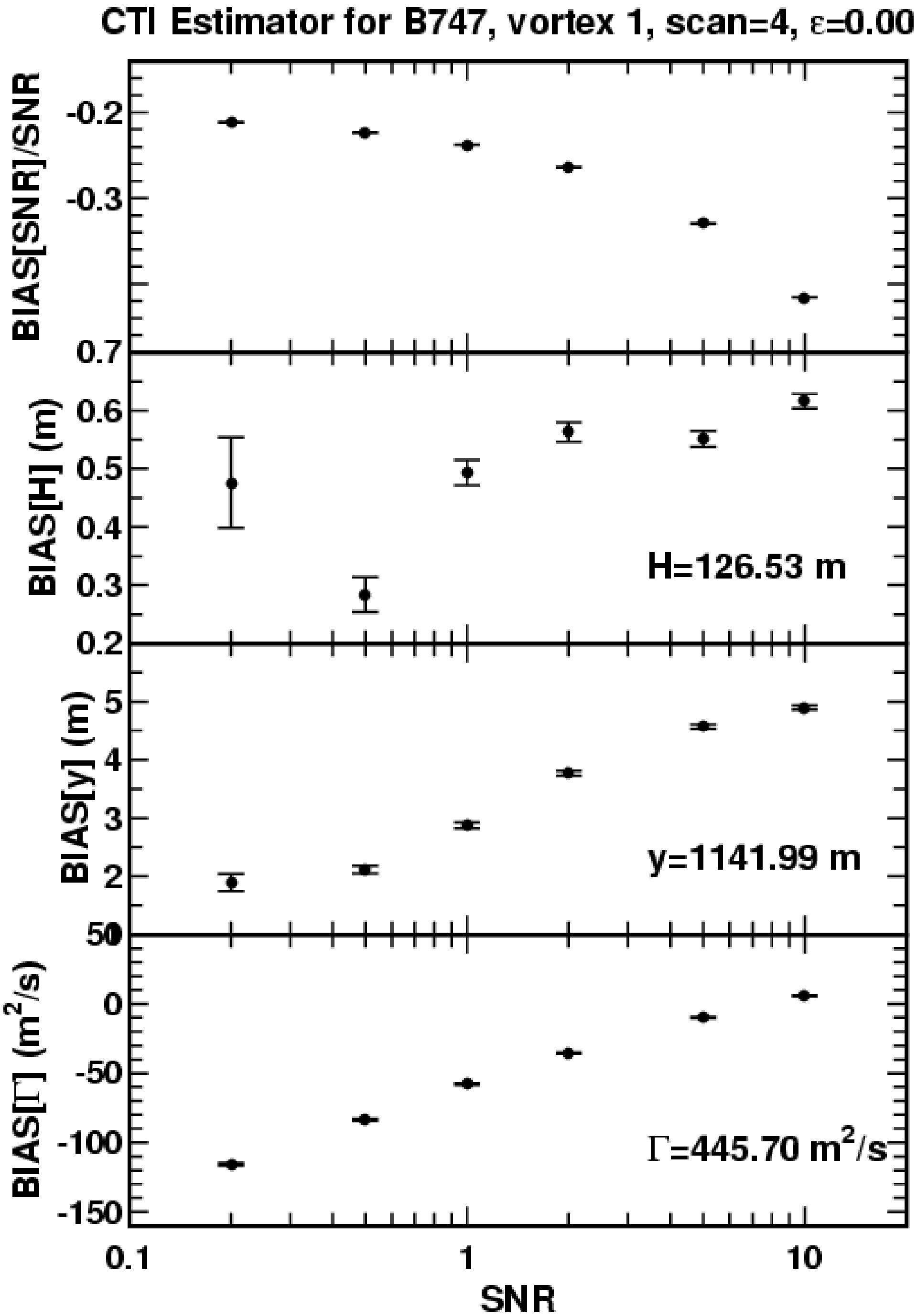

Figure 63. Bias of CTI estimates of the Boeing 747 vortex parameters for vortex 1 of lidar scan 4 as a function of SNR for added turbulence (ε=0.001). The correct values are indicated.

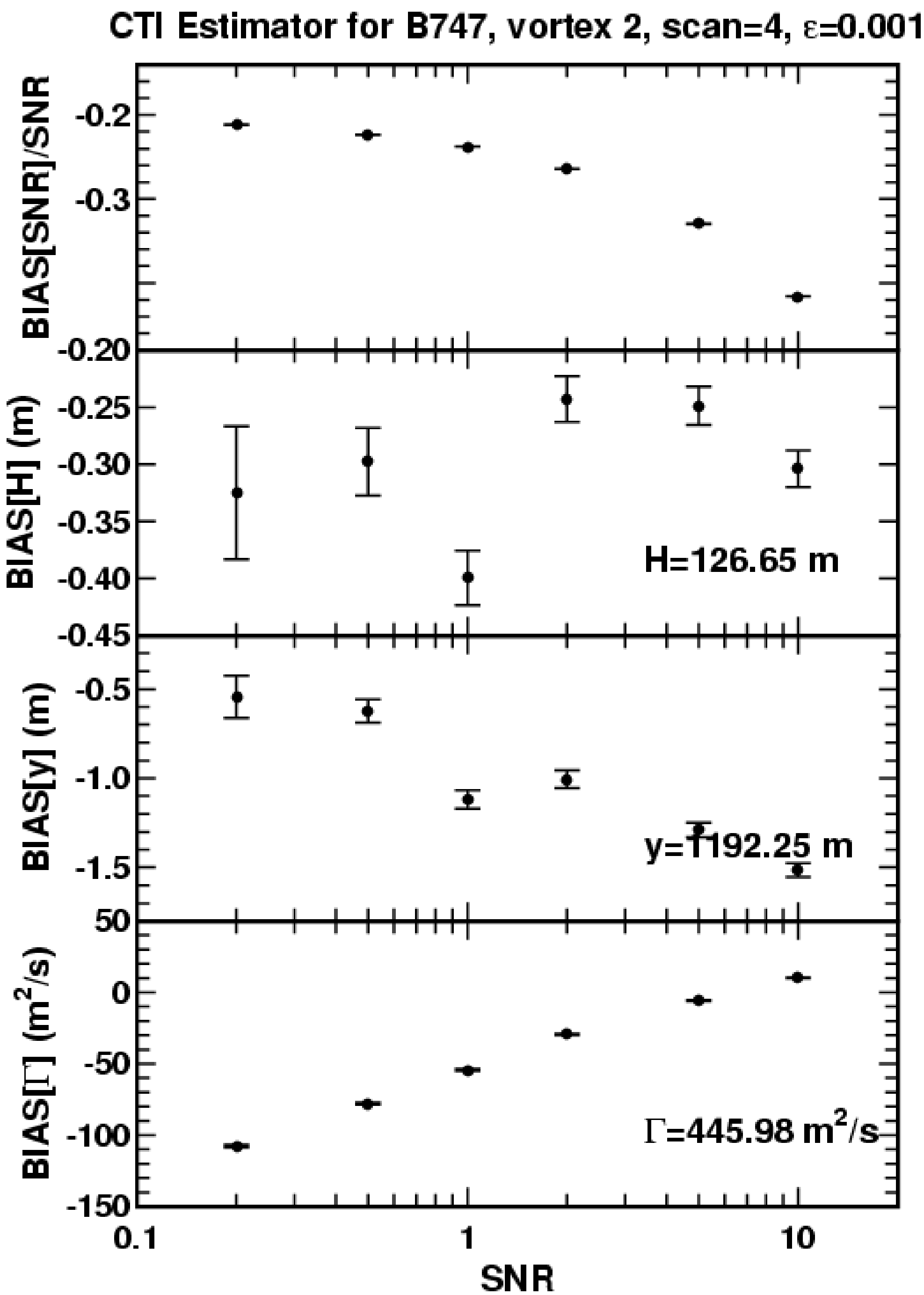

Figure 64. Bias of CTI estimates of the Boeing 747 vortex parameters for vortex 2 of lidar scan 4 as a function of SNR for added turbulence (ε=0.001). The correct values are indicated.

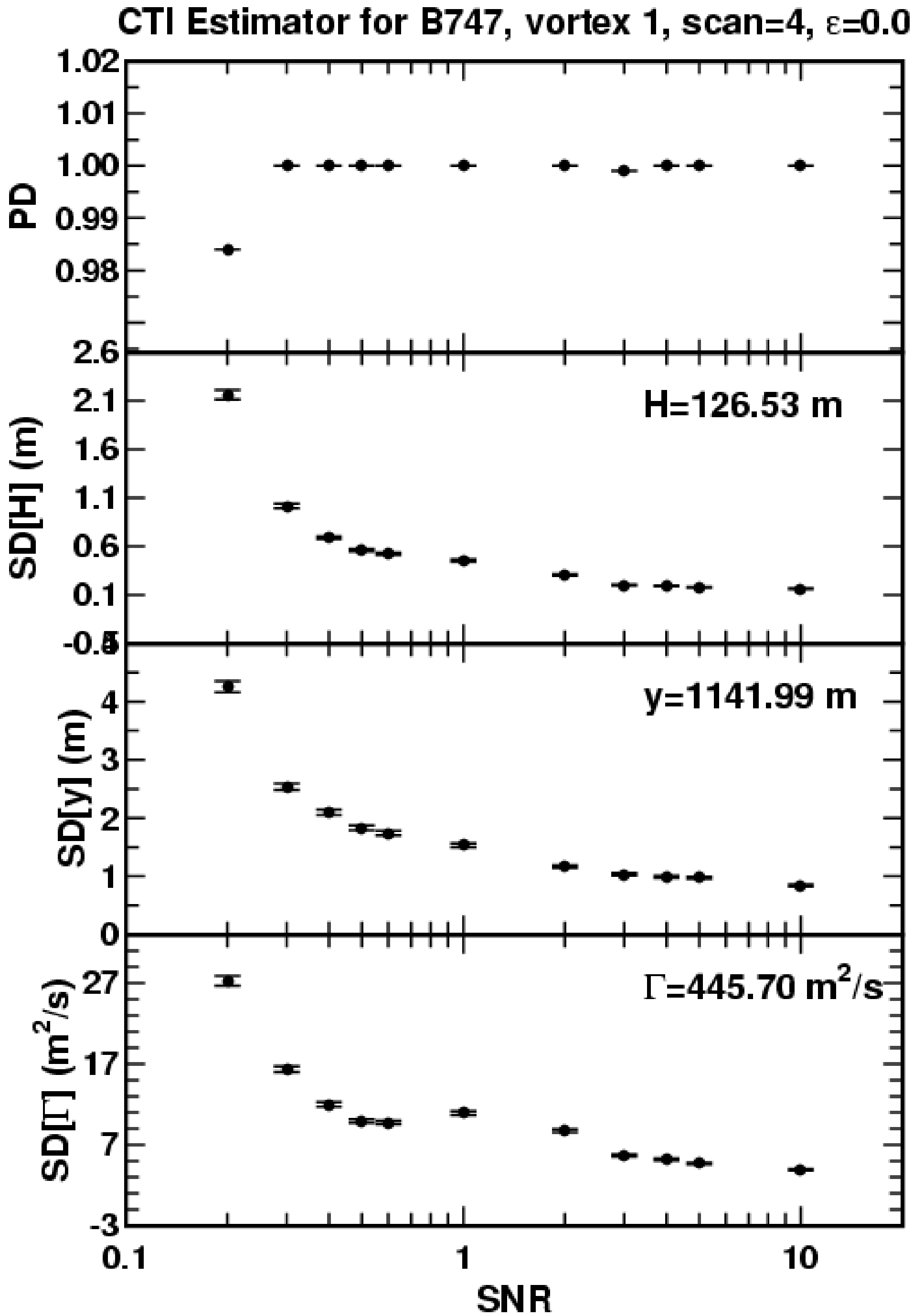

Figure 65. Detection probability (PD) and standard deviation (SD) of CTI estimates of the Boeing 747 vortex parameters for vortex 1 of lidar scan 4 as a function of SNR for no added turbulence (ε=0.0). The correct values are indicated.

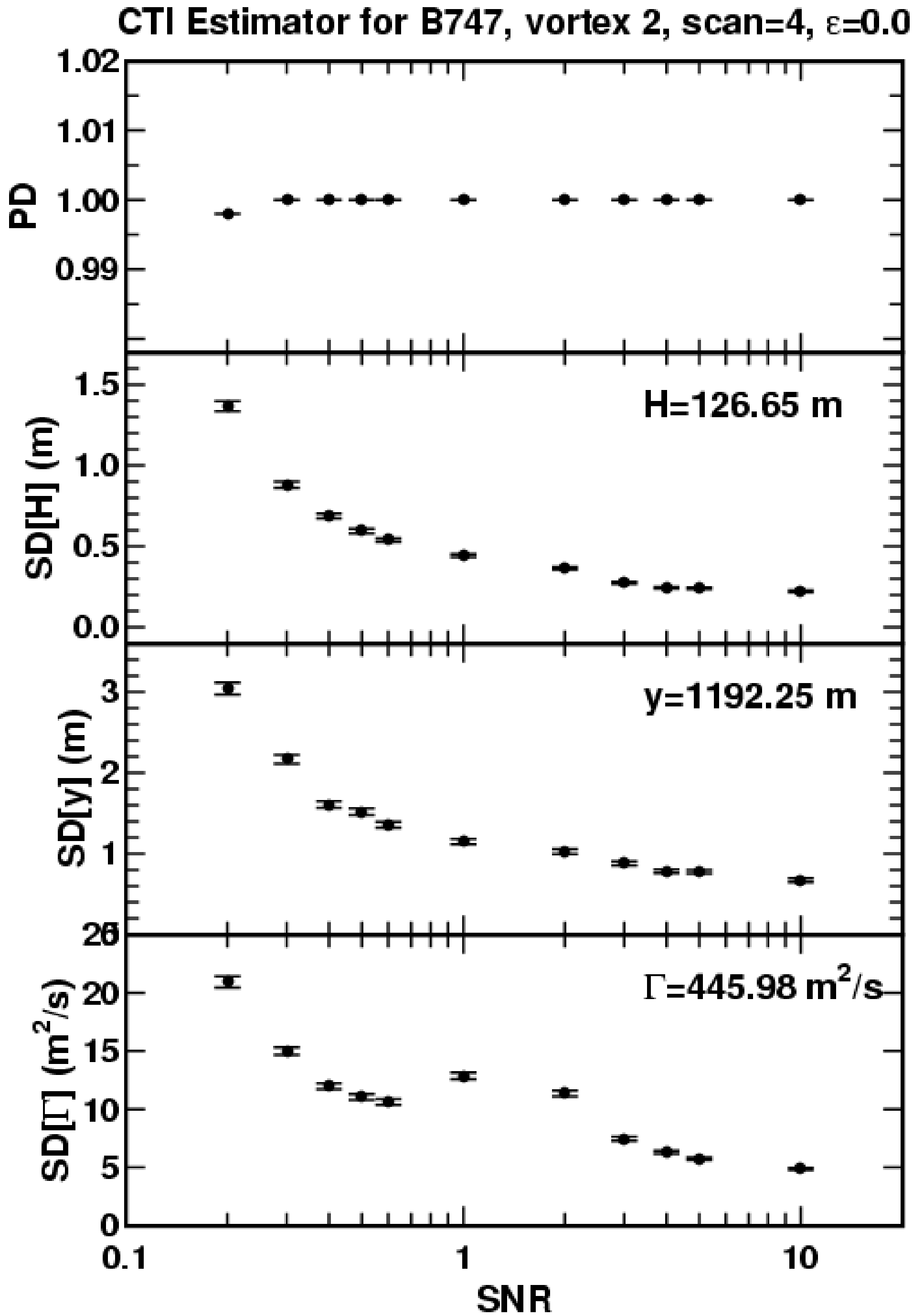

Figure 66. Detection probability (PD) and standard deviation (SD) of CTI estimates of the Boeing 747 vortex parameters for vortex 2 of lidar scan 4 as a function of SNR for no added turbulence (ε=0.0). The correct values are indicated.

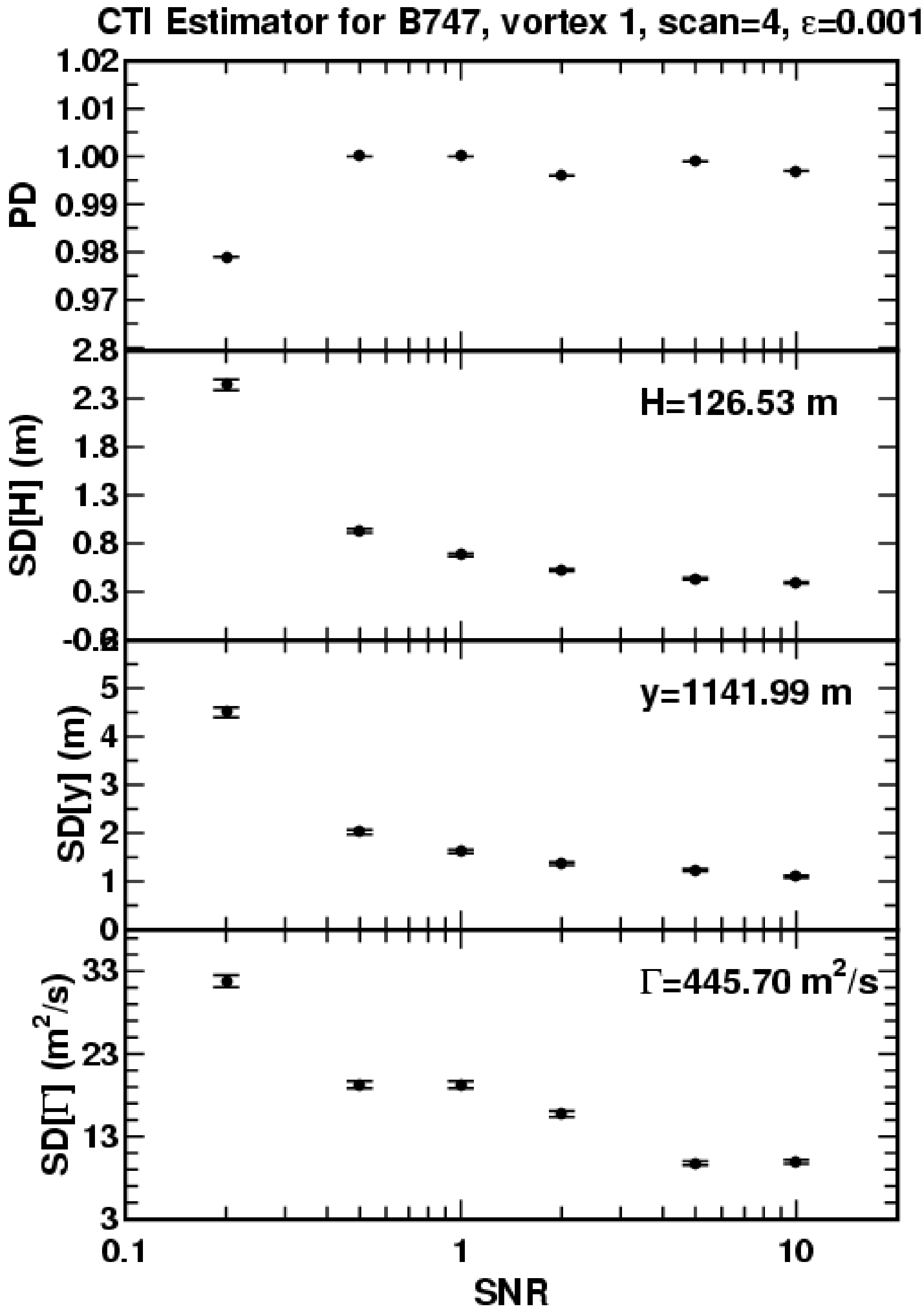

Figure 67. Detection probability (PD) and standard deviation (SD) of CTI estimates of the Boeing 747 vortex parameters for vortex 1 of lidar scan 4 as a function of SNR for added turbulence (ε=0.001). The correct values are indicated.

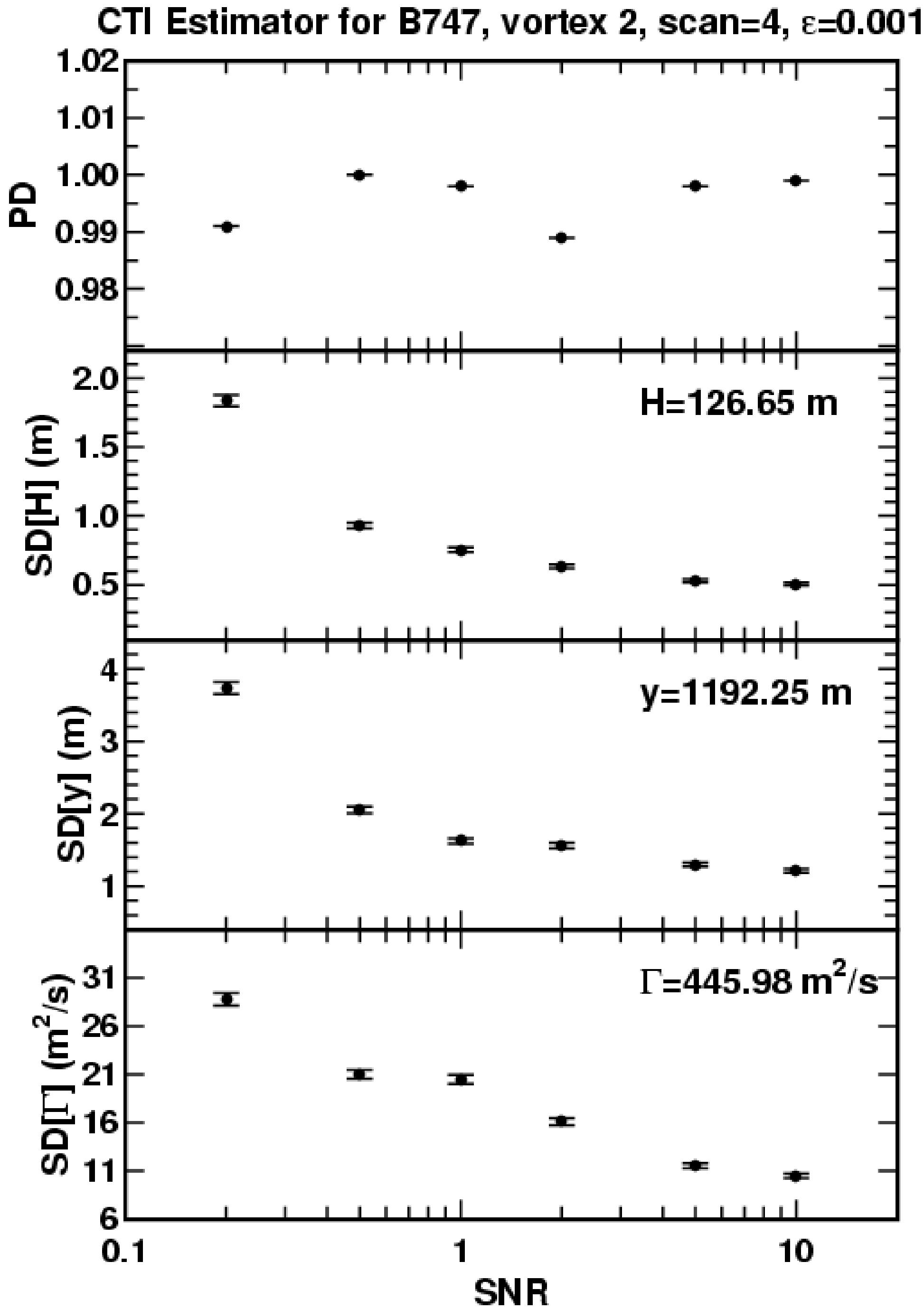

Figure 68. Detection probability (PD) and standard deviation (SD) of CTI estimates of the Boeing 747 vortex parameters for vortex 2 of lidar scan 4 as a function of SNR for added turbulence (ε=0.001). The correct values are indicated.

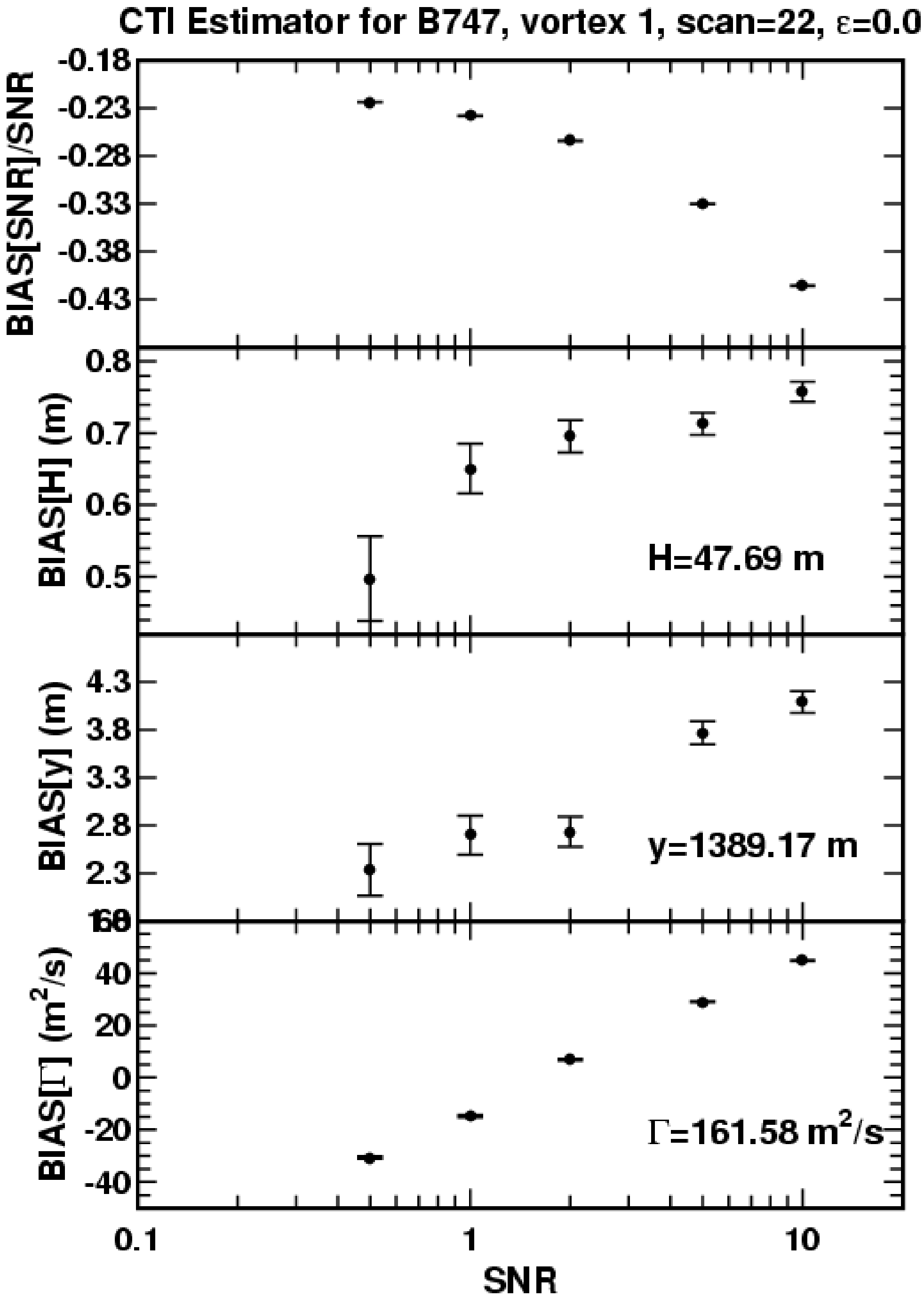

Figure 69. Bias of CTI estimates of the Boeing 747 vortex parameters for vortex 1 of lidar scan 22 as a function of SNR for no added turbulence (ε=0.0). The correct values are indicated.

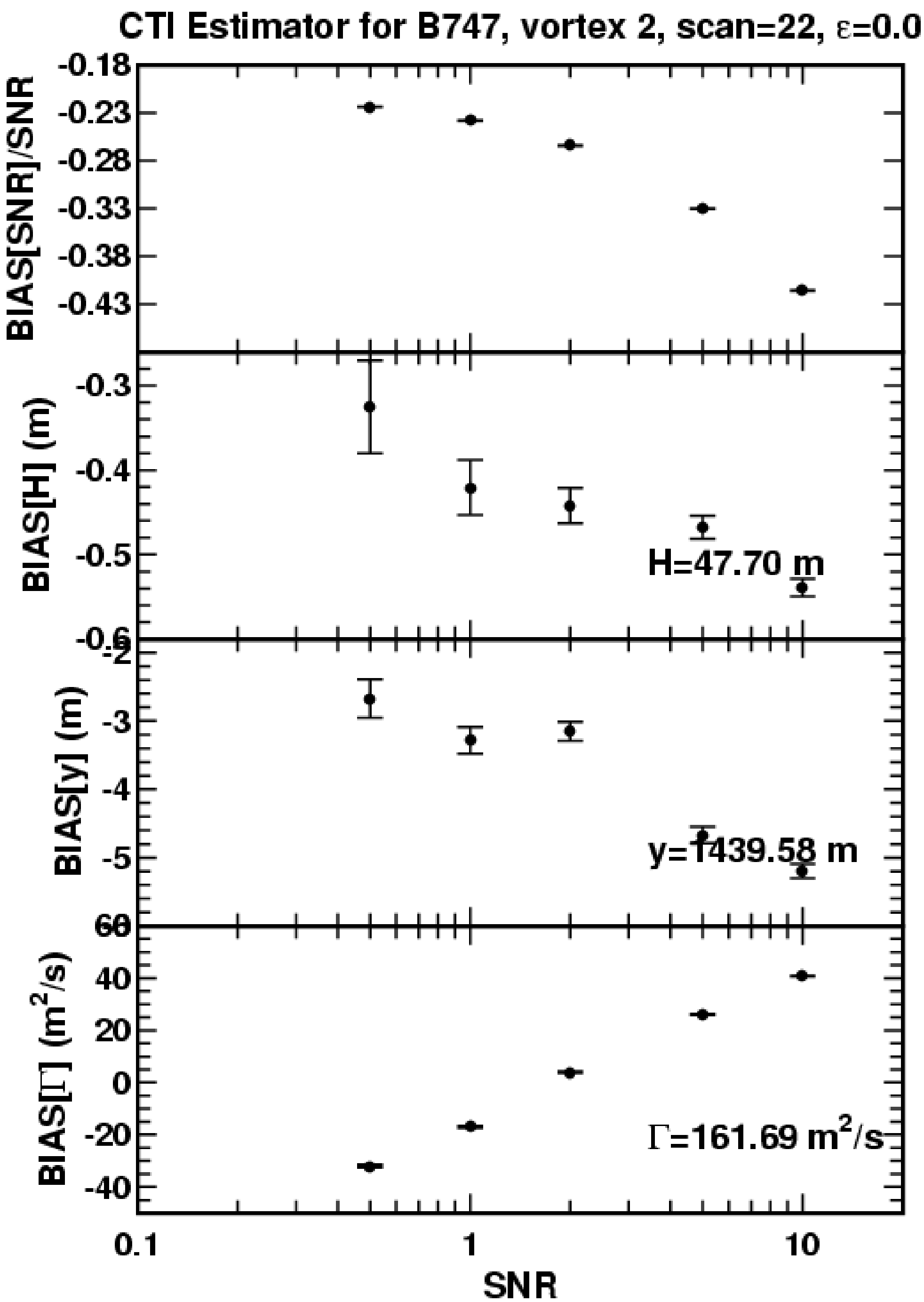

Figure 70. Bias of CTI estimates of the Boeing 747 vortex parameters for vortex 2 of lidar scan 22 as a function of SNR for no added turbulence (ε=0.0). The correct values are indicated.

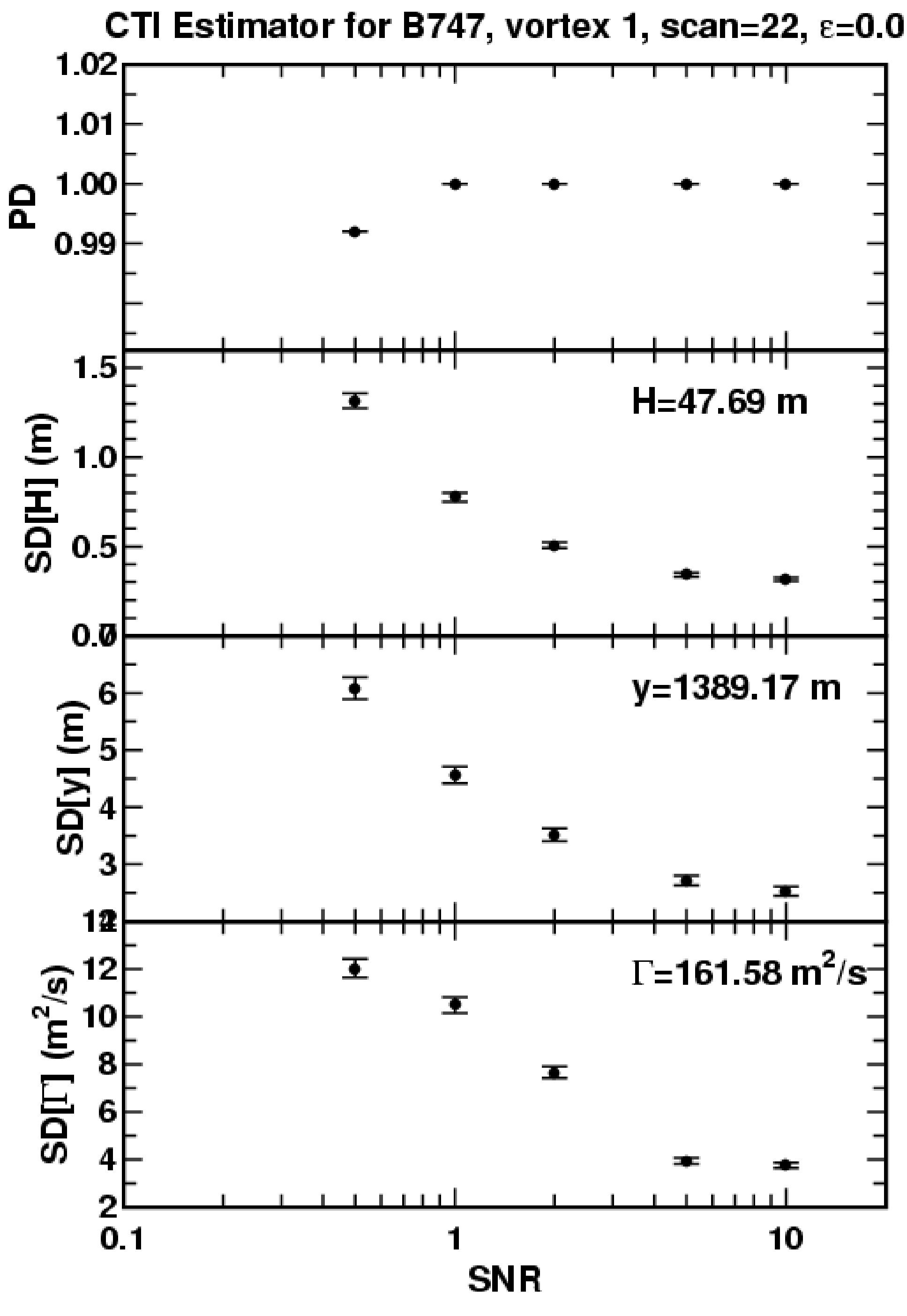

Figure 71. Detection probability (PD) and standard deviation (SD) of CTI estimates of the Boeing 747 vortex parameters for vortex 1 of lidar scan 22 as a function of SNR for no added turbulence (ε=0.0). The correct values are indicated.

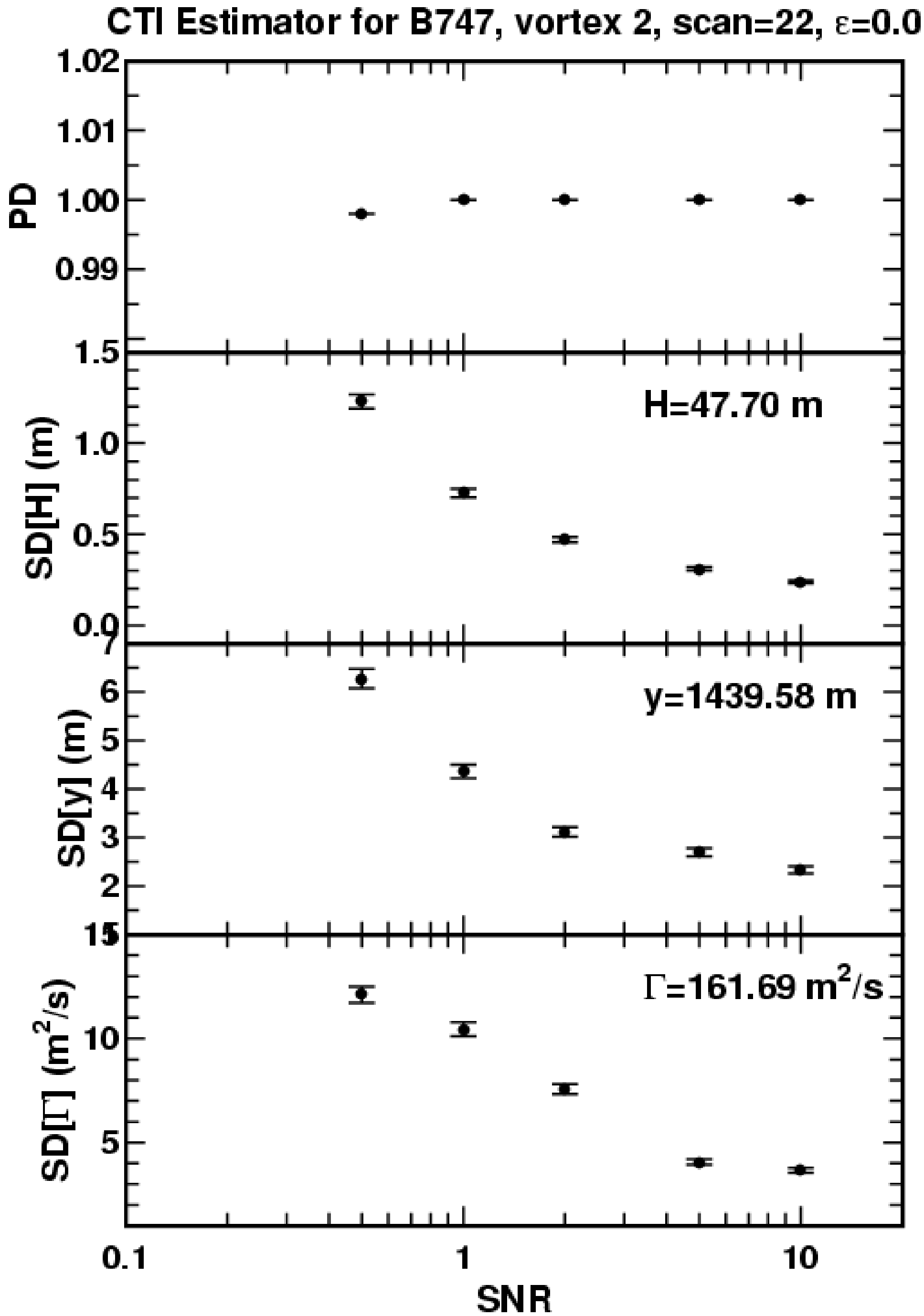

Figure 72. Detection probability (PD) and standard deviation (SD) of CTI estimates of the Boeing 747 vortex parameters for vortex 1 of lidar scan 22 as a function of SNR for no added turbulence (ε=0.0). The correct values are indicated.

3.12 Summary Task 1.1(a)

The performance of CTI's algorithm for wake vortex detection and tracking was determined using rigorous computer simulations of lidar data for two cases of a vortex evolution: a Boeing 737 and a Boeing 747. The rigorous computer simulations produce accurate estimates of the bias and standard deviation of the measurements of the vortex parameters, because truth is known a priori from the input analytic model for the vortex evolution. The grid-size requirements for accurate simulations were determined by a convergence test (see Figure 6) on the statistical properties of the raw lidar signal spectra. For the detection mode, i.e., the first lidar scan of the vortex, the best possible performance was determined by the optimal Maximum Likelihood (ML) estimator (see Section 3.7) for two scenarios: 1) the vortex pairs have the same parameters and a known separation and vortex radius (ML 3 par) and 2) the vortex parameters can have any value but the vortex radius is assumed known (ML 6 par). The results can be summarized as:

- The SNR required for vortex detection depends on vortex type and strength.
- The CTI algorithm bias in vortex location (height H and distance y) is small for SNR above the detection threshold.
- The CTI algorithm bias in vortex strength Γ depends on SNR and on the true value of Γ.
- The CTI algorithm random error (standard deviation SD) is small for all the parameter regime with good detection (PD=1).
- The performance of both the CTI algorithm and the ML estimators is degraded by an additive turbulent velocity field.
- Verification of the performance of the CTI algorithm with independent measurements will be difficult because of the small bias and small random error. The obvious solution is the comparison of two simultaneous vortex measurements from two lidars.
- There is room for improvement in the CTI algorithm based on the comparison with the ML estimators.

These results are the first quantitative evaluation of vortex parameter measurements. Although the parameter regime of the analysis was limited, the general behavior of the CTI algorithm and the ML estimator was determined and possible areas of improvement identified. These include:

- Improve first detection performance by assuming that the parameters of each vortex pair are the same and that the vortex pair separation b_0 and vortex radius r_C are determined by the aircraft type which can then be estimated based on the largest likelihood function of all possible aircraft.
- Use the vortex radius r_C from the aircraft type determined from the first detection in the vortex tracking mode to reduce the errors in the circulation strength estimates Γ.
- Reduce the bias in the circulation strength estimates (more accurate SNR information).
- Evaluate the impact of additive turbulence, ambient velocity, and wind shear on the performance of vortex measurements.

- Produce estimates of the background turbulence from the lidar data or other means to bound the typical atmospheric conditions.

- Determine the threshold vortex parameters that define a hazard to guide algorithm development, i.e., what is the minimum value of circulation strength for each aircraft type that must be measured and what are the accuracy requirements at this threshold (bias, standard deviation).

Future simulations could include spatial variations in aerosol backscatter and more realistic vortex descriptions in simulations of performance. This may require high-resolution 3D numerical models with grid size at least 0.05 m to correctly resolve the scales of motion (see Figure 6). However, an unbiased estimate of the true vortex parameters will be required as well as efficient lidar simulation code using the gridded 3D numerical wind fields as input. Because of the large data sets and intensive numerical effort, both the 3D numerical wind field model of the vortex and the lidar simulation should be performed on the same computer. In addition, the effects of the spatial filtering of the numerical model must be determined to ensure reliable results. This will most likely require a smaller model resolution to mitigate the effects of the model filtering.

4 Task 1.1(b)

4.1 Introduction to Task 1.1(b)

Under Task 1.1(b) the research team addressed the development of a test plan to validate the numerical simulation studies conducted under Task 1.1(a), including the STL field test being conducted by the Volpe National Transportation Systems Center at the time of this report. Therefore, plans for validation field tests were developed in two categories: 1) tests that could be conducted as add-ons to the current STL series of tests, and 2) tests that would require a restricted airspace. In both cases, the objective of the tests was to validate the results of the numerical simulations.

4.2 STL Field Test

In November 2003, a member of the research team visited the STL site where Volpe personnel are conducting tests with the CTI WindTracer for the detection of wake vortices caused by large aircraft during landing. These tests are currently focused primarily on vortices during in ground effect (IGE). Volpe personnel have installed the WindTracer LIDAR and other instruments at the St. Louis airport to collect data on wake vortices. Under the direction of Dr. Frank Wang, of the Surveillance and Sensors Division, Volpe personnel will collect and process the data and then report their findings to the FAA. At the time this report was written, Volpe personnel had not published a test plan, but Volpe personnel provided the drawings, pictures, and information relevant to the field test that is included in this report.

Personnel from the Volpe Center are studying the behavior of vortices with respect to staggered closely spaced parallel runways (CSPRs); specifically, wake transport and wake altitude. Wake transport is self-explanatory, referring to the transport characteristics of wake vortices, and wake altitude refers to wake vortices generated by a lead aircraft on one runway transported into the path of a trailing aircraft on a second runway.

Sections 4.2.1 through 4.2.5 are a summary of the information gathered by GTRI at the St. Louis site visit and through correspondence with Frank Wang since the visit.

4.2.1 STL Project Schedule

Volpe personnel have had the WindTracer LIDAR running since April 2003. As of Nov. 6, 2003, Volpe personnel were still completing the installation of anemometers and sodars that will provide information in addition to the lidar. The Volpe field test period of performance will be 1 year from their declared start date of February 1st, 2004. If needed, and if the FAA funding is still available, the period of performance will be two years. A second phase is also anticipated, but the exact nature of the test depends on what is learned in phase one. However, it is certain that phase two will have another CTI lidar measuring out of ground effect (OGE) wake vortices and perhaps more windlines.

4.2.2 Test Site

STL was chosen as the test site, because it has CSPRs (separated by 1300 feet) and sees mostly heavy aircraft (dominantly 737s and MD-80s). Both of these conditions are of interest to the FAA/NASA study. Additionally, American Airlines donated office space in their flight training building (formerly operated by TWA) for a Volpe control room, and the lidar and one sodar are northwest of runways 12R and 12L in an abandoned American Airlines parking lot. Figure 73 is a diagram of the CSPR at STL. Figure 74 gives the layout of the site, including information such as elevation, with runways 12L and 12R marked by red circles. Figure 75 gives the layout of the instrumentation at STL. A discussion of instrumentation follows in Section 4.2.3.

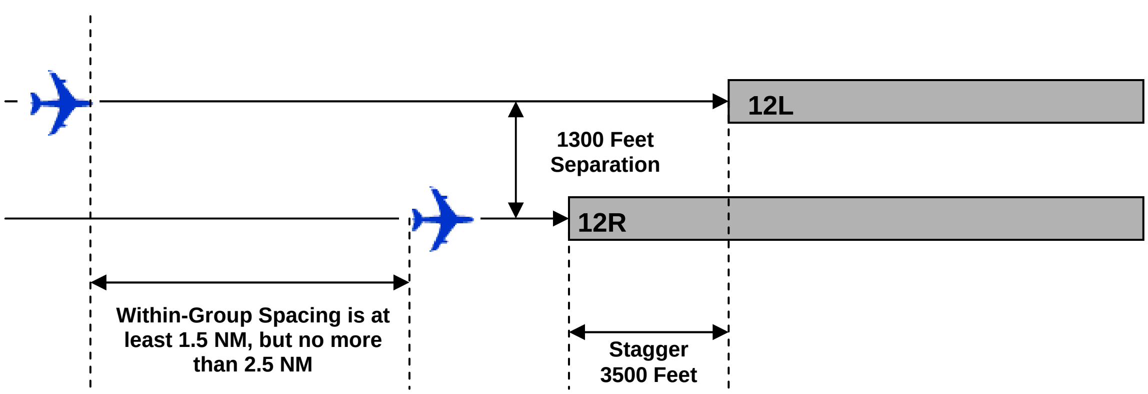

Figure 73. Staggered CSPR layout at STL

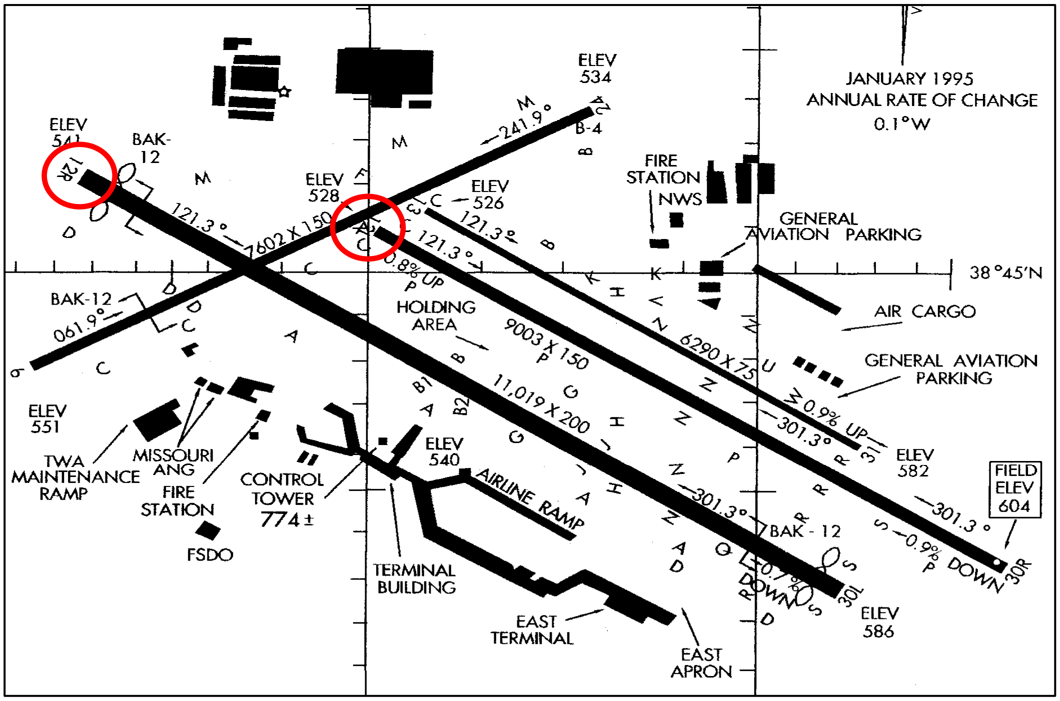

Figure 74. STL plan showing elevations

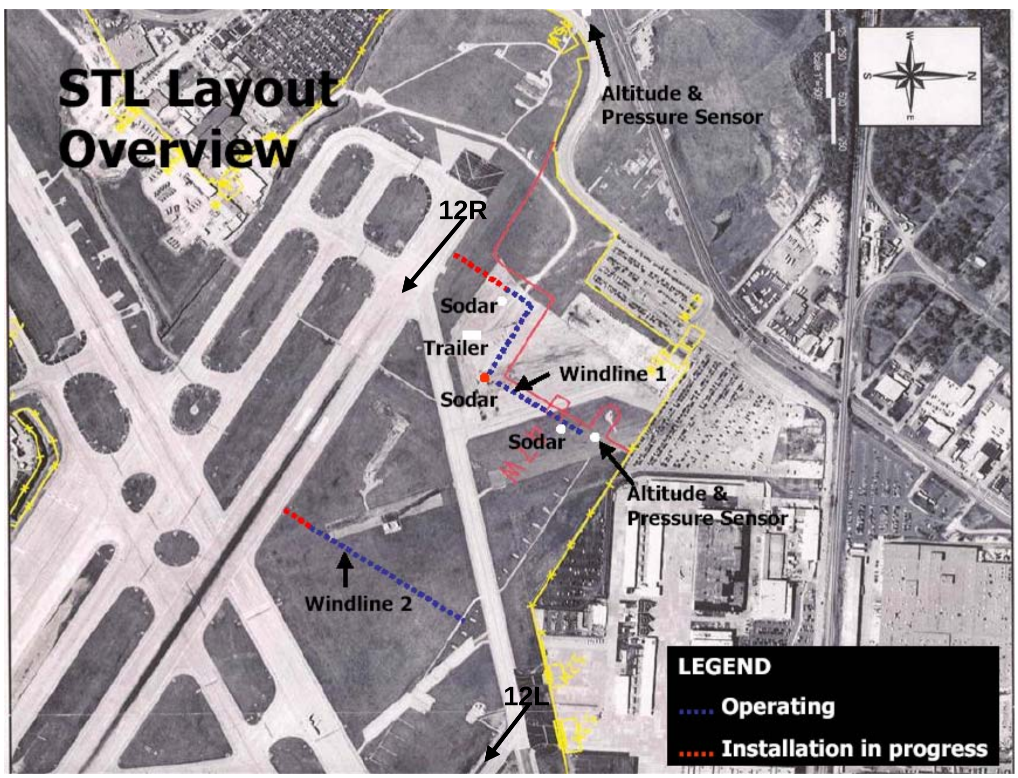

Figure 75. STL layout of instrumentation (October 2003)

4.2.3 Instrumentation

Sections 4.2.3.1 through 4.2.3.5 describe the instrumentation being used in the STL field test. Photographs of the instruments are included, where available.

4.2.3.1 WindTracer Pulsed Doppler Lidar

The WindTracer Lidar is a turnkey system manufactured by CTI. The lidar is a compact, scanning, laser-based system that measures range, height, and strength of aircraft wake vortices. The lidar has a 3-km detection range and can scan for wake vortices in multiple azimuthal planes or "vertical slices". Scanning for vortices in multiple planes allows the axial coherence of the vortices to be established.

The hardware system is made of several units, including a transceiver, scanner, heat exchange / power converter, controller, and signal processor, as well as additional electronics and support equipment. The transmitter is a self-contained unit, as is the transmitter controller. The data system is contained in a small trailer. A GPS receiver is included in the data system and provides the UTC time stamp for all data. The user also has the ability to control the unit and display computed data from a remote location.

Figure 76 is a photograph of the lidar trailer as positioned for the field test at STL, and Figure 77 is a close-up photograph of the lidar trailer. The lidar can be no closer than 1000 feet laterally from the nearest area of interest, i.e. runway 12R. The lidar is positioned such that the lidar is able to scan both runways of interest at the same time. Figure 78 shows how the lidar scans across the runways. The vertical scan angle is just enough to cover the typical glide slope of 3° of a landing aircraft approaching the runways.

Through June 2003, the lidar measured in 4 vertical slices: 31°, 50°, 68°, and 75°, clockwise from north. After a program review, these angles were changed to 31°, 50°, 75°, 86°, and 96°. The scan at 96° gives substantially axial motion (down the runway) of vortices and was eliminated as a scan angle in January 2004. Figure 79 shows the different angles currently being scanned by the lidar. Table 7 gives the altitude of the aircraft over runways 12R and 12L when the lidar scans through its various angles.

Figure 76. WindTracer Lidar at STL

Figure 77. Close-up of the WindTracer Lidar

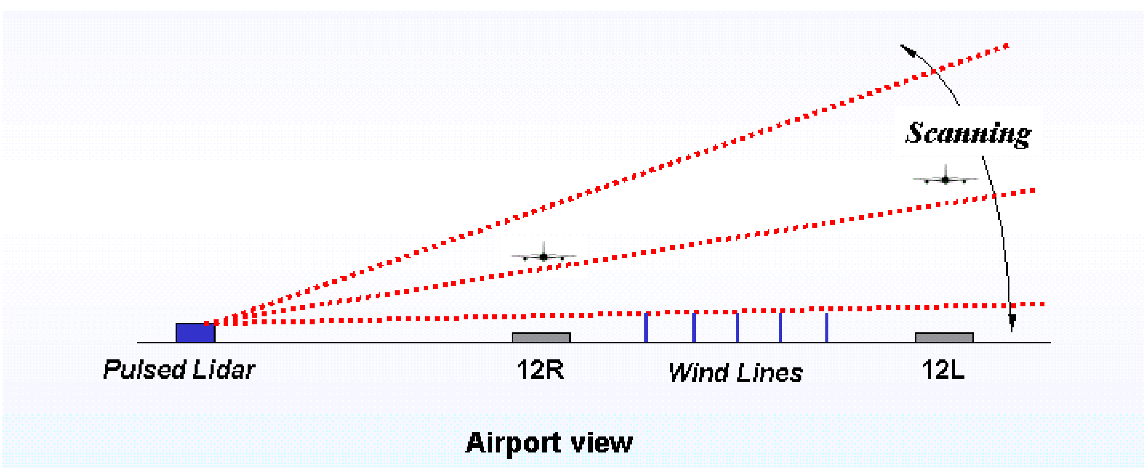

Figure 78. Pulsed lidar scan of runways

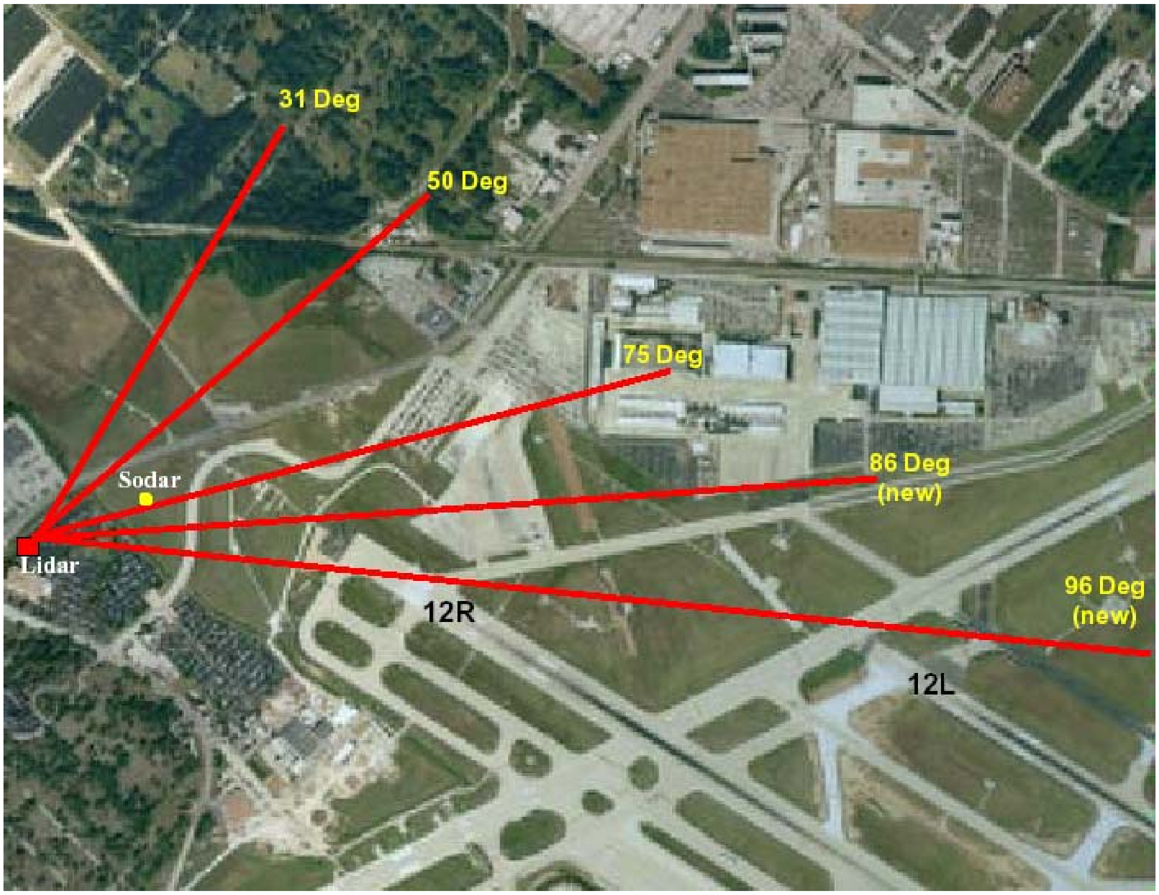

Figure 79. Current (October 2003) lidar scanning angles with respect to the runways of interest (12L and 12R)

Table 7. Scanning angle versus altitude of aircraft over runways 12R and 12L

Scanning Angle (°)	Altitude over 12R (ft)	Altitude over 12L (ft)
31	146	329
50	130	294
75	99	222
86	79	175

4.2.3.2 Sodars

There are 3 sodars at the test site. One sodar is being used as a wind profiler (3 non-orthogonal sound beams measuring wind strength and direction) and has been in operation since April 2003. The other two sodars are being used as vortex sensors (1 vertical pointing beam) and are still being installed as of November 2003. The manufacturer of these sodars is Aeronvironment. Figure 80 is a photograph of the wind sodar.

Figure 80. Wind Sodar at STL

4.2.3.3 Windlines

There are 2 windlines consisting of fixed anemometers mounted on poles of varying heights, depending on the proximity to and location along the runway. The anemometer is a Young Meteorological Instruments model 27106R Gill Propeller Anemometer. The windlines have been collecting data since October 2003. Figure 81 (a) and (b) are photographs of the 2 windlines, including one of the sodars.

(a)

(b)

Figure 81. (a) Windline 1 and a sodar (b) Windline 2

Windline 1 (WL1) consists of 48 poles and has 3 sections, with the middle section perpendicular to the other two sections and parallel to runways 12L and 12R, as shown in Figure 75. The first section (farthest from 12R) has 23 poles spaced 25 feet apart. Poles 1-16 have anemometers placed at a height of 12 ft. Poles 17-22 have anemometers at 3ft and 12ft. Poles 1-22 are all aligned to measure crosswinds. Pole 23 has 7 anemometers: 3 for measuring crosswinds at heights of 3, 6, and 12 ft; 3 for measuring head winds at heights of 3, 6, and 12 ft; and one for measuring vertical winds at 12 ft.

The middle section (or perpendicular section) of WL1 has 4 poles, all measuring crosswinds. These poles are spaced 100 feet apart. All anemometers on these poles are at a height of 12 ft.

The last section of WL1, which lies closest to runway 12R, has 21 poles. Pole 28 has one anemometer at 12 ft; poles 29-38 have anemometers at 3ft and 12 ft; poles 39-48 each have one anemometer at 3 ft. All poles are spaced 25 ft apart (with the exception that poles 38 & 39 are 50 ft apart) and are set up to measure crosswinds.

Windline 2 (WL2) is a straight line that runs perpendicular to 12R. There are 42 poles in WL2, each separated by 25 feet. Consider pole 1 to lie farthest from 12R. Poles 1-4 have anemometers placed at a height of 3 ft, all measuring cross winds. Pole 5 has 4 sensors: 2 measuring crosswinds at 3 ft and 6 ft, and 2 measuring headwinds at 3 ft and 6 ft. Poles 6-12 each have 2 anemometers at 3 ft and 6 ft for crosswinds; poles 13-18 each have one anemometer at 6 ft for crosswinds. Pole 19 has 4 anemometers: 2 for crosswinds at 3 ft and 6 ft, and 2 for headwinds at 3 ft and 6 ft. Poles 20-24 have anemometers at 6 ft to measure crosswinds; poles 25-31 have anemometers at 3 ft and 6 ft to measure crosswinds. Pole 32 has 4 sensors, just like poles 5 and 19. Finally, poles 33-42 each have an anemometer at 3 ft to measure crosswinds.

The heights and spacing of the anemometer poles with respect to Runway 12R, are shown in Figure 82, with the heights of the poles exaggerated.

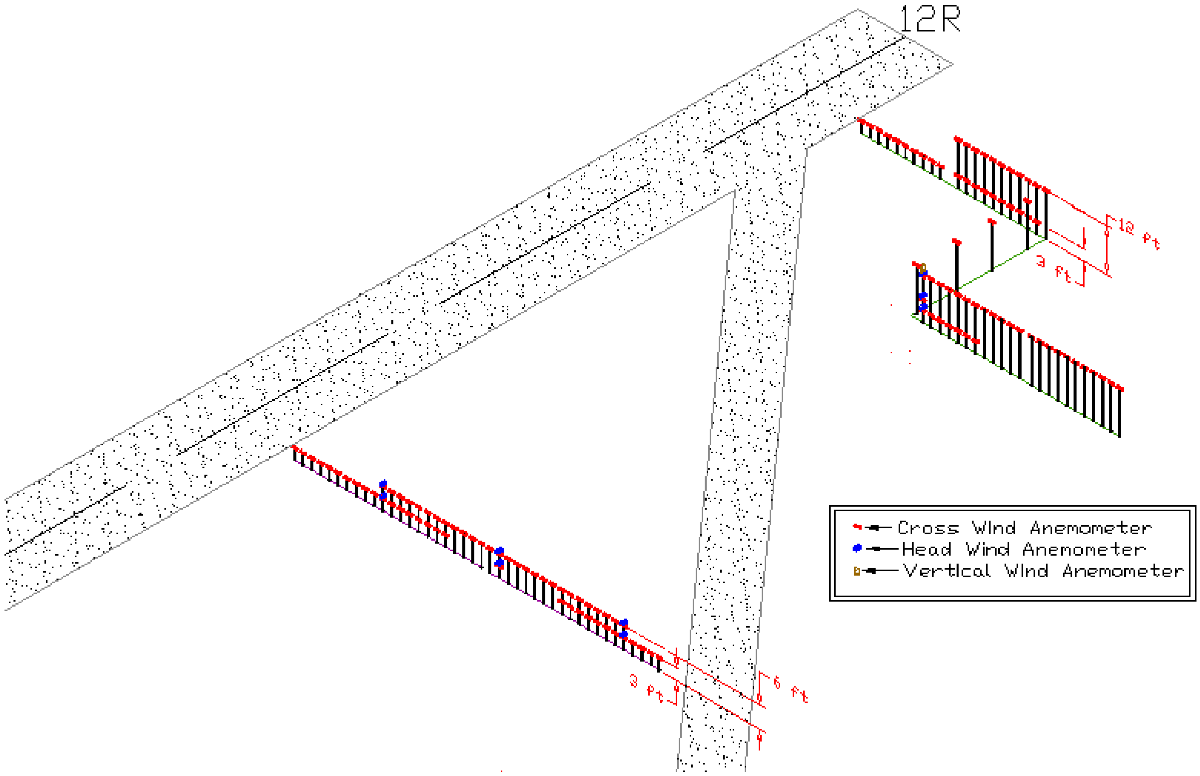

Figure 82. Windline drawing

4.2.3.4 Airplane Detector Suites

There are 2 airplane detector suites; one located at each of the NW ends of runways 12R and 12L. Each suite consists of a pressure transducer and a laser rangefinder in an environmental enclosure. The pressure transducer is model MET3, manufactured by Paroscientific Inc. The MET3 operates at 10 Hz, and the purpose of the sensor is to detect aircraft arrival and estimate aircraft weight. The peak of the recorded pressure indicates that an airplane is overhead. The laser rangefinder is made by Riegl, model LD90-3. The rangefinder laser has a pulse frequency of 200 Hz and points vertically, sensing the presence and distance to planes directly over the end of the runways. Figure 83 (a) and (b) are pictures of the altitude and pressure sensors for runways 12L and 12R, respectively.

(a)

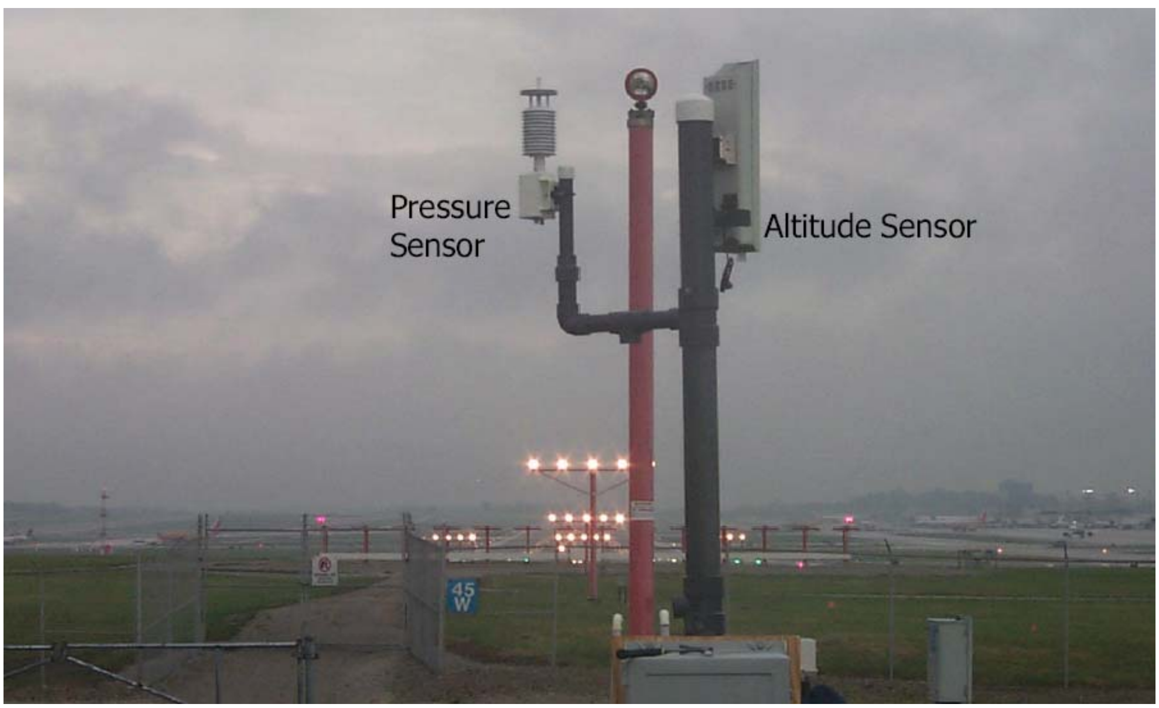

(b)

Figure 83. Pressure and altitude sensors for runways (a) 12L and (b) 12R

4.2.3.5 Mode-S Radio Receiver

The Mode-S system detects a radio downlink from the airplanes landing and departing from runways 12R and 12L. Transmissions include time, make, and model of the aircraft. The information received includes the type of aircraft and its position (altitude) at a series of documented times. The laser rangefinder described in Section 4.2.3.4 verifies the Mode-S altitude data.

4.2.4 Auxiliary information

There is additional data being gathered during the field test. An automated Surface Observing System (ASOS) provides weather information; low-level wind shear alert system (LLWAS) sensors are present; and a Total Airport Management Information System (TAMIS) gives aircraft approach information. The FAA is providing a monthly download of arrival and departure information, including times, aircraft type, aircraft weight, etc. Finally, American Airlines is providing Flight Data Recorder information for approaches during which a pilot reported a wake vortex incident.

4.2.5 Data collection and processing

All instruments are recording data automatically and continuously. The data is stored on a server in the control room. Weekly, a local college student copies the data to DVD and stores the DVDs in the control room. Occasionally the DVDs are picked up by Volpe personnel and delivered to the Volpe Center, where relevant data sets are copied onto their central data server. "Relevant" means approaching aircraft only. The study is not concerned with wake effects from departing aircraft.

Hardware and data collection software are turnkey systems from CTI. Data processing software is still under development, with input from CTI. Processing is being and will always be done as post-processing, not in real time. Real-time checks are done occasionally by personnel from Volpe and CTI via Ethernet connections for confirmation of instrument health.

The only post-processing variable that alters the processing outcome is the choice of a clutter map. The surrounding environment that the laser beam encounters (the ground, buildings, trees, etc.) must be characterized and provided to the processing algorithms. Clutter maps are updated whenever the landscape or environment along the scan path changes. Examples of such changes include differences in foliage as the seasons change and ground height changes due to construction.

In addition to scanning for vortices, the lidar hourly performs 2 types of wind profiles: Plan Position Indicator (PPI) and Velocity Azimuth Display (VAD). VAD is a vertical measurement, and PPI is a conical scan. Data is collected and stored by Volpe personnel, but it is currently not being used.

Occasionally natural eddies are detected by the system. Personnel from the Volpe Center will be able to identify the timing and strength of these occurrences. A value of 100 m^2/sec is a commonly accepted threshold of significant circulation strength.

4.3 Validation of Lidar Simulations

GTRI recommends three types of field tests to validate the simulations performed by NCAR in Task 1.1(a). The major constraint for the validation tests is that the simulations were only done for OGE vortices generated by 737s and 747s. There are several definitions for a vortex to be considered OGE; for example the height of the vortex must be equivalent to one wingspan of the aircraft creating the vortex or to the initial vortex pair horizontal separation (b_o). The current AVOSS model considers a vortex to be OGE when the height of the vortex is 1.5b_o. There are other conditions, however, such as shear and stability that make the boundary for OGE vary. For the purposes of this study, the boundary for OGE was taken to be 1.5b_o. For a 737, the wingspan is 113.2 ft; b_o is 73.6 ft, and 1.5b_o is 110.4 ft. For a 747, the wingspan is 212.5 ft; b_o is 165.8 ft, and 1.5b_o is 248.6 ft.

The focus of the STL tests is on IGE vortices. However, in comparing the b_o values of the 737 and 747 to the altitudes given in Table 7, there are some scanning angles in the current setup that will accommodate the OGE scanning needs. Specifically, the lidar scans to altitudes greater than 248.6 ft at 31° and 50° over runway 12L, which will accommodate the OGE height needed for a 747. In addition, the lidar scans to altitudes greater than 110.4 ft at 31°, 50°, 75°, and 86° over 12L, and 31° and 50° over 12R, which will accommodate OGE needs for the 737.

In section 4.2.1, it was mentioned that a Phase 2 is planned for the STL field test, where a second CTI lidar will be installed to measure OGE vortices. Two of the three recommended field tests described in the following sections will use this second lidar. These tests will validate random measurement errors and track bias found by the simulations of Task 1.1(a) for OGE vortices. The recommended tests are envisioned as short-term or temporary configurations of the two lidars, to interfere as little as possible with the long-term measurements being taken by Volpe personnel.

The third recommended field test is discussed in Section 4.3.3. The concept is to use a tall "vertical windline" as opposed to the standard 6 ft-12 ft windlines that are usually placed between runways at an airport. Windlines near the ground have proven very useful in several field studies for tracking vortices, and they have been used to validate lidar track data. Windlines, however, have apparently not been used to validate lidar circulation measurements, and of course ground windlines are used for IGE vortices, not OGE.

4.3.1 Side-by-Side CTI Lidars

The first recommended validation test is a very simple test involving two CTI lidars at STL. Two identical lidars scanning side-by-side will be able to measure the random errors of the lidars in track and circulation. Figure 84 gives the suggested layout of the two side-by-side lidars. During the visit to the STL test site in November, it was determined that this configuration is possible; there is space beside the current lidar for an additional lidar.

Placing the lidars as close as possible side-by-side will allow them to scan in parallel planes in virtually the same airspace, thereby detecting the same vortices at the same point in time. As shown in the simulations from Task1.1(a), the lidar has random errors in track and circulation of the vortices. Statistical analysis of the data from two identical lidars operating as recommended in this section will validate the random error found in the simulations.

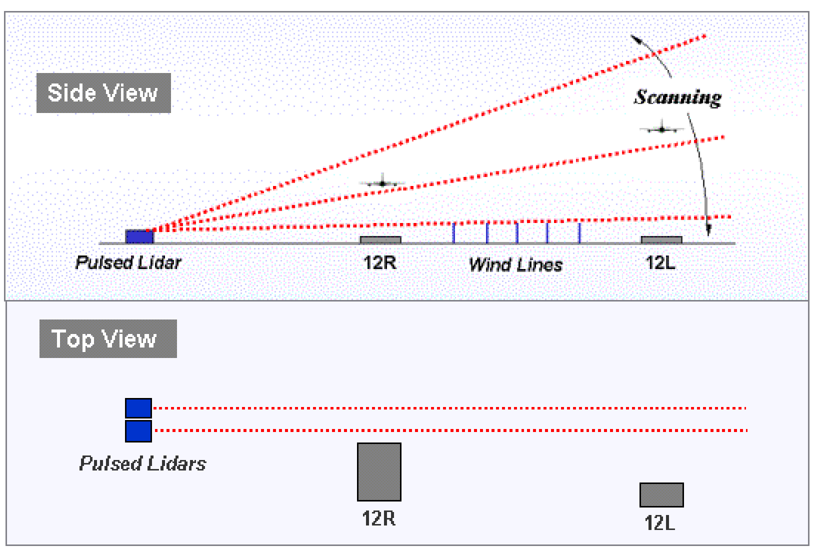

Figure 84. Side-by-side lidars scanning in parallel planes

4.3.2 *Facing CTI Lidars*

Simulations conducted under Task 1.1(a) showed that the algorithm bias for vortex location is small. To confirm the algorithm bias, the following test is recommended. By scanning the same space from equal distances on opposite sides of runway 12L, any horizontal track bias can be detected in the lidar data. Two identical lidars in such a configuration should give equal and opposite horizontal track biases. Runway 12L is chosen because it contains two OGE azimuth scanning angles that meet the boundary requirement for a 747, and four that meet the requirement for a 737, as discussed in Section 4.3.

In this recommended field test, two identical CTI lidars would scan parallel planes while facing each other, as shown in Figure 85. Actual location possibilities for the second lidar are marked in Figure 86, using 12L as a centerline. The possible positions marked in the figure are only examples based on open areas in the photograph that still meet the OGE angle requirement discussed in Section 4.3. A visit to STL and a careful review of possible sites will be necessary to choose the best location for accessibility, convenience, and a clear LOS.

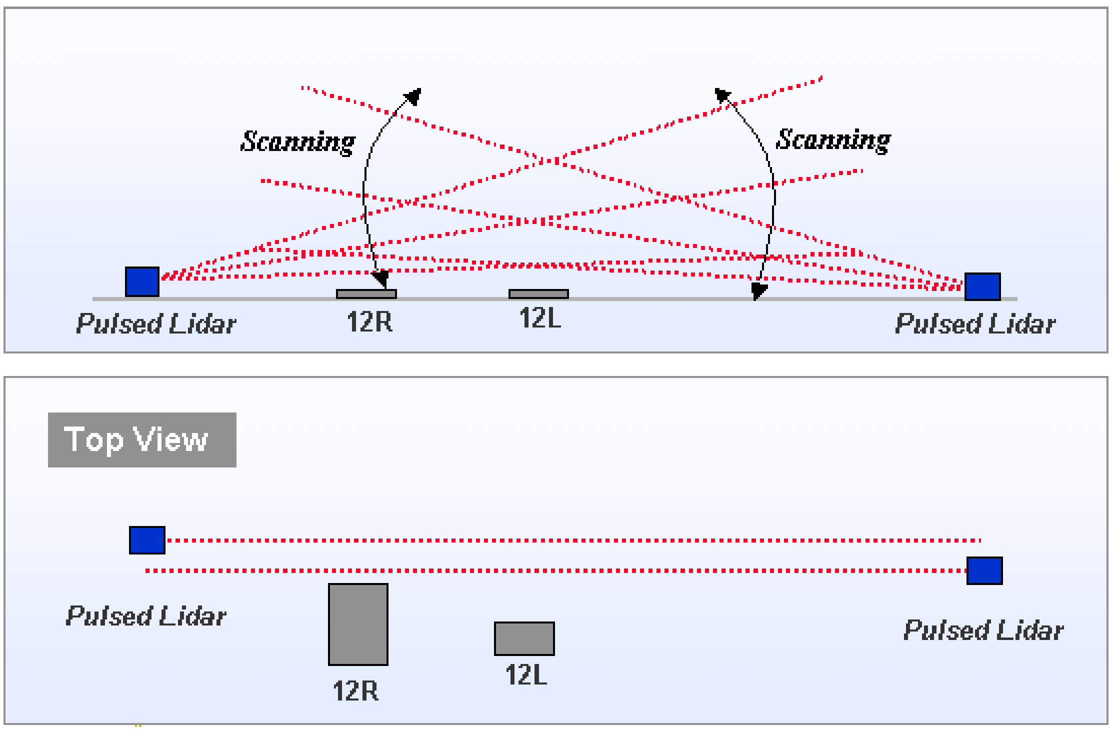

Figure 85. Facing lidars scanning in parallel planes

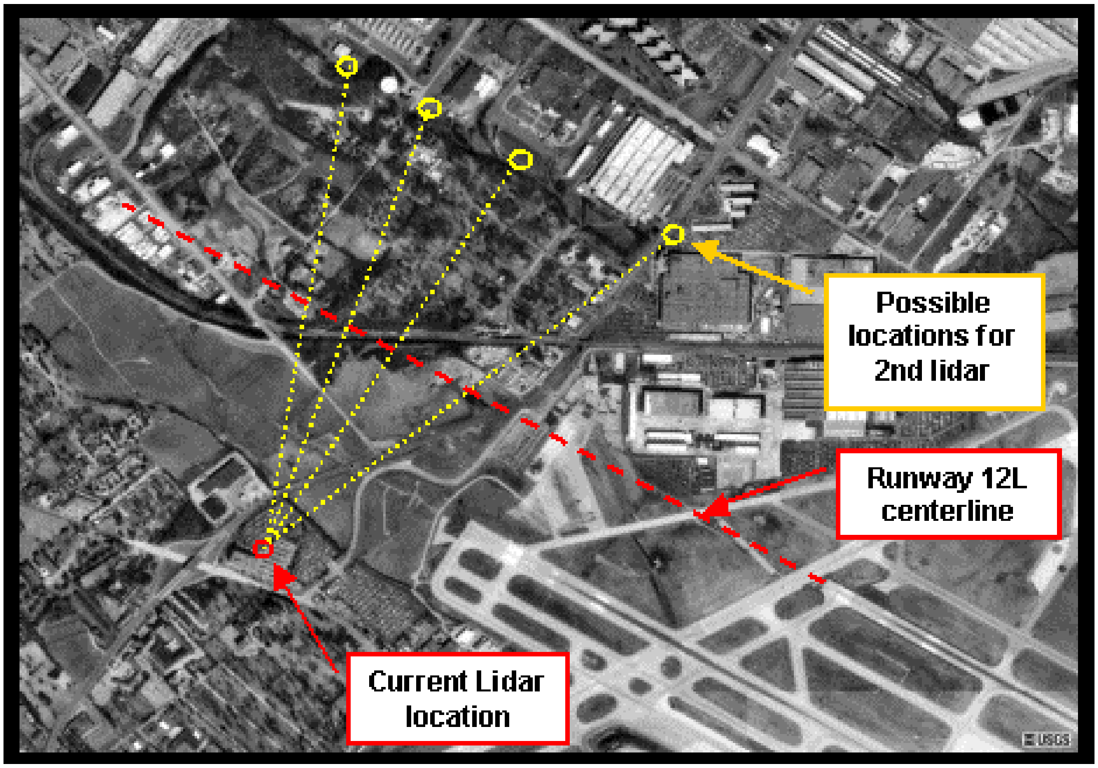

Figure 86. Possibilities for 2nd lidar location

4.3.3 CTI Lidar versus Vertical Windline

Simulations conducted under Task 1.1(a) found the circulation bias to be relatively large. Measuring the accuracy of the lidar's vortex circulation values is difficult, because this test cannot be performed with two identical lidars. In addition, no other instrument samples the wind field in the same way, with the same resolution, as a scanned pulsed Doppler lidar. Circulation values from a pulsed Doppler lidar have been compared to CW lidar results, and the values were quite different when the vortices were new (although they converged as the vortices aged). [19]

The validation approach recommended here is based on 3-axis acoustic anemometers, because they provide high accuracy, high temporal resolution, and a wind vector that can be resolved to find the component along the lidar's LOS. Acoustic anemometers also have a successful history in windlines for wake vortex tracking. [20]

Attempting to sample a vortex wind field with a two-dimensional array of anemometers at the same resolution provided by the lidar would be prohibitively expensive. For this reason, the plan presented here relies on an ambient crosswind to transport the vortices across an array of 3-axis anemometers mounted on a tower (essentially a vertical wind line) while the lidar performs vertical scans in a plane adjacent to the tower, in the direction of the prevailing crosswind.

The test configuration is shown schematically in Figure 87. The vortex decay times are on the order of 100 seconds, so their properties will be almost constant during the time required to transit the tower (a few seconds). The vertical anemometer array will essentially provide a two-dimensional slice through the vortex wind field. The wind fields measured in this way will provide an independent check of both the track and circulation measurement accuracies of the lidar.

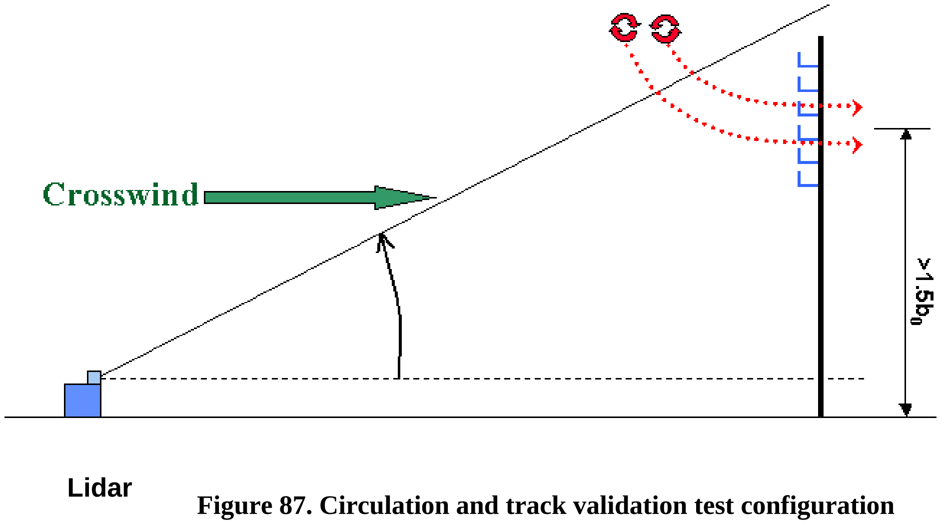

Figure 87. Circulation and track validation test configuration

In order to plan the recommended field test, the tracks of the vortices from their initial positions to the tower were estimated, as well as their expected wind fields when they reached the tower, using the same vortex model as in Task 1.1(a). Wind fields were calculated using Equation 1, the sink rate from Equation 2, and the circulation strength as a function of time from Equation 3. The vortex parameters used are also the same as for Task 1.1(a), listed in Table 1.

As a guide to planning the field test, a vortex is considered to be dissipated when its circulation reaches 90 m^2/s. [21] Using the parameters in Table 1 and Equation 3, a 737 vortex is dissipated in about 64 seconds and a 747 vortex in about 120 seconds.

Vortex tracks were calculated by assuming that horizontal transport is determined by the ambient crosswind speed (as shown is previous field measurements) and by calculating the vertical sink rate using Equation 2. For the examples shown here, the crosswind speed was chosen to be the same as for Task 1.1(a), 3 m/s. Tracks for the 737 and 747 vortices are shown in Figure 88 and Figure 89. The vortex pair was initially centered at the location (0,0) in these plots.

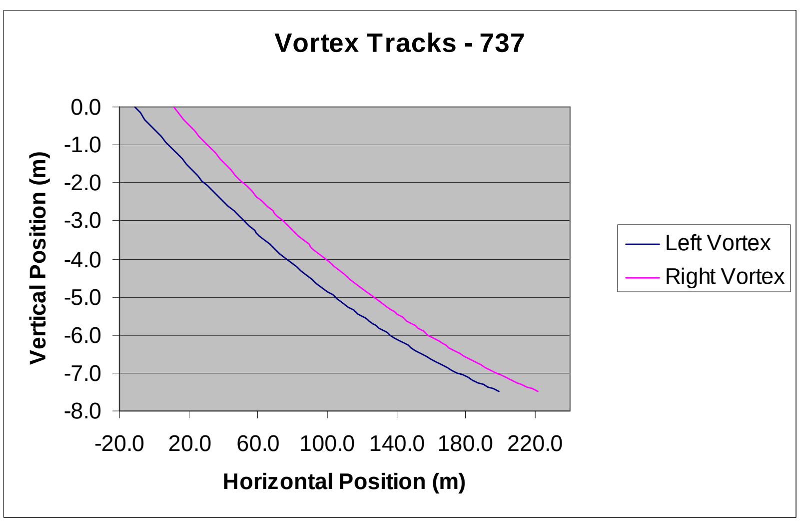

Figure 88. Predicted 737 vortex tracks with a 3 m/s crosswind.

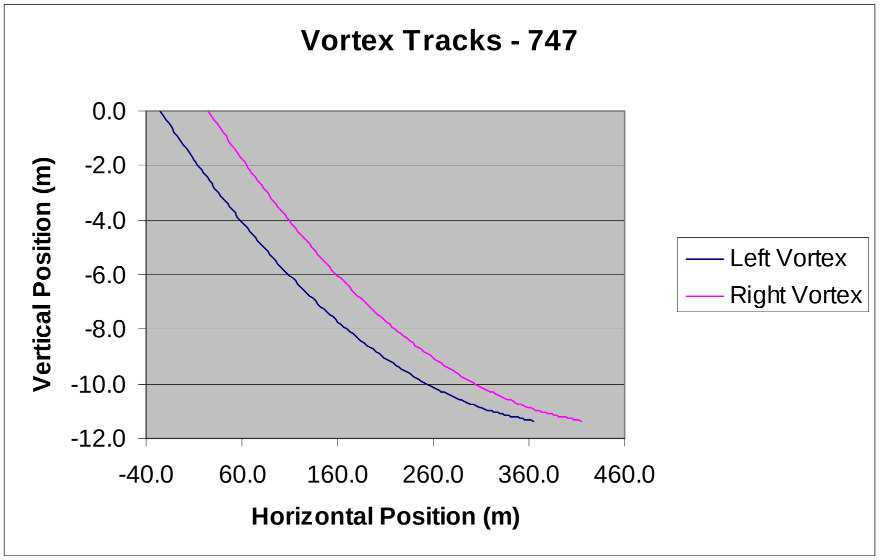

Figure 89. Predicted 747 vortex tracks with a 3 m/s crosswind.

As noted above, the sink rate and the wind field velocities are calculated from $\Gamma(t)$, which is plotted versus horizontal position (again assuming a crosswind of 3 m/s) for the 737 and 747 in Figure 90 and Figure 91, respectively.

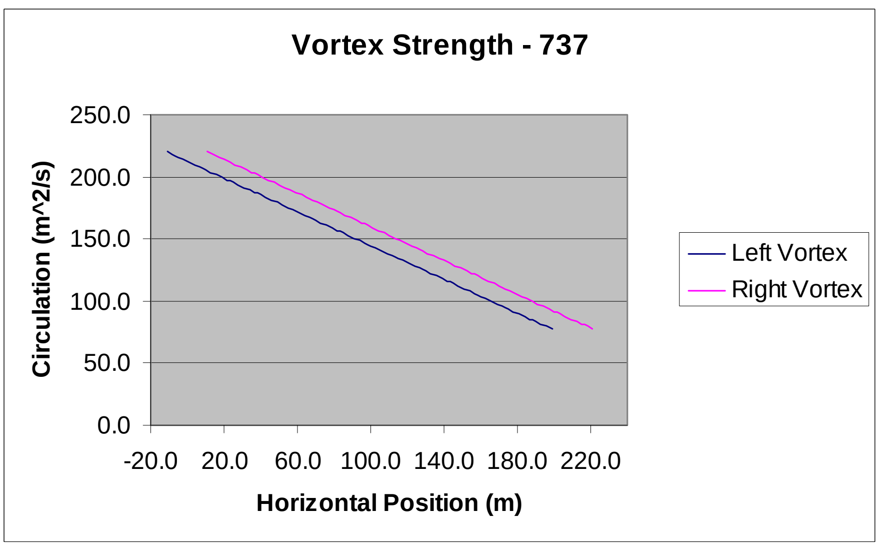

Figure 90. 737 vortex circulation versus horizontal position for 3 m/s crosswind.

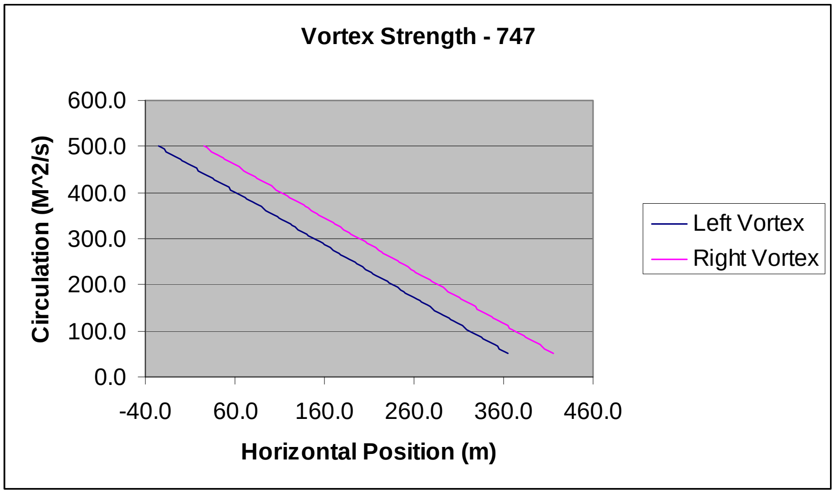

Figure 91. 747 vortex circulation versus horizontal position for 3 m/s crosswind.

Inferring from Figure 90 and Figure 91, the vortices will be nearly dissipated after they are transported horizontally by 180 m (737) and 360 m (747), so the tower fly-bys should have offsets lower than these figures for a 3 m/s crosswind. For example, offsets of about 100 m and 260 m would ensure that the circulations are at least 150 m^2/s.

In order to choose the spacing between anemometers, it is necessary to calculate the expected wind fields as a function of distance from the center of the vortex core, using Equation 1. Tangential velocities are shown in Figure 92 for the 737 and 747 vortices when $\Gamma(t)$ has decayed to 150 m^2/s. The values range from about 14 m/s decreasing to less than 2 m/s at distances from 2 to 20 m, respectively, from the vortex centers. Considering that the ambient winds are assumed to be 3 m/s and that there will be an unknown turbulent wind field, the values shown in Figure 92 suggest that anemometer spacing should not exceed 5-10 m. In this case, the closest anemometers will register wind speeds of a few m/s when the vortex crosses the tower, assuming it crosses somewhere within the anemometer array.

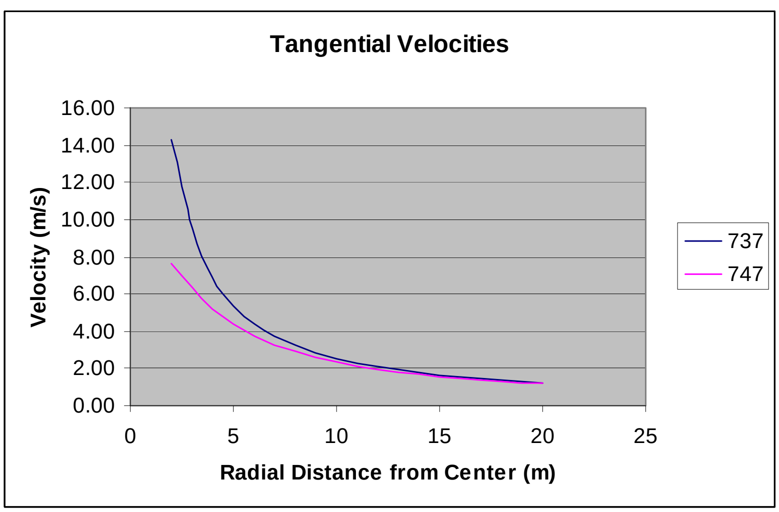

Figure 92. Tangential velocities for 737 and 747 vortices, $\Gamma(t)$ = 150 m^2/s

The expected vortex wind fields are shown graphically in Figure 93 for a 747 vortex with a circulation of 150 m^2/s centered on a vertical array of six anemometers that spans 50 m vertically. The wind speeds range from 2.13 m/s to 7.35 m/s.

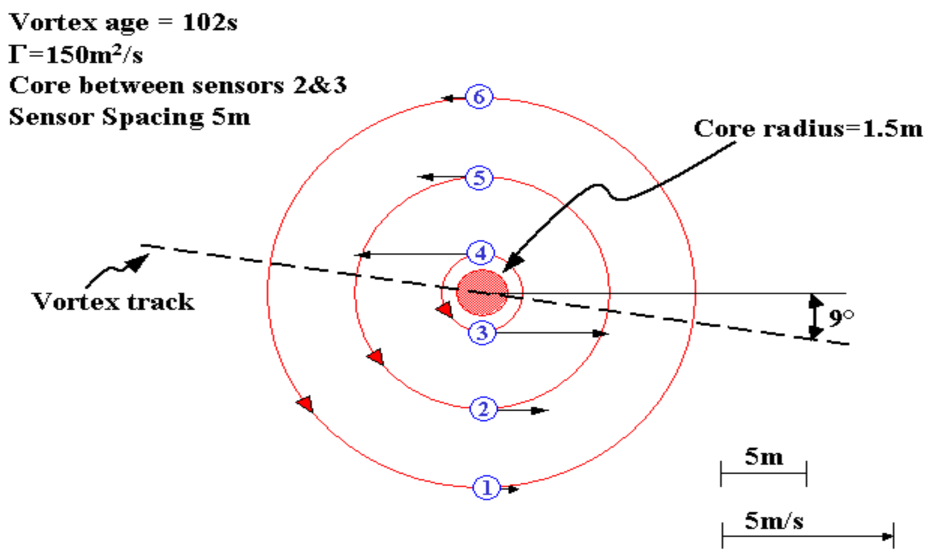

Figure 93. 747 vortex wind fields and anemometer array, $\Gamma(t)$ = 150 m^2/s

In order to insure that the vortices are OGE, the center of the anemometer array should be at least $1.5b_o$. Additionally, the aircraft altitude and lateral offset distance from the tower should be adjusted, depending on the ambient wind speed, so that the vortices are approximately centered on the sensor array when they cross the tower. Each vortex will require several seconds to transit the tower, depending on the crosswind speed and the vortex size. For example, if the vortex is 30 m in diameter, it will cross the tower in 10 s with a 3 m/s crosswind.

Assuming the lidar is located 1120 m from the tower, as in Task 1.1(a), its spatial resolution will be the same as in the SFO tests. Its temporal resolution could be much better, because it will only be necessary to scan a range of angles that encompasses the sensor array. Using the same vertical scan speed as in Task 1.1(a) of 3.3 degrees per second, vertical scans could be repeated as often as every second. The lidar would then scan each vortex several times as it crossed the tower.

Because the lidar and the anemometer array will sample the vortex wind fields in different ways with differing time and space resolutions, a direct comparison can only be performed on raw data such as maximum wind velocity. When the vortex is directly over the anemometer array, the position data from the array and the lidar should agree. Beyond the maximum value, data from the anemometers and the lidar must be modeled to determine position and strength. For example, a fitting procedure can be developed to find the circulation and track parameters for the model described in Equation 1 that best agrees with the anemometer data, and then the time-dependent circulation and track parameters can be compared with the lidar data files.

The anemometer array can be used to measure the mean crosswind, as well as the statistical properties of the turbulent wind field. However, the lidar measurements will be affected by the instantaneous turbulent wind field, which is random and unpredictable. The fact that the instantaneous turbulent wind field will not be known along each LOS during the measurements means that there will be some inherent level of uncertainty in the instrument comparisons. In addition, the turbulent wind field will complicate the model-fitting procedure described above by introducing another type of uncertainty, and the standard axially-symmetric model may not describe the real-world vortices accurately. Therefore, the end goal of the analysis should be to determine whether or not the lidar track and circulation results are consistent with modeled values constrained by the anemometer data, within the limits of the measuring and modeling uncertainties.

Because tall vertical towers are not allowed near runways at airports, a dedicated facility must be located. To determine the feasibility of installing a 150-200 foot tower* at any flight facility, GTRI contacted the Wallops Island Flight Facility (WFF). After discussions with Mike Hitch in Technology Relations at WFF, it appears possible to install anemometers on tall towers that are sturdy enough to hold the lightweight anemometers, while keeping the bulk of the tower small so as to interfere as little as possible with the wake vortices generated. (The tower will cause some distortion to the axial flow of the vortex.) WFF can support the project technically and can procure and install the tower in the event that this test is conducted. In addition, the tower can be placed near a runway, but it is not necessary as long as the test aircraft can simulate a landing near it.

4.4 Summary Task 1.1(b)

Under Task 1.1(b), GTRI documented the planning, procedures, and operations to date of the STL field test currently being conducted by the Volpe National Transportation Systems Center. The descriptions and layout of the equipment are noted, along with the reasoning that went into the choice of measurement devices, the logistics of the site, and the means of assimilating and processing the resulting data.

The other aspect of Task 1.1(b), the development of a test plan to validate the simulation studies conducted under Task 1.1(a), was also completed and included in this report. The test plan calls for three possible field experiments. This first test places two CTI lidars side-by-side to measure the random errors of the lidars in track and circulation. The second test places two CTI lidars at equal and opposite positions around the centerline of an active runway, thereby quantifying any horizontal track bias in the lidar data. The third test calls for the superposition of a CTI lidar scan with a vertical anemometer windline. Such a correlation between lidar and windline out of ground effect has never been attempted and it may be pivotal in confirming the lidar's ability to measure vortex strength and position.

5 Conclusions

Under Task 1.1(a), the performance of the CTI WindTracer algorithm was determined for wake vortex detection and tracking using Monte Carlo computer simulations of lidar data for two cases of OGE vortex evolution. Simulated lidar data were generated for various vortex and lidar parameters, and the results of CTI's algorithm (which was implemented on a mainframe computer at the National Center for Atmospheric Research) were compared with the known input parameters or "truth". This approach permits a rigorous statistical analysis of the detection of the vortex and the accuracy of the resulting estimates of vortex location and strength as a function of the lidar Signal to Noise Ratio (SNR), the key lidar signal quality parameter.

For each set of input parameters, 1,000 realizations were generated in order to insure good statistical accuracy. The lidar signals were generated with sophisticated algorithms that

* A 150-200 foot tower is needed to reach the boundary height for OGE, however, near ground effect (NGE) is sufficient for the tests. The vortex circulation strength and structure is still intact in NGE as it is in OGE. NGE occurs at $0.5b_o$, therefore the tower size can probably be reduced significantly.

accounted for the fact that a wake vortex is much smaller than the lidar pulse, and realistic atmospheric conditions such as the background turbulence were included. An ambient wind speed of 3 m/s away from the lidar was assumed.

Simulations were performed for two different aircraft selected by NASA - the Boeing 737 for a smaller aircraft and the Boeing 747 for a large aircraft. Two cases were considered: an ideal analytic vortex model with no turbulence, and the same vortex model with an added turbulent velocity field satisfying a von Karman spatial spectrum and having an energy dissipation rate of 0.001 m^2/s^3.

The research team modified an existing ML estimation algorithm developed at the University of Colorado to produce optimal estimates of wake vortex parameters, as a reference for the performance of the CTI algorithm. To ensure robust results, both the simulations of lidar signals and the calculation of the ML estimates were produced with minimal approximations, which resulted in an intensive computational load. The vortex and lidar parameters were selected by NASA and CTI to match the conditions at the 2001 San Francisco airport (SFO) tests.

CTI's algorithm operates in two distinct modes: a detection mode and a tracking mode. Therefore, two situations were simulated: 1) a detection scenario where many realizations of the first 4 scans of lidar data were generated and processed, and 2) a tracking scenario where 22 scans of the vortex were generated and analyzed. Three main statistical metrics were produced: the probability of detection of the vortex, and the bias and the standard deviation of the resulting estimates of the vortex parameters. In addition, the probability density function (histogram) of the estimates was also produced to quantify the performance of CTI's algorithm.

In general, the performance of the CTI algorithm was very good. For SNR = 10, the errors in the CTI vertical and horizontal track measurements were often very small compared to the vortex dimensions, in the 0.2 m range. The largest biases observed were 4 m, with a random error of about 1 m. The results for vortex circulation showed that the lidar algorithm was very accurate when the vortex was first detected, but that it overestimated circulation more and more as the vortex decayed. Circulation biases as large as 60 m^2/s were observed for vortices 100 seconds old. The addition of turbulence increased the standard deviations of the estimates but had little effect on bias. An investigation of algorithm performance as a function of SNR showed that the probability of vortex detection is very high for SNR values over 0.5, and for SNR = 1 or greater, the tracking errors are very small. Bias error in the circulation estimates is a function of SNR, however, growing larger as SNR decreases.

Under Task 1.1(b), the STL field test being conducted by the Volpe National Transportation Systems Center was documented, and the possibilities for using the STL test site to validate the CTI lidar performance were investigated.

The research team visited the STL site and developed a written description of the tests. The description includes several diagrams and photographs to illustrate the position and scan patterns of the lidar, as well as the positions of associated instruments such as wind lines. Auxiliary information and the data collection and processing procedures were also documented.

One lidar had been installed, and a second, identical lidar was being procured for STL. The second lidar was to be installed further up the glide slope from the first, and the existence of two lidars at one airport provided a unique opportunity for cost-effective add-ons to the STL tests. Plans for validation field tests were therefore developed in two categories: 1) tests that could be conducted as add-ons to the current STL series of tests; and 2) tests that would require a separate series of tests in a restricted airspace. In both cases, the objective of the tests was to validate the results of the numerical simulations conducted under Task 1.1(a).

Two short-term tests using the two lidars were recommended for STL. In the first test, the lidars were to be installed adjacent to each other, scanning in adjacent vertical planes, so as to measure the same vortices simultaneously with both lidars. A statistical analysis of the vortex track and circulation data files would then provide a measure of the random measurement errors of the two lidars. In the second test, the lidars were to face each other across the glide slope, again scanning adjacent vertical planes. An analysis of the resulting track files would then determine any track bias along the range direction.

Tests of two CTI lidars together cannot be used to validate the circulation biases in low SNR shown by the simulations. Circulation bias will require a separate type of instrument. Scanning the lidar in a vertical plane adjacent to a vertical array of acoustic anemometers was recommended, while wake vortices were transported across the array by the ambient wind. Point sensors cannot characterize the vortex wind field with the temporal and spatial resolution of the lidar, but acoustic anemometers do provide fast, accurate, three-axis wind measurements. The tower supporting the sensor array would have to be fairly tall, so this test was to be conducted in controlled airspace, not at a commercial airport.

6 Acknowledgements

The research team would like to acknowledge the support of Steve Hannon and Eugene Bazyl of Coherent Technologies, Inc. for test and delivery of the CTI wake vortex detection and tracking algorithm, as well as demonstrating the CTI lidar interface. The research team would also like to acknowledge Frank Wang of the Volpe National Transportation Systems Center for all of his support providing data for the STL test section of this report. Additionally, Mike Hitch of the Wallops Island Flight Facility was most helpful in determining the feasibility of the vertical windline field test.

7 References

[1] Henderson, S. W., C. P. Hale, J. R. Magee, M. J. Kavaya, and A. V. Huffaker, 1991: Eye-safe coherent laser radar system at 2.1 μm using Tm,Ho:YAG lasers. Opt. Lett., **16**, 773-775.

[2] Henderson, S. W., P. J. M. Suni, C. P. Hale, S. M. Hannon, J. R. Magee, D. L. Bruns, and E. H. Yuen, 1993: Coherent laser radar at 2 μm using solid-state lasers. IEEE Trans. Geo. Remote Sensing, **31**, 4-15.

[3] Hannon, S. M. and S. W. Henderson, 1995: Wind measurement applications of coherent lidar. Rev. Laser Eng., **23**, 124-130.

[4] Hannon, S. M. and J. A. Thomson, 1994: Aircraft wake vortex detection and measurement with pulsed solid-state coherent laser radar. Mod Opt., **41**, 2175-2196.

[5] Constant, G., R. Foord, P. A. Forrester, and J. M. Vaughan, 1994: Coherent laser radar and the problem of aircraft wake vortices. J. Mod. Optics, **41**, 2153-2173.

[6] Brockman, P., B. C. Barker, G. J. Koch, D. P. C. Nguyen, and C. L. Britt, 1999: Coherent pulsed lidar sensing of wake vortex position and strength, winds and turbulence in the terminal area. Tenth Biennial Coherent Laser Radar Technology and Applications Conference, Mount Hood, Oregon, June 28-July 2, 12-15.

[7] Kopp, F., S. Rahm, R. Simmet, and I. Smalikho, 2003: Wake-vortex characterization by pulsed Doppler lidar. 12th Coherent Laser Radar Technology and Applications Conference, Bar Harbor, Maine, June 15-20, 152-155.

[8] Frehlich, R. G., 1996: Simulation of coherent Doppler lidar performance in the weak signal regime. J. Atmos. Oceanic Technol., **13**, 646-658.

[9] Frehlich, R. G., 1997: Effects of wind turbulence on coherent Doppler lidar performance. J. Atmos. Oceanic Technol., **14**, 54-75.

[10] Frehlich, R. G., 2000: Simulation of coherent Doppler lidar performance for space-based platforms. J. Appl. Meteor., **39**, 245-262.

[11] Frehlich, R. G., 2001: Estimation of velocity error for Doppler lidar measurements. J. Atmos. Ocean. Tech., **18**, 1628-1639.

[12] Frehlich, R. G., and L. Cornman, 1999: Coherent Doppler lidar signal spectrum with wind turbulence. Applied Optics, 38, 7456-7466.

[13] Frehlich, R. G., L. Cornman, and R. Sharman, 2001: Simulation of Three-dimensional turbulent velocity fields. J. Appl. Meteor, **40**, 246-258.

[14] Burnham, D. C., and J. N. Hallock, 1982: Chicago monostatic acoustic vortex sensing system. report No. DOT-TSC-FAA-79-103.IV, July.

[15] Frehlich, R. G., S. Hannon, and S. Henderson, 1998: Coherent Doppler lidar measurements of wind field statistics. Boundary-Layer Meteor, **86**, 233-256.

[16] Hannon, S. M., 2000: Autonomous infrared Doppler radar: Airport surveillance applications. Phys. Chem. Earth (B), **25**, 1005-1011.

[17] Frehlich, R. G., 1993: Cramer Rao Bounds for Gaussian random processes and applications to radar processing of atmospheric signals. IEEE Trans. Geoscience and Remote Sensing, **31**, 1123-1131.

[18] Rye, B. J. and R. M. Hardesty, 1993: Discrete spectral peak estimation in incoherent backscatter heterodyne lidar. I. Spectral accumulation and the Cramer-Rao lower bound. IEEE Trans. Geoscience and Remote Sensing, **31**, 16-27.

[19] WAKE VORTEX JFK 2 Final Report, D.P.C. Nguyen, Report No. RTI/4903-032-03S, Research Triangle Institute, Final Report under NASA Contract NAS1-19214, Task 32 (1998).

[20] J.N. Hallock, S.P. Osgood, and J. Kanopka, WAKE VORTEX EFFECTS ON PARALLEL RUNWAY OPERATIONS, American Institute of Aeronautics and Astronautics, 41st Aerospace Sciences Meeting and Exhibit, Reno, NV, 6-9 Jan 2003.

[21] NASA Langley Research Center Wake Vortex Research Supporting VAMS, D.K. Rutishauser, Briefing dated 22 May 2002.

REPORT DOCUMENTATION PAGE	*Form Approved* *OMB No. 0704-0188*

1. REPORT DATE *(DD-MM-YYYY)*	**2. REPORT TYPE**	**3. DATES COVERED** *(From - To)*
01-	Contractor Report	

4. TITLE AND SUBTITLE
Pulsed Lidar Performance/Technical Maturity Assessment

5a. CONTRACT NUMBER
NAS1-02056-6008

5b. GRANT NUMBER

5c. PROGRAM ELEMENT NUMBER

6. AUTHOR(S)
Gimmestad Gray G.
West, Leanne L.
Wood, Jack W.
Frehlich, Fred

5d. PROJECT NUMBER

5e. TASK NUMBER
6008

5f. WORK UNIT NUMBER
305295.02.07.07.20

7. PERFORMING ORGANIZATION NAME(S) AND ADDRESS(ES)
NASA Langley Research Center
Hampton, VA 23681-2199

Georgia Institute Of Technology
Atlanta, GA 30332-0800

8. PERFORMING ORGANIZATION REPORT NUMBER

9. SPONSORING/MONITORING AGENCY NAME(S) AND ADDRESS(ES)
National Aeronautics and Space Administration
Washington, DC 20546-0001

10. SPONSOR/MONITOR'S ACRONYM(S)
NASA

11. SPONSOR/MONITOR'S REPORT NUMBER(S)

12. DISTRIBUTION/AVAILABILITY STATEMENT
Unclassified - Unlimited
Subject Category-03
Availability: NASA CASI (301) 621-0390

13. SUPPLEMENTARY NOTES
Original COTR: Ben Barker (retired) then transferred to David Rutishauser
An electronic version can be found at http://ntrs.nasa.gov

14. ABSTRACT
The performance and technical maturity of the Coherent Technologies, Inc. (CTI) WindTracer lidar have been assessed for wake vortex detection and tracking at airports. The performance assessments described here were conducted with Monte Carlo simulations, and general plans were developed for field tests to validate the simulations.

To quantify the performance of CTI's algorithm, simulated lidar data were generated for various vortex and lidar parameters, and the results of CTI's algorithm (which was implemented on a mainframe computer at the National Center for Atmospheric Research) were compared with the known input parameters or "truth". This approach permits a rigorous statistical analysis of the detection of the vortex and the accuracy of the resulting estimates of vortex location and strength as a function of the lidar Signal to Noise Ratio (SNR), the key lidar signal quality parameter.

15. SUBJECT TERMS
wake vortex, wake turbulence, airport sensors, wake vortex detection, pulsed Lidar, wake vortex sensor, Lidar simulation

16. SECURITY CLASSIFICATION OF:			**17. LIMITATION OF ABSTRACT**	**18. NUMBER OF PAGES**	**19a. NAME OF RESPONSIBLE PERSON**
a. REPORT	**b. ABSTRACT**	**c. THIS PAGE**			STI Help Desk (email: help@sti.nasa.gov)
					19b. TELEPHONE NUMBER *(Include area code)*
U	U	U	UU	112	(301) 621-0390